ITER TECHNICAL REPORT

iter
china eu india japan korea russia usa

REPORT NO.

ITR-24-004

TITLE

Initial evaluations in support of the new ITER baseline and Research Plan

AUTHOR/AUTHORS

A. Loarte, R.A. Pitts, T. Wauters, I. Nunes, F. Köchl, A.R. Polevoi, S-H. Kim, M. Lehnen, J.Artola, L. Chen, S.D. Pinches, X. Bai, P. de Vries, I. Carvalho, M. Dubrov, Y. Gribov, M. Schneider, L. Zabeo

AUTHOR EMAIL(S)

alberto.loarte@iter.org

DATE

29th March 2024

Initial evaluations in support of the new ITER baseline and Research Plan

A. Loarte, R.A. Pitts, T. Wauters, I. Nunes, F. Köchl, A.R. Polevoi, S-H. Kim, M. Lehnen, J.Artola, L. Chen, S.D. Pinches, X, Bai, P. de Vries, I. Carvalho, M. Dubrov, Y. Gribov,

M. Schneider, L. Zabeo.

(ITER staff members).

With contributions from ITER Fellow Scientists and collaborators: K. Schimd, Y. Liu, J.R. Martín-Solís, C. Angioni, I. Pustzai.

And

Members of the new ITER baseline Task Force: J. Rapp, Ph. Snyder, Z. Unterberg, M. Xu, G. Xu, T. Nakano, T. Suzuki, N. Oyama, J. Ghosh, V. Menon, A. K. Singh, H. Zohm, A. Kallenbach,F. Rimini, J. Bucalossi, E. Tsitrone, C. Bourdelle, J. Hobirk, S-W. Yoon, S. Konovalov, V. Rozhansky, N. Kirneva.

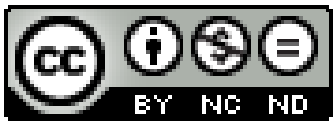

CONTENTS

Glossary and Acronyms

2016-FP	ITER First Plasma planned in the FP phase of the 2016-IRP
2016-IRP	Staged Approach Baseline 2016 ITER Research Plan (2XUY9N)
AFP	Augmented First Plasma
AP	Assembly Phase
ASDEX	Axially Symmetric Divertor Experiment
Be	Beryllium
CIS	Central Interlock System
CQ	Current Quench of a disruption
CSS	Central Safety System
CXN	Charge-Exchange Neutrals
DD	Deuterium Deuterium
DEMO	Demonstration power plant
DMS	Disruption Mitigation System
DNB	Diagnostic Neutral Beam
DT	Deuterium-Tritium
DT-1	First set of DT campaigns in the new baseline with the objective to demonstrate the Q = 10 project goal
DT-1	First DT phase of FPO in New Baseline Research Plan
DT-2	Second DT phase of FPO in New Baseline Research Plan
EAST	Experimental Advanced Superconducting Tokamak
ECH	Electron Cyclotron Heating
ELM	Edge Localized Mode
FP	First Plasma
FPE	First Plasma Exhaust System
FPO	Fusion Power Operation phase of IRP
FW	First Wall
FWP	First Wall Panel
GDC	Glow Discharge Cleaning
HFS	High Field Side

HNB	Heating Neutral Beam
HV	High Voltage
ICH	Ion Cyclotron Heating
ICWC	Ion Cyclotron Wall Cleaning
ILW	ITER-like Wall (Be) installed at JET
IntCom	Integrated Commissioning
IRP	ITER Research Plan
ITPA	International Tokamak Physics Activity
ITR	ITER Technical Report
JET	Joint European Torus
LCFS	Last Closed Flux Surface
LFS	Low Field Side
LTM	Long Term Maintenance
MHD	Magnet Hydro Dynamic
NB	New Baseline
NB-FP	ITER First Plasma planned at the end of IntCom-I of the new baseline
NBI	Neutral Beam Injection
NB-IRP	New Baseline ITER Research Plan
NBMFRS	Neutral Beam Magnetic Field Reduction System
Ne	Neon
n_{GW}	Greenwald density limit
NTM	Neoclassical Tearing mode
OMP	Outer Mid Plane
PCS	Plasma Control System
PFC	Plasma-Facing Components
PFPO-1	Pre-Fusion Power Operation 1 phase of 2016-IRP
PFPO-2	Pre-Fusion Power Operation 2 phase of 2016-IRP
RE	Runaway Electrons
RMS	Root Mean Square
SNU	Switching Network Units
SOL	Scrape Off Layer

SQRS	Simplified Q2 Recycling System
STM	Short Term Maintenance
TBMs	4 Test Blanket Modules
TF	Toroidal Field
TFTR	Tokamak Fusion Tet Reactor
TORE SUPRA	Torus Superconductor Tokamak
TQ	Thermal Quench of a disruption
VDE	Vertical Displacement Event
W	Tungsten
WEST	W-Environment in Steady-State Tokamak

Part I: Consequences of Changing the First Wall Material in ITER

Executive Summary

This report addresses the proposed modifications to the ITER baseline regarding the change of the first wall material from Be to W in order to mitigate the associated risks and taking in consideration the foreseen objectives and constraints for the DT-1 operational campaigns (namely the demonstration of Q = 10 with 500 MW of fusion power and a burn length of at least 300 s within a total fluence of ~ 3×10^{25} neutrons).

The main modifications concern the change of the heating and current drive mix and power levels for DT-1 compared to that foreseen in the 2016 baseline and the introduction of a boronization system. The rationale for the specific choices proposed is given, including the minimization of risks for the research programme to demonstrate the expected goals (in AFP and DT-1). This rationale is supported by physics assessments based on guidelines from present experiments and extensive modelling studies. Open areas where further R&D is required to either validate the models used for ITER predictions or to strengthen these predictions are discussed.

In addition, the impact of a W wall on ITER operation with the proposed new baseline systems is assessed for Q = 10 and a range of key scenarios in the AFP phase. This includes risk minimization operational approaches as well as minor modification to components beyond the change of wall material (i.e. detailed design of first wall panels for increased resilience to disruption loads).

The conclusion of these studies is that, with the proposed modifications to the baseline, the risks of the change of wall material to ITER achieving its Q = 10 goal are low to medium. Additional systems being considered for the baseline proposal are described that could reduce these risks to just low for a restricted set of Q = 10 plasma pulses.

1. Introduction

The new ITER baseline considers the change of first wall material from Be to W. This has potential positive impacts compared to Be on a range of issues such as those related to in-vessel T retention, dust production and resilience to disruption thermal loads during unmitigated or partially mitigated disruptions. However, it increases the risk related to increased core plasma radiation that can lead to the non-sustainment of H-mode plasmas and the radiative collapse of the discharge with direct impact on the achievement of the ITER high Q goals. To mitigate these risks, in particular with a view to the demonstration of the Q = 10 goal in DT-1 within a total neutron fluence of 3 10^{25} neutrons, the new baseline considers a modified heating and current drive mix and power level and a boronization system. In this report we describe the rationale and the physics assessments that support the specific choices made for the new baseline as well as operational strategies and minor design modifications to mitigate the risks of a W wall on the achievement of the ITER mission.

2. Review of the experimental physics basis for W wall operation and overall implications for ITER

Operation with W plasma-facing components (PFCs) can cause increased core plasma radiation, which decreases the operational range of H-mode plasmas and may lead to uncontrolled W accumulation (i.e. uncontrolled rise of the core W density at constant edge density). As will be discussed later in this section, the direct empirical extrapolation of the findings in present experiments to ITER is not straightforward. For some cases, the physics processes driving W transport differ between present experiments and ITER (e.g. core particle sources), or the experimental plasma conditions showing large W core densities are not accessible in ITER (e.g. low density plasma conditions leading to excessive divertor loads).

With these caveats, guidance from experiments can be used to evaluate the impact that a W wall may have in the expected range of operational conditions to be explored in ITER. We note that this is not a fully exhaustive review of the literature and we use, for simplicity, many examples from ASDEX Upgrade since it has operated with full W PFCs since 2007; the findings from ASDEX Upgrade are similar to those of other tokamak experiments operating with high Z PFCs (namely Alcator C-Mod, EAST, WEST and JET), or that have addressed high Z core impurity transport (e.g. DIII-D).

Experiments in ASDEX-Upgrade [Kallenbach 2009] with boronized and unboronized W walls show that stationary H-mode conditions can be maintained for a separatrix power flux 50% higher than the H-mode threshold power ($P_{sep} \geq 1.5\ P_{LH}$), with a typical level of core plasma radiation $P_{rad}^{core} \leq (0.4\text{-}0.5)\ P_{heat}$, as shown in Fig. 2-1. The operational space for JET with a Be wall and W divertor (ITER-like Wall or ILW) in terms of the same parameters has been re-examined for the initial ILW H-mode operation [Joffrin 2014] when such scenarios were first developed and the results are shown in Fig. 2-2. In terms of maximum P_{rad}^{core}/P_{heat} the values are comparable to those in ASDEX Upgrade, while in terms of the margin to the L-H threshold power, these initial JET ILW H-mode plasmas operated with $1.0 \leq P_{sep}/P_{LH} \leq 1.5$ and, thus, with lower margin than ASDEX-Upgrade. It should be noted, however, that in the case of JET, P_{LH} is evaluated from the 2008 scaling [Martin 2008] and the real H-mode threshold in JET with the ILW tends to be lower than the value derived from this scaling.

A quantitative comparison of the effect of the W wall on H-mode performance in ASDEX Upgrade can be found in [Kallenbach 2009, Schweinzer 2016] in which plasmas with no/low boron (B) coverage of the wall are compared with similar plasmas with large B coverage. As can be seen in Fig. 2-3 the W wall increases the radiation level by 50% compared to a low Z wall (boronized) and increases the W concentration. Despite this, the W concentration can be maintained at levels of ~ few 10^{-5}, as required for Q = 10 in ITER, by the application of ECH or ICH heating as shown in Figs. 2-4 and 2-5. An essential ingredient to achieve these acceptable concentrations under stationary operating conditions is to ensure that ELMs are maintained controlled at sufficient frequency since, in present experiments, they provide a very effective means to exhaust W from the edge plasma. Note that, as discussed below, W transport at the plasma edge between ELMs is directed inwards in present experiments and this may not apply in ITER.

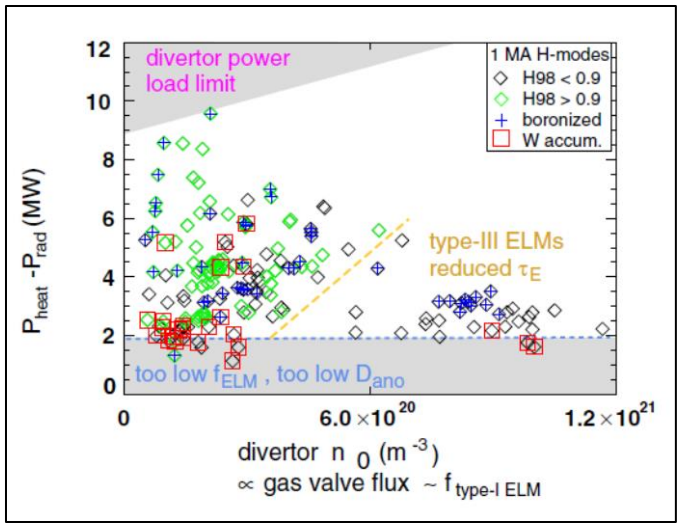

Figure 2-1. H-mode operational space in terms of divertor neutral density, $n_{0,div}$, and target heat load, $P_{heat} - P_{rad}$. Data points represent either steady-state flattop phases or phases leading to central W accumulation (red squares), averaging time is typically 0.5 s. The divertor neutral density is nearly proportional to the total gas valve flux. Black diamonds denote discharges with H-factors, H_{98y2} below 0.9, which are typically Type-III ELMy H-modes. The limits indicated are just sketches guided by the data points. Plasma current I_p = 1 MA. The typical L-H transition power for these plasma conditions is 1.5 MW [Ryter 2013].

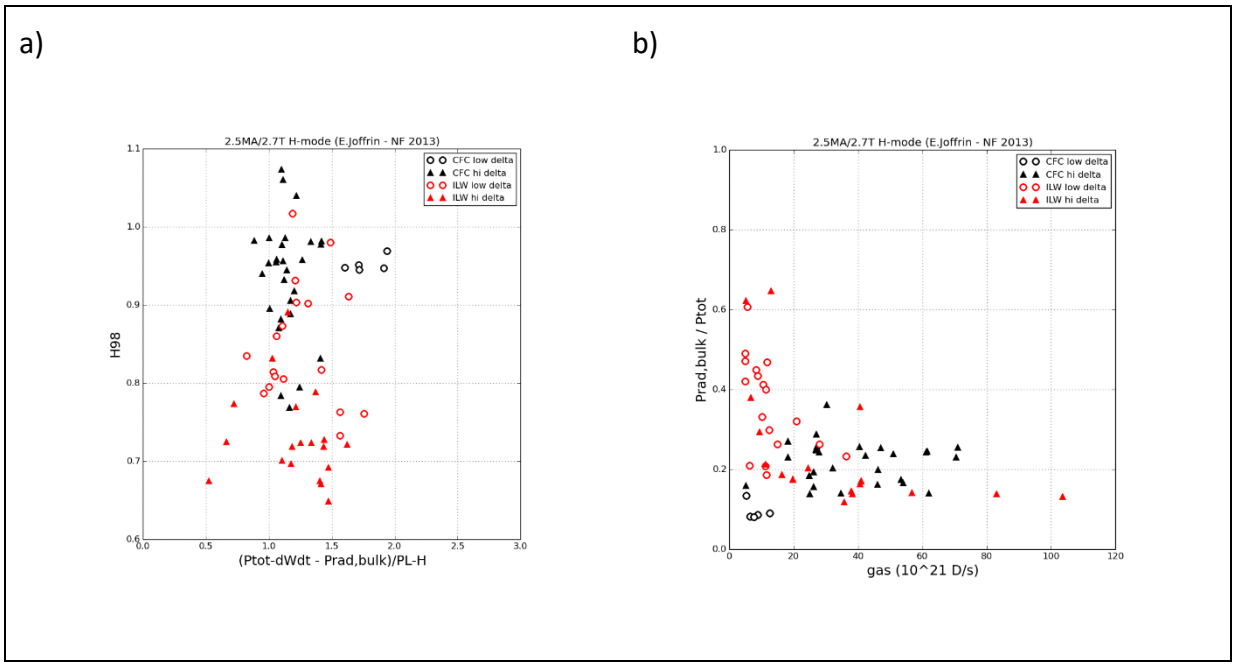

Figure 2-2. a) H_{98} versus P_{sep}/P_{LH} and b) P_{rad}^{core}/P_{heat} versus gas fuelling rates for JET initial H-mode plasmas with the ILW compared with carbon PFC operation.

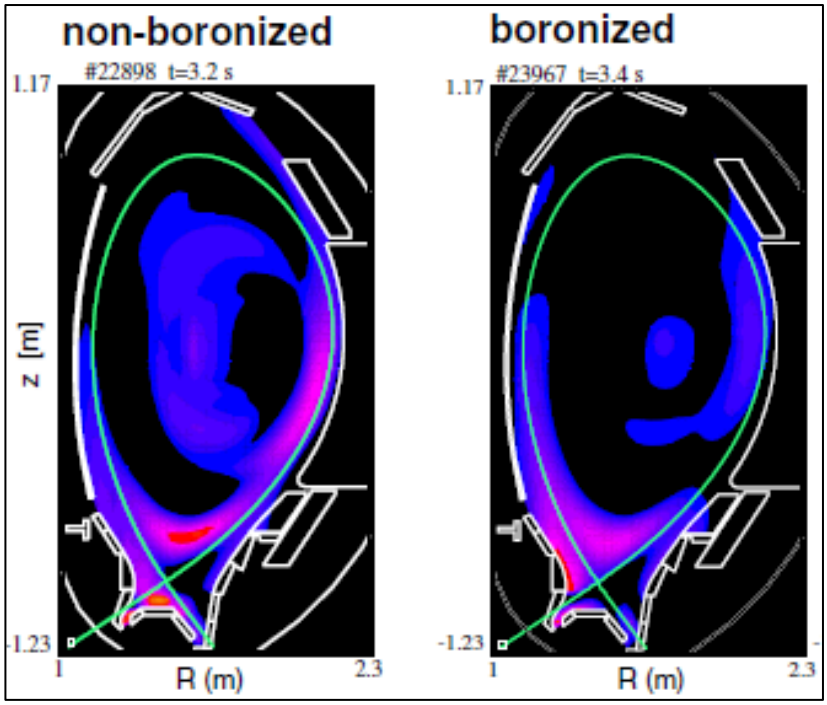

Figure 2-3. Comparison of the radiation distribution from bolometry of two ASDEX Upgrade discharges with identical heating power and D fuelling for non-boronized and boronized conditions. The total radiated powers are 4.5MW for the non-boronized and 3.4MW for the boronized discharge.

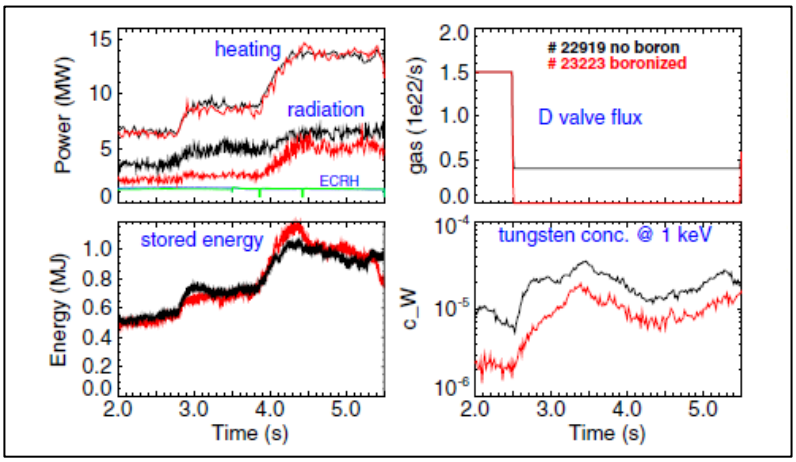

Figure 2-4. Comparison between high power improved H-mode discharges with identical heating schemes under non-boronized and boronized conditions in ASDEX Upgrade. Shown are the heating power (almost identical) and total radiation time traces, the gas puff, stored energy and W concentration. The H-factor H98y,2 at t = 4.3 s is 1.1 for the unboronized and 1.3 for the boronized discharge without D puff. For the latter discharge, confinement is slightly decreased by moderate neoclassical tearing mode activity. I_p = 1 MA, q_{95} = 4.7.

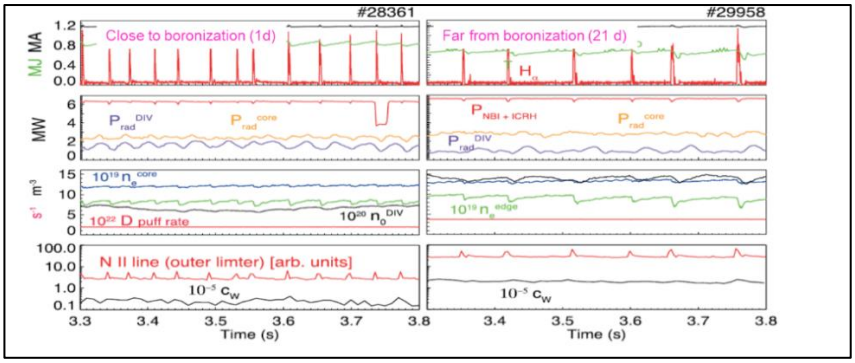

Figure 2-5. Comparison of ITER Baseline ASDEX Upgrade discharges during phases of 0.5 s duration. Discharge parameters are identical except gas puff and 'freshness' of boronization. While the discharge on the left (#28361) was conducted 1 day after a boronization, the one on the right (#29958) was executed 21 days after a boronization. Different gas puff levels 1.9 x 10^{22} and 3.8 x 10^{22} atoms s^{-1} were necessary to reach stationarity for discharges #28361 and #29958, respectively.

Central ECH heating is effective to avoid uncontrolled W accumulation in present experiments, as shown in Fig. 2-6.a. ICH can also provide a similar effect, as shown in Fig. 2-6.b, provided that the additional W influx generated by specific ICH-W plasma-wall interactions remains small [Angioni 2017]. This can be achieved by the installation of low Z PFCs at the antenna sides or by covering the W side elements by boronization; these schemes are not suitable for ITER with a full-W wall. Approaches to accomplish the same goal by antenna design that are relevant for ITER have been demonstrated in present experiments such as ASDEX Upgrade [Bobkov 2010, Bobkov 2017] (see Fig. 2-7.b) and Alcator C-Mod [Wukitch 2013]. Separate studies have shown that the flexibility provided by the ITER ICH antenna design can be deployed to reduce the ICH-induced W source [Helou 2023].

The temperature anisotropy of ICH resonant species leads to direct effects on W transport and to poloidal asymmetries of the electrostatic potential [Angioni 2021] which also affect W transport. The combination of such ICH-driven effects can impact core W transport positively (i.e. outwards) or negatively (inwards) depending on plasma conditions [Manas 2022].

i) ii)

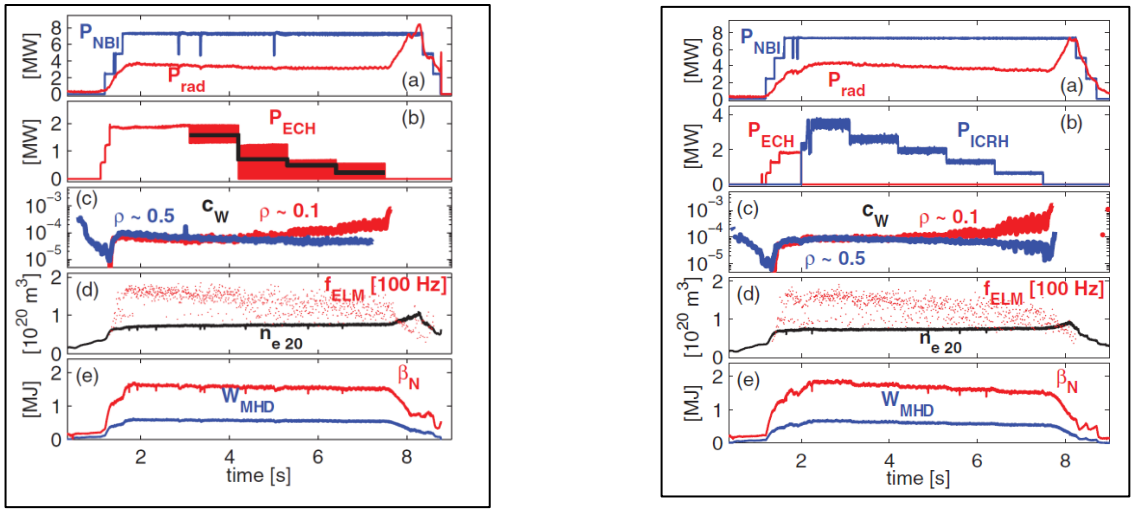

Figure 2.6. Time traces of ASDEX Upgrade shot (i – 32408 and ii -32404) with decreasing steps of ECH and ICH, respectively: a) total NBI and radiated powers, b) total ECH and ICH powers, c) W concentration c_W at □ ~ 0.1 and □ ~0.5, d) ELM frequency and line averaged density, e) normalized β and total stored energy [Angioni 2017].

a) b)

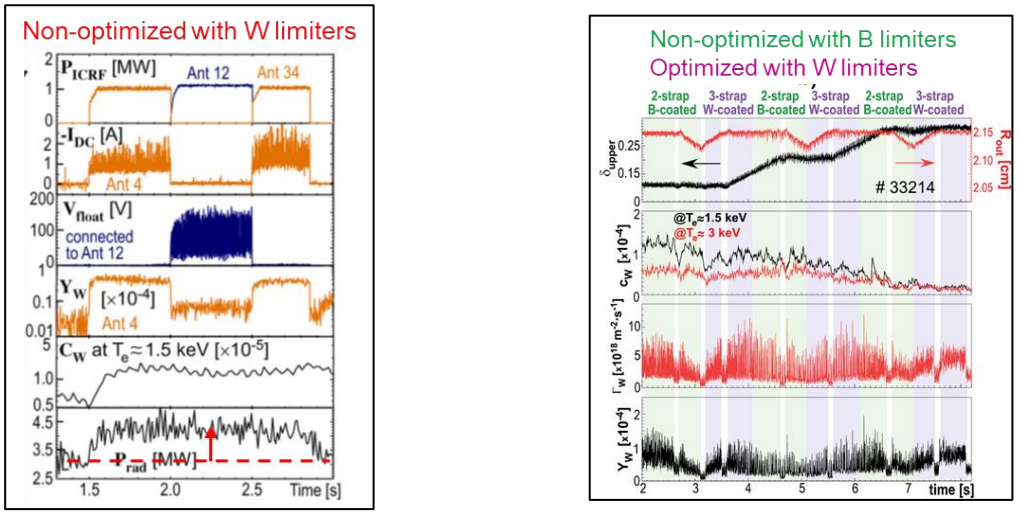

Figure 2-7. a) Characterization of the W release during ICH power input from antenna pairs 12 and 34 for shot #22797 before boronization in ASDEX Upgrade with non-optimized (2-strap) antennas [Bobkov 2010]. b) Comparison of the B-coated antennas with the W-coated antennas during scans of plasma triangularity and the radial position in deuterium plasmas in ASDEX Upgrade. Every antenna pair provides $P_{ICH} = 1.5$ MW in the highlighted time windows on top of $P_{aux} = 6.3$ MW. The non-optimized (2-strap) antennas are B-coated and the optimized (3-strap) antennas are W-coated [Bobkov 2017].

Regarding the W influxes from the divertor and the wall, present experiments find that the gross wall W source is much smaller than that from the divertor, a factor of 5-10 for typical

conditions in ASDEX Upgrade [Dux 2011], as shown in Fig. 2-8.a. For ELMy H-modes, the W wall source can be dominated by the ELMs or by the inter-ELM plasma flux depending on whether the plasma-wall distance is small (inter-ELM dominated) or large (ELM dominated) compared to the characteristic distance for radial particle flux decay. An example for ELM dominated W wall influx [Dux 2011] is shown in Fig. 2-8-b.

a) b)

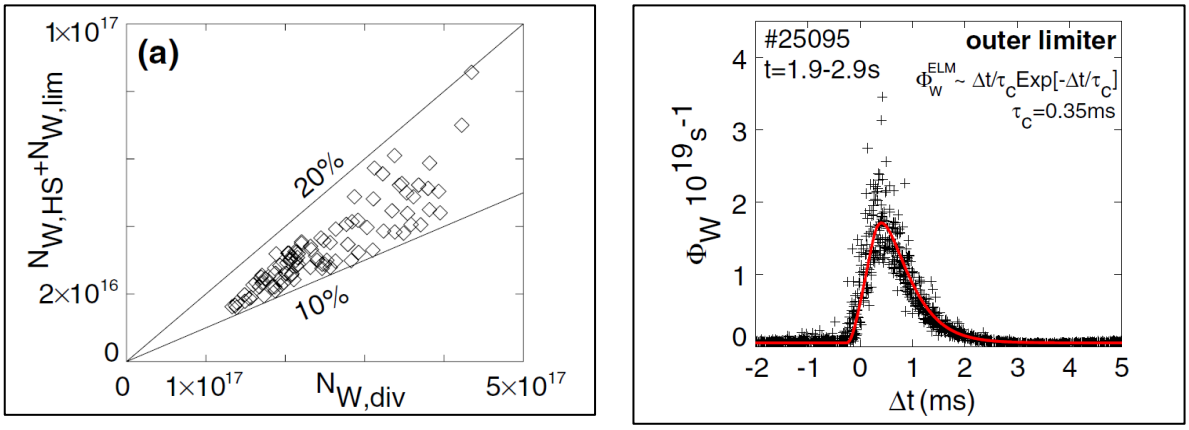

Figure 2-8. a) ELM W source at the main chamber components versus the divertor W source in ASDEX Upgrade. b) Evolution of the W source rate at the outboard limiters during a type-I ELM. The temporal coordinate Δt is the time difference to the arrival time of the ELM in the outboard divertor and the data of 117 ELMs are overlaid. [Dux 2011].

Despite the much smaller magnitude of the W wall source its effect on the core W plasma density is sizeable. This is due to the fact that W prompt redeposition is smaller at the wall than at the divertor and to the less efficient penetration of divertor produced impurities by screening in the divertor plasma. To document this experimentally, plasma-wall distance scans at constant plasma and divertor conditions were performed in ASDEX Upgrade; results are shown in Fig. 2.-9 [Dux 2009]. Increasing the gross W influx from the LFS leads to an increase by a factor of ~ 2 of the core W concentration, even if the LFS W gross influx remains about an order of magnitude lower than that from the divertor. This implies an effective contamination efficiency for LFS wall produced W an order of magnitude larger than from the divertor.

The W that enters the edge plasma has to be transported across the pedestal of H-mode plasmas. Experimental and modelling studies have shown that impurity transport in the H-mode pedestal between ELMs can be described by neoclassical transport. The direction and magnitude of the W transport is, thus, determined by the density and temperature gradients in the pedestal. For the usual experimental conditions achievable in today's experiments (with $|R/L_n| > |R/2L_T|$, where L_n and L_T are the density and temperature gradient scale lengths in the pedestal) this implies a negative inwards pinch and thus a significant increase of the impurity density from the separatrix to the top of the pedestal, as shown in Fig. 2-10 [Pütterich 2011]. For conditions obtained at JET in plasmas with high ion temperatures, in which $|R/L_n| < |R/2L_T|$, a decreased W density at the edge is observed as expected from neoclassical transport predictions [Field 2023] see Fig. 2.-11.

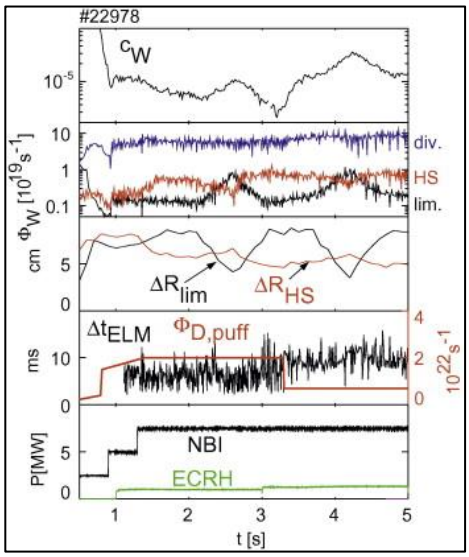

Figure 2-9. Time traces for an ASDEX Upgrade discharge (#22978) with variations of the outer separatrix radius at two levels of gas puffing showing the increase of the W core density when the LFS (lim) W wall flux increases. From top to bottom: W concentration, gross W sources from the divertor, HFS and LFS, distance between the separatrix and the wall at the LFS and HFS, gas puffing level and resulting ELM frequency, NBI and ECH heating waveforms [Dux 2009].

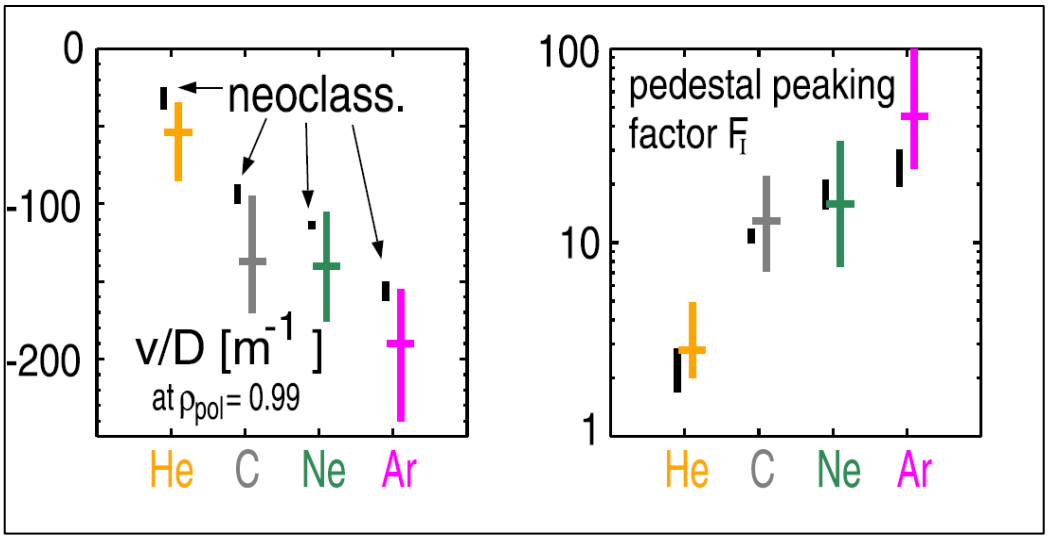

Figure 2-10. Measured and modelled (assuming neoclassical transport) inverse scale lengths for a range of impurities in the ASDEX Upgrade pedestal and resulting pedestal peaking (namely the ratio of the impurity density at the top of the pedestal and at the separatrix) [Pütterich 2011].

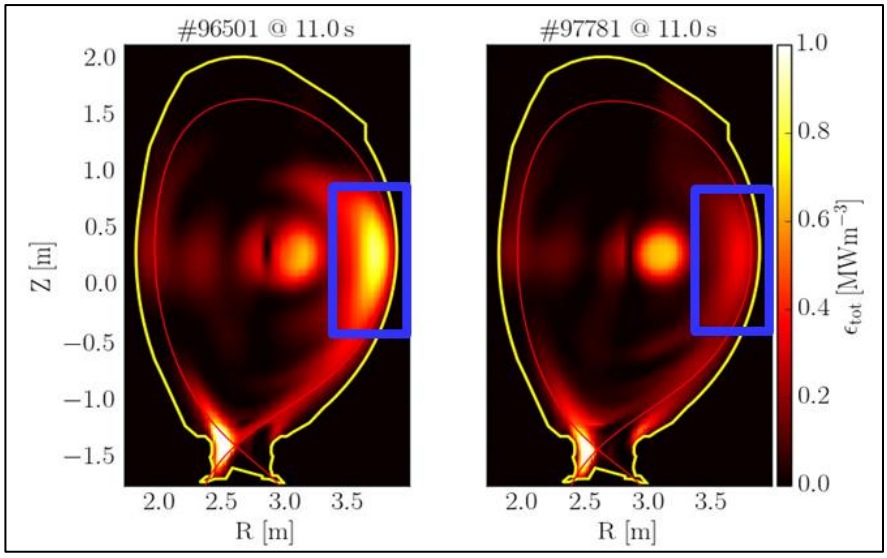

Figure 2-11. Comparison of the total radiated emissivity distributions, dominated by W radiation, from tomographic inversions of bolometric measurements for two hybrid JET pulses (#96501 (left) and #97781 (right) at 11 s) showing the decrease of the edge W density associated with neoclassical screening in pulse #97781. The first wall and separatrix contours are shown yellow and red respectively [Field 2023].

As mentioned at the start of this section, drawing direct conclusions on the implications of a W wall for ITER solely based on direct extrapolation of experimental results is not simple since quantitative extrapolation is subject to large uncertainties and also because for some key specific issues it is already known that the behaviour expected in ITER is qualitatively different from that in present experiments. For such specific issues, direct extrapolation is simply incorrect. Taking this into account, the following overall implications can be considered for ITER:

- Robust H-mode operation with a W wall should be maintained in ITER up to core radiative power fractions of $P_{rad}^{core}/P^{heat} \leq 0.5$. These are typical radiated power fractions found in the development of H-modes for devices with W PFCs. When the net W impurity influxes into the plasma are optimized (e.g. by source reduction or increased outflux by ELMs), lower radiation fractions can be achieved with all-W PFCs;
- Robust H-mode operation (in DD/DT plasma) requires that the edge power flow with some margin above the L-H power threshold be maintained. Based on experimental results, $P_{sep} \geq 1.5\ P_{LH}$ can be adopted for ITER;
- Sufficient capability for central ECH heating should be maintained to ensure efficient plasma heating and good core W accumulation control. This should be in addition to other control missions of the ECH system in ITER such as NTM control;
- Sufficient capability for central ICH heating is desirable for W control and for the flexibility of the experimental programme. Note that, as discussed in the next section, ICWC is required in ITER for fuel removal occurring during boronization;
- Good ELM control is mandatory for operation in H-mode with all-W PFCs.

Two key aspects of W transport physics that are already known to be different from most present experimental evidence, due to physics differences or integration aspects in ITER, are:

- Mechanisms driving core W accumulation.

In present experiments, the existence of a strong core particle source (usually provided by NBI) is key to drive the uncontrolled accumulation of W, as confirmed in Alcator C-Mod, ASDEX Upgrade and WEST [Loarte 2015, Manas 2021, Yang 2020]. A source of comparable strength is not provided by ITER NBIs because the high energy of the injected ions (~1 MeV) entails a very low core particle source for similar levels of injected power (~10's of MW) [Loarte 2015]. One should note that to model W accumulation driven by neoclassical effects, the evaluations of impurity neoclassical transport must include the correct physics model. The plasma collisionality affects the magnitude and direction of the temperature screening term, being positive (screening) in the Pfirsch–Schlüter regime and negative in the Banana-Plateau (BP) regime at lower collisionalities. Application of such appropriate physics models to ITER leads to very low inwards/outwards neoclassical velocities in the core plasma [-0.04, 0.02] m/s which are much smaller than those that could be expected from anomalous transport [Fajardo 2022]. We note that the Mach number of ITER plasmas is low and, thus, does not significantly enhance neoclassical W transport, unlike in present experiments [Angioni 2014, Loarte 2016]. This implies that evolution of the W density in ITER core plasma will take place over long timescales, many tens of seconds compared with typically a few seconds in present experiments. As a consequence, if W accumulation were to occur in ITER, it would be easily detected and means to control/arrest it could be deployed.

- Pedestal transport and W exhaust by ELMs.

Pedestal transport in ITER H-modes between ELMs is expected to be regulated by neoclassical physics as in present experiments, although uncertainties remain regarding the level of accuracy to which neoclassical physics can describe W transport across the ITER pedestal [Reynolds-Barredo 2020]. On this basis, the relationship between edge density and temperature gradients is key to determine the radial direction of the W flow at the edge. Integration of ITER plasmas with acceptable divertor power loads, particularly with high levels of additional heating and for high Q operation, implies that the separatrix density typically has to be in the range of $n_{sep}/n_{ped} > 0.5$ [Pitts 2019]. This results in moderate edge density gradients at the plasma edge compared to those for the temperature for which, typically, $T_{sep}/T_{ped} < 0.1$. Under such conditions, edge temperature screening dominates and W transport is outwards in the pedestal [Dux 2014], as shown in Fig. 2-12. This is unlike the vast majority of experimental evidence, except the JET results quoted above [Fields 2023], in which ITER-like pedestal edge gradients were obtained. Therefore, assuming by default that W transport at the ITER plasma edge between ELMs would be inwards and drawing consequences from present experiments along these lines is incorrect. We note, in addition, that ELMs are expected to melt the divertor monoblocks at least in some locations (e.g. toroidal gap edges) for plasma current above ~5 MA in ITER and they need to be strongly mitigated or suppressed for higher current levels. Therefore, even if it were effective (see below), increasing the ELM frequency cannot be considered as an edge W control scheme for plasma currents above 5 MA, since the associated ELM power fluxes would be intolerable in the divertor.

It is similarly incorrect to assume that ELM control through ELM frequency increase will routinely provide appropriate W density control in ITER. The efficiency of ELM control by frequency increase to provide W exhaust from the edge plasma is directly correlated with the shape of the edge W density profile. For conditions in which edge W transport is inwards and W profiles in the pedestal are peaked, as is the case in the vast majority of present experiments, ELMs provide efficient W exhaust. On the contrary, for conditions in which W screening dominates (high power and/or high Q in ITER) and W density profiles in the pedestal are hollow, ELMs produce an inwards W influx and therefore increase the core W concentration rather than decrease it. This was originally identified for ITER in [van Vugt 2019, Dux 2017], as shown in Fig. 2-13 and confirmed in the JET experiments mentioned above. It implies that in conditions with W screening in ITER, ELM suppression rather than controlled ELM triggering will be required for W control, independently of the needs for divertor ELM power flux control (melt avoidance).

a) b)

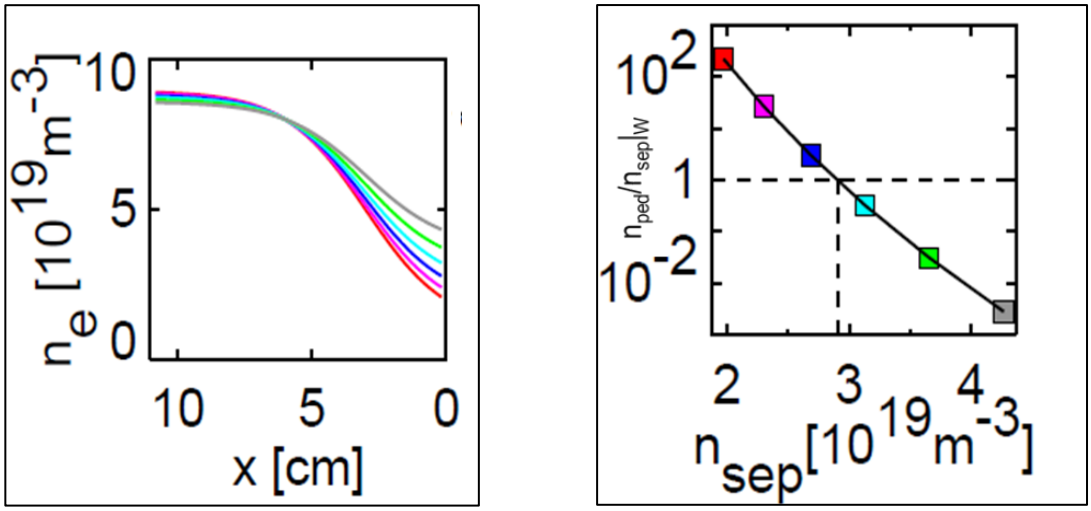

Figure 2-12. Modelled ratio of the W density peaking (W density at pedestal top divided by that at the separatrix) in the ITER pedestal for Q = 10 plasma conditions for a range of separatrix densities. For separatrix densities above 3 x 10^{19} m^{-3}, screening of the W (i.e. lower W pedestal density than at the separatrix) is expected [Dux 2014]. Note that for appropriate power exhaust for Q = 10 plasmas $n_{esep} \geq 4 \times 10^{19}$ m^{-3} is required [Pitts 2019].

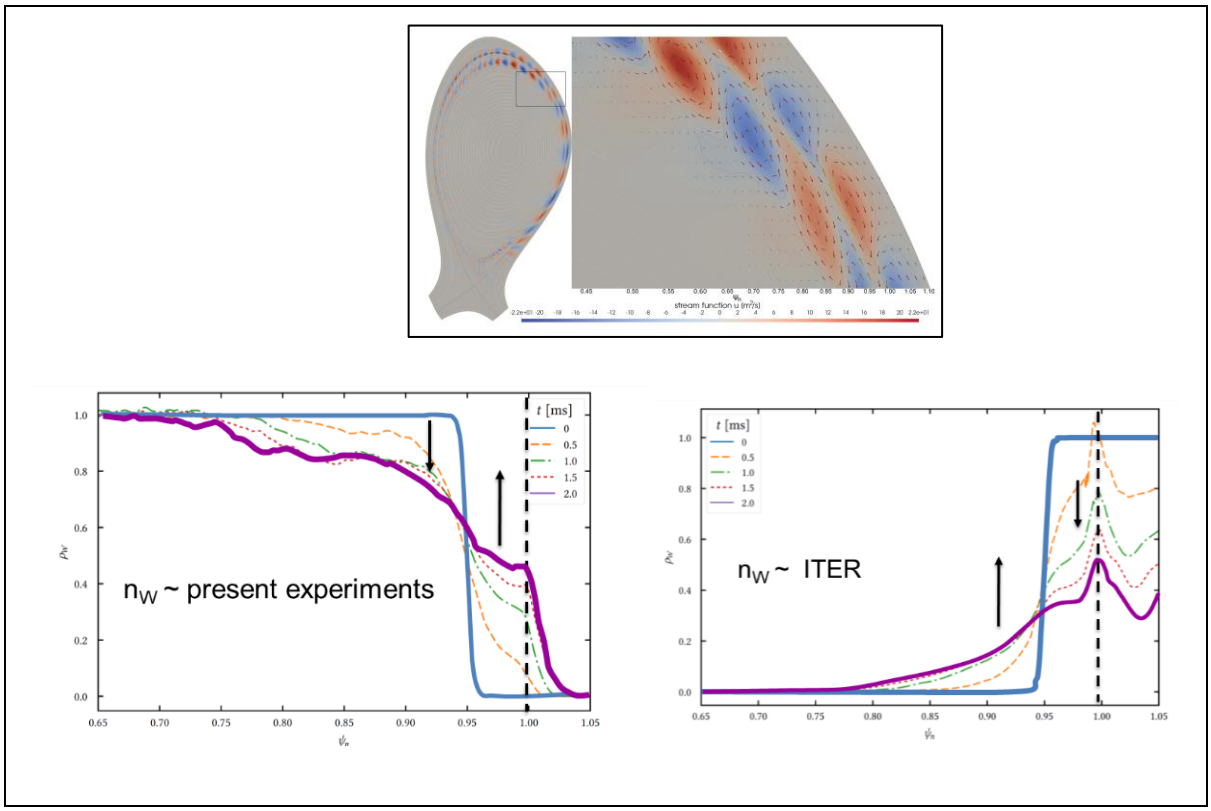

Figure 2-13. Upper: JOREK model fluid velocity during ELMs for ASDEX Upgrade (arrows indicate the direction of the drift, with the colour indicating the magnitude). Lower left: W impurity distribution before (blue) and after (violet) the ELM assuming inwards edge W transport between ELMs as in present experiments. Lower right: W impurity distribution before (blue) and after (violet) the ELM assuming outwards edge W transport between ELMs as expected in ITER. The dashed vertical line corresponds to the separatrix and the horizontal axis is in normalized flux units [van Vugt 2019].

3. Rationale, requirements for the boronization system and implications for ITER

In addition to discharge cleaning techniques, gettering in tokamaks has been used since 1975 as a powerful tool for controlling the impurity influx into fusion plasmas [Winter 1990]. A key effect is the reduction of the oxygen impurity concentration, achieved through both Be gettering and the application of boronization. Since the new proposed baseline scenario excludes the use of Be, an alternative approach for wall conditioning is necessary to minimize the influx of impurities, notably oxygen. Boronization is proposed as the method of choice for a W main chamber wall, ensuring favourable plasma conditions for effective plasma operation.

Boronization in fusion devices involves applying a thin, amorphous B layer covering the plasma-facing surfaces through the process of plasma-enhanced chemical vapour deposition. The first boronization was accomplished in TEXTOR through GDC plasma with diluted diborane (B_2D_6) in helium [Winter 1989]. Since then, and until the present day, this technique has been routinely and effectively employed in numerous fusion devices. Note that alternative techniques for applying B coatings are being developed in fusion research. Solid injection of

boron9ATR8M is being considered in ITER to create temporary low-Z wall conditions at plasma-wetted surfaces, potentially enhancing plasma performance in a selected number of high-Q experiments, but its integration into ITER is not simple. Boronization via pulsed ICWC plasma, as demonstrated in HT-7 and EAST [Li 1999, Gao 2009], may need multiple ICH antennas for layer uniformity, which cannot be implemented in ITER. Therefore, to achieve a long-lasting oxygen gettering effect in ITER, GDC boronization remains the best reliable approach.

3.1. Experimental basis for boronization with a W wall

After completing its conversion into a full W device, the ASDEX Upgrade tokamak operated the first experimental campaigns without boronization [Kallenbach 2009]. The relatively high impurity level in the unboronized machine led to restrictions of the H-mode operational space, since low-medium Z impurities dominated the physical sputtering of tungsten, predominantly under low or medium power conditions. The presence of oxygen also impacted the plasma limiter start-up.

Fig. 3.1.-1 illustrates that boronization in ASDEX Upgrade effectively removes residual oxygen for hundreds of discharges. Fig. 3.1-2 shows a similar the reduction of the intrinsic oxygen contamination in consecutive boronizations of the full W WEST tokamak. The reduction is most pronounced in the first boronization, lasting hundreds of discharges after the third. Boronization in WEST improves plasma start-up by almost completely suppressing RE beam formation, extending prefill ranges and reducing the edge radiation levels [Bucalossi 2022]. The first L-H transition in WEST was achieved after a fresh boronization.

3.2. Evaluations of GDC boronization in ITER

The proposed approach to B coating in ITER follows the extensive experience accumulated in present devices and will be applied through GDC plasma, utilizing diluted diborane (B_2H_6 or B_2D_6) in either H, D or helium (He). The toroidal field will not be present during this process, limiting the procedure to short term maintenance (STM) or long term maintenance (LTM) periods. Note that the repetition of boronization in present experiments is usually driven by low-density programmes, needing hydrogen pumping and a low-Z wall for their successful implementation, rather than by oxygen gettering. Boronization in ITER, however, aims at maintaining a low oxygen level to ease plasma operations. In particular, based on the experience of ASDEX Upgrade and WEST (as already discussed in Section 3.1), EAST [Liu 2007], and on the W start-up simulations for ITER described later in Section 5.2, the operational space for ITER limiter start-up on high-Z PFCs is expected to be rather narrow. As a consequence, the impurity levels during this initial phase have a significant potential impact in ITER operation.

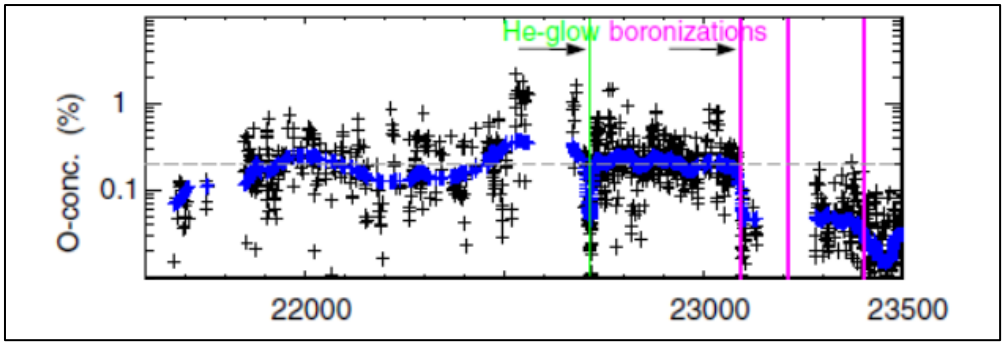

Figure 3.1-1. Development of O concentrations during the unboronized, full-W ASDEX Upgrade campaign and after boronization, from X-ray lines measured by a Bragg crystal spectrometer ($n_e > 4.5 \times 10^{19}$ m^{-3}) [Kallenbach 2009].

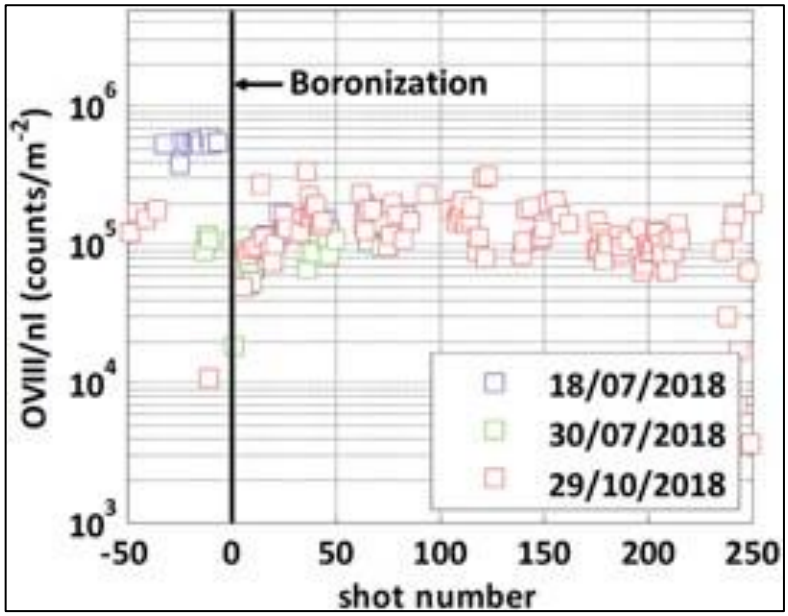

Figure 3.1-2. Oxygen radiation before and after the first, second and third boronizations performed on WEST [Bucalossi 2022].

Reviews by [Buzhinskij 1997] and [Hong JNM 2011] indicate that layers of 50-100 nm will be required in ITER to provide the appropriate gettering effect. Based on [Ennaceur 2000], a 50 nm coating can bind an estimated ~1-5x10^{20} oxygen atoms per m^2. For a conservative effective O-gettering surface area of ~10% of the ITER first wall (65 m^2), considering a maximum impurity outgassing rate of 1x10^{-9} Pa.m^3.s^{-1}.m^{-2} from the in-vessel surfaces (2x10^4 m^2) [ITR-19-004], and assuming that the outgassing is all water (which is conservative for baked steel), one boronization corresponds to a possible oxygen storage capacity of 2.5 to 12.5 weeks of ITER operation. Note that the maximum leak rate in ITER is two orders of magnitude below the outgassing rate [ITR-19-004].

To evaluate the lifetime of boronized layers on the plasma-facing surfaces, simulations have been carried out with the WallDYN3D code for Q = 10 plasma conditions with highest expected ion fluxes to the FW (namely close to double-null operation and high far SOL transport) [Schmid 2023]. The results of these simulations, shown in Fig. 3.2-1, demonstrate

that for plasma exposed surfaces, the boronized layers last only for very short periods (~100 s), while for remote areas these layers can survive for long plasma exposure periods (~10^4 s). We note that for two weeks of plasma operation (12 operational days), with an average of 13 pulses per day, this 10^4 s corresponds to an average high power duration of 65 s per pulse.

The required boronization frequency in ITER to maintain good vacuum conditions is determined by both the oxygen uptake capacity and the erosion rate of the B layers due to plasma operations. Based on the above estimates, the procedure needs to be performed at most once every two weeks. The application of B layers by GDC boronization is therefore consistent with the ITER operation cycle which includes STM shutdowns (2-3 days) every two weeks. During STM, the toroidal field can be ramped to zero, as required for GDC if a boronization is needed.

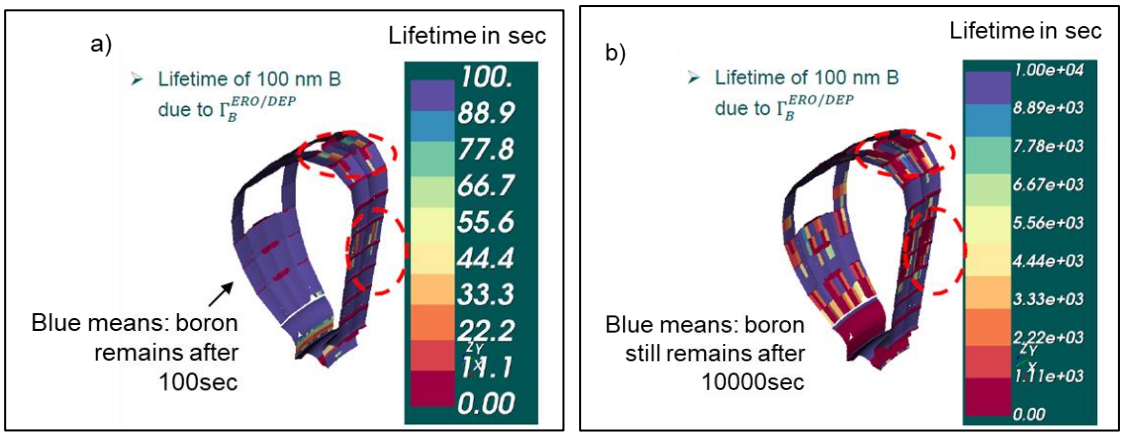

Figure 3.2-1. Lifetime of a 100 nm thick B layer exposed to a Q = 10 plasma with large high SOL transport and near double-null operation evaluated with the WallDYN3D code. a) Plasma exposed areas with short erosion lifetime for B layers and b) remote areas with long layer erosion lifetime.

Besides oxygen, the boronization layers also absorb hydrogen. The introduction of B in present devices improves density control by decreasing hydrogen recycling. While this is not the envisaged aim of boronization in ITER, the introduced B does have the potential to trap a significant amount of T in-vessel. Evidently, this T retention will be capped by the quantity of B introduced and is estimated at 370g T for DT-1 if no specific action to remove the in-vessel T within or between campaigns is taken.

As in the case of Be, eroded B is expected to accumulate into thick co-deposited layers at the divertor as well as in recessed main chamber wall areas. Desorption of D or T from such B deposits requires respectively 177°C, 427°C and 577°C to break chemical B–D–B, B–D, B–O–D bonds [Yoshikawa 2009]. A 350°C gas bake of the divertor (foreseen for removal of trapped T in Be deposits) versus a 240°C water bake therefore brings little gain for this purpose with B deposits so that this capability is no longer required in the new baseline. Thus, a combination of fuel removal techniques is expected to be necessary in ITER to maintain a low level of retained T by B layers, similar to those applied to remove T from Be co-deposits in JET following the DTE2 experiment [Matveev 2023].

Methods to recover T rely on thermal release, isotopic exchange, or a combination of both. Isotopic exchange occurs through plasma exposure of surfaces, and in the specific case of B layers, the depth of effective interaction depends strongly on the energy of the plasma particles impacting on the surface. Following a boronization, the WallDYN simulations in Figure 3.2-1 predict that layers can accumulate at the divertor up to a thickness of tens of nm per Q=10 discharge. Exchanging T from such layers requires energies above 300 eV. Tokamak pulses, ICWC, and GDC meet this requirement, but because GDC requires that the toroidal field be zero, its use is constrained to shutdown periods (STM, LTM). Thick layers are thus expected to accumulate over plasma campaigns. Note that GDC combined with baking, restricted to LTM in ITER, has shown to be effective to recover T in JET [Matveev 2023], but the same with regard to fuel removal from B layers has yet to be demonstrated.

Dedicated tokamak discharges have been developed for JET [Wauters 2022] and investigated theoretically for ITER [Park 2023] to recover fuel from divertor deposits. The common scenario involves raising the divertor strike lines onto deposition-dominated areas, bringing heat and particle flux to these locations. A concern in this scenario is the possibility of re-depositing T along with B onto other PFCs, rendering them inaccessible for subsequent cleaning through tokamak discharges. This risk can be reduced by decreasing the T content in tokamak cleaning pulses, and consequently in newly formed deposits, using prior implementation of ICWC, as demonstrated in JET [Matveev 2023]. Main chamber deposits, accumulating at lower rates, may be accessed directly by ICWC.

The required duration of an ICWC procedure depends on the achievable particle flux arriving at the B deposits. Energy spectra of charge exchange neutrals (CXN) during ICWC, accessing shadowed areas on the main chamber, measured above 1-5 keV in JET, TORE SUPRA and ASDEX Upgrade, show relatively low integral flux. Figure 3.2.-2 shows a specific example from TORE SUPRA, for which a flux of 10^{17} (H+D) $m^{-2}s^{-1}$ above 1 keV can be inferred [de la Cal PPCF 2006]. These neutrals stem from the energetic tail of a non-Maxwellian distribution and represent less than 1% of the ion population. When extrapolating this data to 300 eV (the energy required for isotope exchange – see above), the flux increases to $9x10^{17}$ (H+D) $m^{-2}s^{-1}$, constituting ~4% of the estimated 50 kW of coupled ICH power. No measurements are available under ITER-relevant conditions within the range relevant for T recovery (> 300 eV).

At low toroidal field in TOMAS, these energetic neutrals represent 1% of the 1.5 kW of coupled ICH power (example spectra in Figure 3.2-2). The energy and total flux of CXN fluxes in ICWC increase with increasing toroidal field and ICH coupled power. Scaling by ICH power (2 MW coupled in ITER) and PFC surface area, CXN fluxes above 10^{18} $m^{-2}s^{-1}$ seem feasible in ITER, allowing effective use of ICWC for T removal.

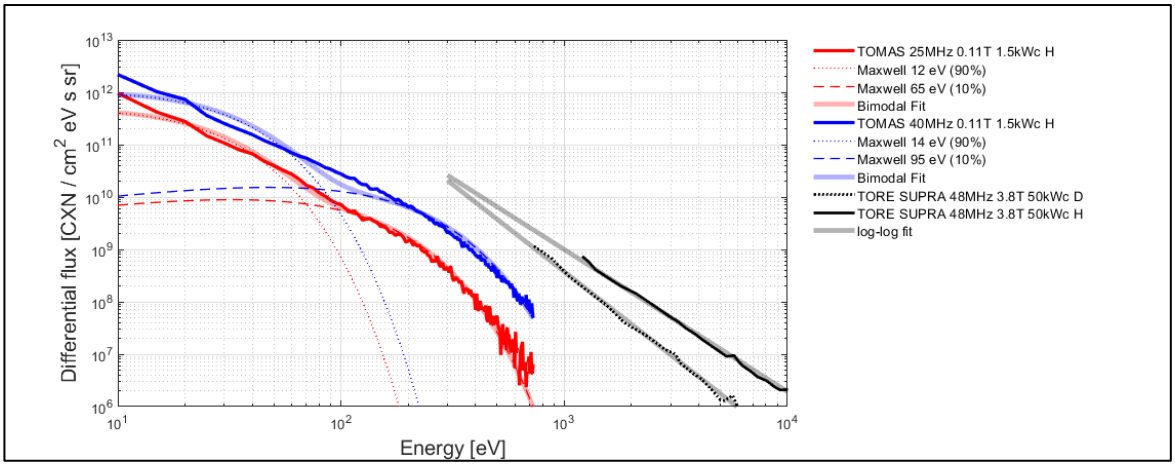

Figure 3.2-2. Differential CXN flux spectra of ICWC in TOMAS [Lopez 2023] and TORE SUPRA [de la Cal 2006].

3.3.A GDC boronization system in ITER

A modelling study has been conducted to provide physics guidelines for a boronization system design which would lead to a reasonably uniform B coating of the main chamber plasma-facing surfaces [96SPT4]. The assessment is based on Monte Carlo tracing of diborane molecules in the ITER GDC plasma, from the injection point, taking into account elastic collisions with neutrals, to the point of ionization or dissociation. The reaction products, B-carrying radicals and ions, will subsequently coat the plasma-facing surfaces. The spatial distribution of diborane reactions in the plasma is studied by varying anode and gas injection configurations, as well as the carrier gas, in order to assess their impact on the achievement of uniform surface coatings. Two-dimensional density and temperature maps of the background H_2 and He GDC plasma parameters are obtained from plasma fluid simulations of the ITER glow plasma [Hagelaar 2014, Kogut 2014]. With 7 anodes powered simultaneously at 30A (the 2016 baseline ITER GDC design) these backgrounds predict a uniform wall ion current density of 0.21 A/m^2.

The GDC boronization process on present devices is in the vast majority of cases performed by fuelling a glow discharge with a mix of diborane gas (usually deuterated diborane, B_2D_6) in He. Hydrogen has been proposed as a carrier gas to reduce sputtering of (stainless steel) surfaces which occurs at a much higher rate with energetic He ions. The carrier gas determines the plasma parameters in the plasma volume. The low electron temperature (< 1 eV) away from the anodes in case of a H glow compared to that of the He glow (> 1 eV), makes diborane ionize and dissociate mostly in the vicinity of the anode glow, resulting in thicker layers around the anodes. For He, the diborane reaction Monte Carlo counts decay from the injection points into the volume with a scale length of 1-2 m, which is shorter than the mean-free-path for diborane ionization and dissociation (3-4 m) due to collisions with background neutrals.

Besides improved system reliability, increasing the number of GDC anodes enhances the uniformity of the boronization layer since the 6 H atoms per diborane molecule affect the GDC parameters compared to a pure H_2 glow. A uniform distribution of gas injection points, 4-6 m apart, provides uniform B coatings in the case of the higher temperatures of the He glow in ITER. Gas injection points at the HFS are recommended for coating the inboard plasma-facing

surfaces. Separating anodes and gas injection points by several meters is also clearly suggested by the modelling.

Figure 3.3-1 shows the normalized distribution of diborane reaction counts for an anode and gas injection point configuration in the ITER mid-plane for a He GDC plasma background at 0.3 Pa. The configuration shows 6 LFS anodes (green squares) spaced pi/4 apart, leaving a gap north and south. The B is injected via 6 LFS points (red diamonds), also spaced pi/4 apart, leaving one larger gap north, and 5 HFS points spaced pi/3 apart leaving a gap east. This example mirrors the kind of distribution of equatorial LFS anodes (placed in the port plugs) which might be the reality on ITER (e.g. no anodes possible in the NBI sectors). As can be seen, leaving substantial toroidal gaps in anode distribution or gas feed points causes large asymmetries on boron deposition. An additional number of anodes in the upper ports, as well as vertically distributed gas feed points, seem mandatory for ITER to achieve a uniform boronization on the basis of this analysis. Thus, the proposed 3D configuration in ITER needs to consider an additional 6 anodes in the upper ports as well as diborane gas feed points at the level of the upper ports.

The risk has been raised that diborane may affect the performance of the active charcoal surfaces in the torus cryopump, essential to pumping of He and hydrogenic fuels during ITER operations. The proposed mitigation strategies require input regarding the minimum pumping efficiency needed for GDC boronization. To guarantee stable glow discharges with diborane in ITER, in the absence of dedicated tests at present, it is proposed to maintain a glow discharge content that closely matches that of current devices. This can be achieved by matching their fuelling and pumping conditions. Table 3.3-1 provides a summary of essential parameters to compare the pumping conditions of GDC boronization in current devices. The total flow rate, operational pressure, and vessel volume determine the residence time of the carrier gas within the vacuum vessel. Being determined by vacuum conductance through pumping ducts, the residence time scales to other products of the boronization glow, such as hydrogen molecules. Note that GDC boronization shows typically a nearly perfect diborane decomposition efficiency [Dibon 2021]. The high process efficiency is understood as a result of the short mean-free-path of diborane in the He glow, as illustrated in Figure 3.3-1. To ensure a glow discharge content which closely matches that of current devices, the gas residence time in ITER needs to be similar to that found in these devices. If pumping conditions are constrained, a higher residence time may be compensated by reducing the diborane content in the fuelling mix. Taking ASDEX Upgrade as an example, doubling the residence time to 100 s in ITER may require halving the diborane flow to 5% in He (example 2 in Table 3.3-1). The duration needed to deposit a 50 nm layer (2.3 g/cm^3) on the PFCs (750 m^2) depends on the diborane flow rate. At 5% diborane in He, a boronization procedure can be completed within 16 hours in ITER.

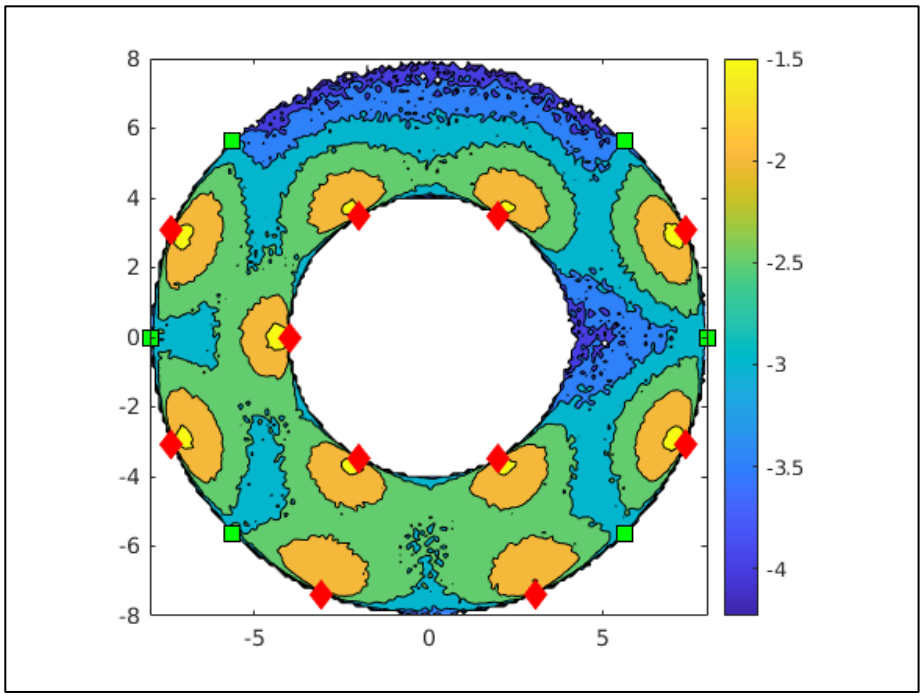

Figure 3.3-1. Normalized reaction counts (log scale) of diborane molecules injected from the locations of the red diamonds in a He glow at 0.3 Pa with 6 anodes (30 A each), with locations indicated by green squares. The 2D simulation is representative of a possible configuration in the equatorial plane in ITER [96SPT4].

	Flow rate (Pa.m^3/s)	**% B_2H_6 in He**	**Pressure (Pa)**	**Volume m^3**	**Residence time (s)**	**Ref**
ASDEX Upgrade	0.38	10	0.5	40	52.6	[Dibon 2021]
JT-60U	0.64	1.4 (decaborane)	0.2	130	40.5	[Saidoh 1993]
TEXTOR	0.169	10	0.2	17.4	20.6	[Winter 1989]
WEST	0.61	7.5	0.6	50	24.5	Priv. comm.
DIII-D	0.21-0.53	15	0.27-0.67	37	46.3	Priv. comm.
ITER example 1	8.2-19.6	10	0.3-0.7	1400	50	
ITER example 2	**4.2-9.8**	**5**	**0.3-0.7**	**1400**	**100**	

Table 3.3-1 Summary of fuelling and pumping conditions of GDC boronization in current devices, including possible operational range in ITER.

3.4.A boron solid injection system in ITER

GDC boronization in ITER aims at oxygen gettering by boron layers deposited on recessed surfaces, rather than covering plasma-exposed W surfaces (in the vicinity of the apex of First Wall Panels (FWPs)) for routine plasma operation. Boron layers in these latter areas are quickly eroded in high-Q discharges. Therefore, a successful demonstration of ITER operation with a W wall at high Q, relevant to fusion reactors, is not impaired by the use of boronization since this only remains in the long-term in recessed areas.

Given the modelled size of the W wall source in Q = 10 plasmas and its impact on plasma performance (see Sect. 5.1), the risk to Q = 10 operation of a W first wall armour is considered to be medium/low, with the risk to lower Q operation (Q = 5) being considered low. However, a significant level of uncertainty remains regarding the evaluation of the W wall source and W screening at the plasma edge, which is intrinsically associated with uncertainties on the level of anomalous transport in the far-SOL and pedestal plasmas in ITER.

Therefore, as an ultimate risk mitigation measure with particular focus on demonstrating Q = 10 in ITER, a B solid injection system is being considered. The primary objective of this system is to establish lasting low-Z wall conditions at plasma-exposed surfaces by replenishing the B coating of these areas during tokamak plasma discharges. Note that this may necessitate the use of tens of grams of B powder to maintain the B coverage for a Q = 10 ITER pulse, based on present experience [9ATR8M]. Due to the associated T retention (0.7 g of retained T per 10 g of boron injected, for 50-50 DT plasmas), this approach can only be applied in a limited number of discharges. A preliminary assessment by the ITER Organization and PPPL experts found no showstoppers to integrating a B powder dropper system in ITER and further studies will be carried out to reach a final conclusion on whether such scheme or alternative ones can be applied for this function in ITER. If successful, it is proposed to include such B solid injection system into the new baseline.

As can be gathered from the above discussions the rationale and basis for a boronization system in ITER are well developed while the optimization of its application in ITER as well for the minimization and removal of in-vessel retained T remain more uncertain. To progress in this area, dedicated experiments (supported by modelling when appropriate) are required; the highest priority topics for R&D in this area for ITER are discussed in [8YFSB3].

4. Rationale and requirements for a revised plasma heating power and mix with a W wall in the context of AFP and DT-1

To define the required heating level and mix for ITER operation with a W wall not only do the issues related to the wall material need to be considered, but also the objectives, experimental strategy and constraints of the AFP and DT-1 phases of the new baseline IRP. These are described in detail in the accompanying report [Part II: new baseline outline IRP] and are repeated below:

For AFP the key objectives are:

- To commission control and protection systems with plasma up to 15 MA/5.3 T;

- To demonstrate disruption mitigation up to up to 15 MA/5.3 T;

- To develop plasma scenarios up to 15 MA/5.3 T in L-mode;

- To develop plasma scenarios up to, at least, 5 MA/2.65 T in H-mode with deuterium (DD) plasmas.

For DT-1 the key objectives are:

- To commission control and protection systems with plasma up to Q = 10;

- To demonstrate disruption mitigation up to Q = 10;

- To develop plasma scenarios in DT up to 15 MA/5.3 T in H-mode with Q = 10 over 300s (or lower plasma current if Q = 10 can be demonstrated at those levels);

- To study the physics of burning plasmas and their integration with an all-W PFC configuration;

The DT-1 programme needs to be implemented within a total neutron fluence of ~ 3 10^{25} neutrons, which is 1% of the Project Specification goal. To achieve these goals within this fluence it is foreseen to interleave the development of H-mode scenarios in DD and DT plasmas as the plasma current/toroidal field levels increase towards 15 MA/5.3T [Part II: new baseline outline IRP].

The additional heating power levels required to sustain H-mode operation in ITER and to demonstrate the AFP (DD) and DT-1 goals (DD and DT) can be evaluated following the guidelines from experiments in Sect. 2. These are: a) to sustain H-mode plasmas a sufficient edge power level is required ($P_{sep} \geq 1.5\ P_{LH}$), and b) the expected level of radiated core power with a W wall will be in the range from $0.25 \leq P_{rad}^{core}/P_{heat} \leq 0.5$. The resulting operational spaces are illustrated in Fig. 4.-1 for a plasma density range that is expected to be above the minimum density for H-mode access in ITER [Loarte 2021]. We note that in the L-H transition evaluation we include the isotopic effect of T on the L-H transition. For the latter it is assumed that for 50-50 DT plasmas, $P_{LH,DT}/P_{LH,DD} = 0.8$ [Righi 1999]; an inverse scaling of the H-mode threshold from D to T has been confirmed in the recent DTE2 experiments at JET with the ILW [Solano 2023]. For plasmas with T/D = 0.1-0.3 it is assumed that $P_{LH,DT}/P_{LH,DD} = 0.9$, which is an intermediate value between that of DD and 50-50 DT plasmas. This assumption is based on the findings of mixed-species H-mode plasmas [Hillesheim 2018]. Results from JET with H-T plasmas show a decrease of the H-mode threshold from pure H plasmas to pure T plasmas as the T concentration increases [Birkenmeier 2023].

From these experimental guidelines we can conclude that to demonstrate DD H-modes at 5 MA/2.65 T in AFP, an additional heating power of at least 40 MW is required. This allows robust operation in H-mode ($P_{sep} \geq 1.5\ P_{LH}$) in these conditions at $n_e = 0.5\ n_{GW}$ and with core radiated power fractions of up to 43%. If lower radiation fractions, down to 25%, can be achieved by optimization of W wall interactions/core W concentration control, H-mode operation in DD could be expanded to 7.0-7.5 MA at this density level.

For DT-1, the limited neutron fluence calls for a substantial part of the H-mode development programme to be performed in DD plasmas to as close as possible to the corresponding DT

plasmas up to 15 MA/5.3 T, if possible [Part II: new baseline outline IRP]. To support this, an additional heating power level of 100 MW is required to ensure robust operation in H-mode ($P_{sep} \geq 1.5\ P_{LH}$) at $n_e = 0.5\ n_{GW}$ up to 10.5 → 13.5 MA depending on the radiated power level (25-50%).

An important ingredient in the above evaluations is the choice of $n_e = 0.5\ n_{GW}$ as the minimum density for sustained H-mode operation in ITER, since the required power to sustain H-mode plasmas scales as $\sim <n_e>^{0.72}$ [Martin 2008]. This choice is based on the finding that the edge ion heat flux is a key physics parameter to trigger the H-mode transition [Ryter 2013]; applied to ITER plasmas leads to $n_e = 0.5\ n_{GW}$ being an appropriate level for the lowest density to plan H-mode operation [Loarte 2021]. Since ITER plasmas are dominantly electron heated, a sufficient density is required for enough equipartition and edge ion heat flux. The criterion $n_e = 0.5\ n_{GW}$ provides the optimum compromise between sufficient edge ion heat flux and overall power level required for H-mode operation (because the required ion power increases with plasma density). The validity of such assumptions has been verified in dedicated studies on the access to H-mode in deuterium 5MA/2.65 T ECH heated plasmas modelled by ASTRA with the TGLF-SAT2 transport model and using a scaling for H-mode access based on the ion heat flux value [Schmidtmayr 2018]. This analysis shows that, in terms of the margin above the required ion heat flux for H-mode access for operation with $P_{ECH} = 40$ MW, the optimum density is $\sim 1.8 \times 10^{19}$ m^{-3} which corresponds to 45 % of n_{GW}, as shown in Fig. 4-2. At this density, the resulting edge ion heat flux exceeds by 6-8 MW that required for H-mode access.

In the context of the ITER W wall, we note that the presence of W in these plasmas even to significant concentrations ($\sim 10^{-4}$) is not detrimental for H-mode, even given the much higher atomic number and radiation efficiency of W compared with Be. This is due to the fact that, although larger W radiation reduces the total edge heat flux, the resulting lower electron temperature leads to a higher equipartition and increased ion heat flux which compensates the lower total power heating the plasma. In addition, the lower impunity content with W compared to Be leads to a smaller effect of impurity dilution on turbulence in the SAT2 model, which increases ion conductivity and, thus, edge ion heat flux.

We note that because of the need for high levels of additional heating in DD H-mode plasmas at high currents, the H-mode development programme in the 2016 IRP switched to DT already at 7.5 MA/2.65 T. This strategy was conceived to take advantage both of the lower power requirements for H-mode operation in DT plasmas due to the lower H-mode threshold and the contribution of the alpha heating to sustain the H-mode scenario with increasing I_p. In the context of DT-1 in the new baseline, such a strategy has two major disadvantages:

- Maximizes the neutron fluence since increasing levels of alpha heating (and thus neutron production) are intrinsically required for the expansion of the H-mode operational space;
- Optimization of alpha heating becomes an important aspect of scenario development, beyond a topic of research, towards high I_p even at moderate Q. This is because alpha heating becomes a sizeable (even if not dominant) contributor to the total heating required to maintain the plasma in H-mode (e.g. $P_\alpha/P_{add} = 0.4$ for $Q = 2$). The need for sufficient alpha heating to sustain H-mode scenarios in DT, even at moderate Q,

restricts the range of D/T concentrations that can be explored at a given current level and has the potential to slow down the development to Q = 10 (resulting in increased neutron fluence).

In this context, the availability of additional heating power of ~ 100 MW opens the operational space for H-modes containing T (> 10 %) up to very high I_p, as shown in Fig. 4-1. This allows the development towards high Q scenarios without the need to optimize alpha heating at each single step. This would be a scenario development strategy similar to that already successfully implemented in present tokamak DT experiments such as JET and TFTR. Optimization of alpha heating is, of course, always required at the largest values of I_p to enable the reduction of the additional heating power to levels closer to 50 MW in order to achieve $Q \geq 5$ in ITER for plasmas with standard H-mode confinement.

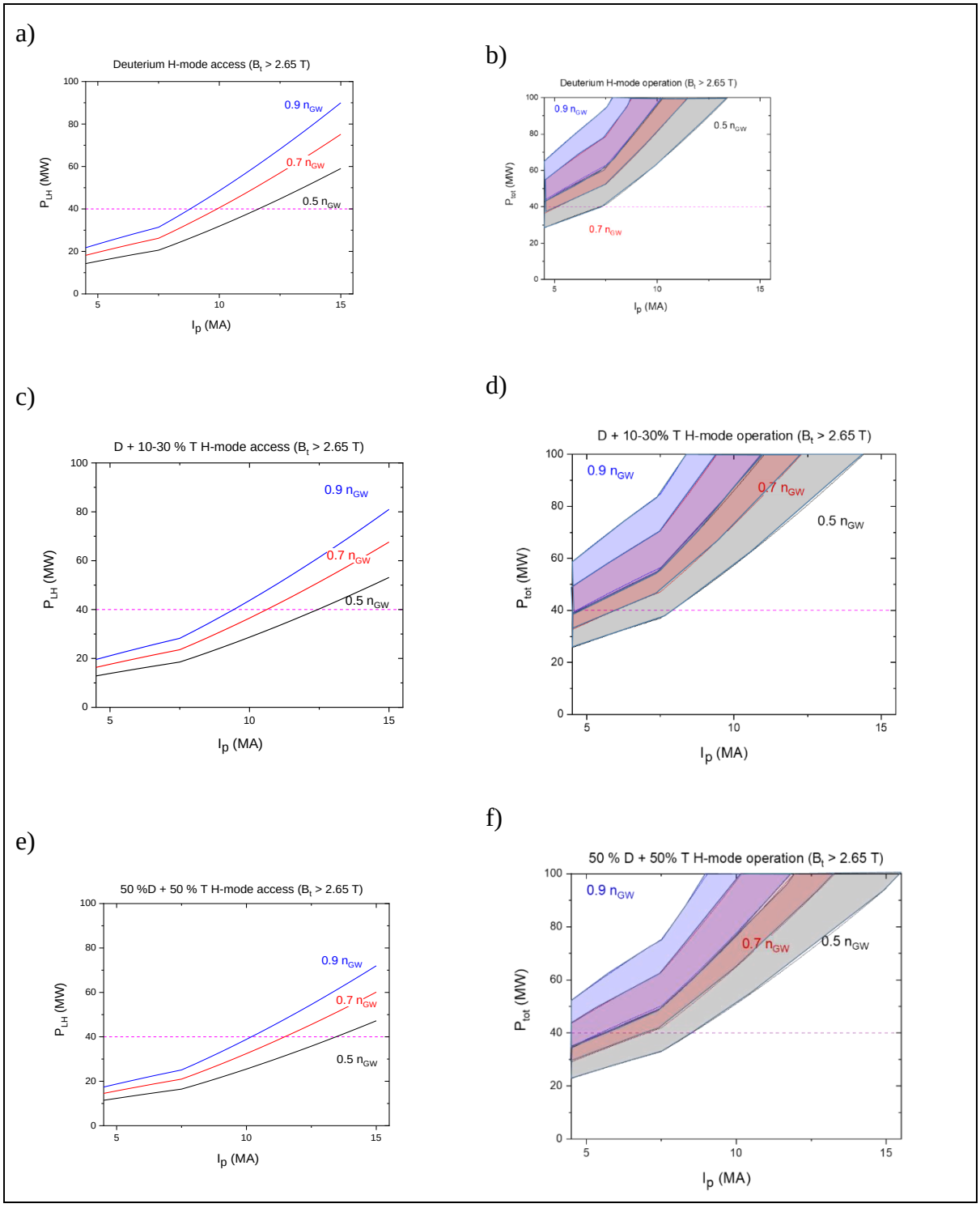

Figure 4-1. Power required to access H-mode (a, c, e) and H-mode operational range (b, d, f) for DD, D+10-30% T and 50% D – 50% T plasmas and a range of operational densities. Note that for plasmas with D and T, P_{tot} includes not only the additional heating power but also the alpha heating.

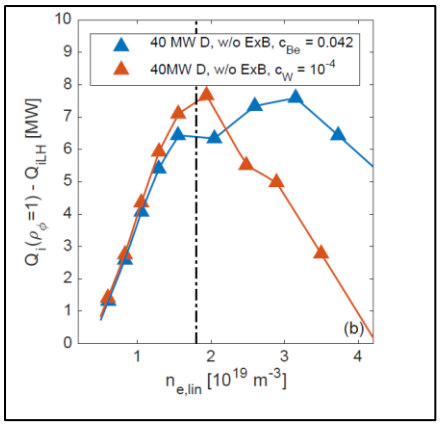

Figure 4-2. Ion heat fluxes in MW at ρ = 1.0 minus the L–H transition ion heat flux scaling [Schmidtmayr 2018] for simulations with $n_{ne,sep} \simeq n_{e,lin}/2.5$ and $T_{i,sep} = T_{e,sep} = 120$ eV, without the inclusion of the impact of the E×B shearing rate in TGLF–SAT2, for different impurity species, with Be concentration of 0.042 and with W in concentration of 10^{-4}. The vertical dash–dotted line identifies the minimum density according to [Ryter 2013, Loarte 2021] [Angioni 2023].

From the arguments above, since no NBI will be available in AFP and 33 MW will be available in DT-1, the required RF power is 40 MW (AFP) and 67 MW (DT-1).

Once the rationale for the levels of additional heating power in the AFP and DT-1 phases of the new baseline is explained, we discuss the choice of the RF heating mix to implement the research in ITER, which is strongly linked to the choice of W as wall material. As discussed in Section 2, operating with a W wall increases the risk of core W contamination and the uncontrolled accumulation of W in the central part. Although there are differences in the physics driving the W accumulation processes in ITER, it cannot be ruled out that this will not happen. As an example, W accumulation has been modelled to occur in the exit phase of ITER H-modes [Loarte 2016] when heating and fuelling rates are not reduced appropriately, as shown in Fig. 4-3.

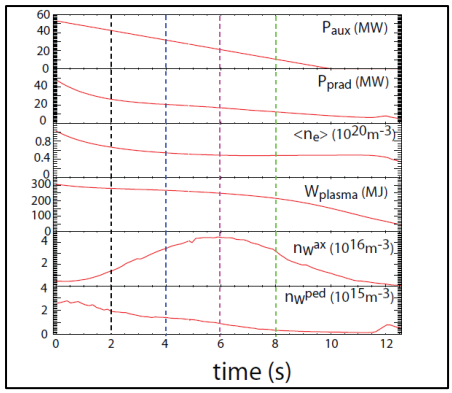

Figure 4-3. Evolution of auxiliary heating power, radiated power and plasma parameters (electron density, energy, axial and pedestal W densities) in the termination phase of ITER Q=10 plasmas for a 10 s ramp of the auxiliary heating power with immediate pellet fuelling switch-off modelled with JINTRAC. The W axial density increases along the power ramp while the pedestal W density decreases, leading to a strong central peaking of the W density profile without increasing the edge W source [Loarte 2016].

These considerations and the experimental evidence in Section 2 calls for efficient central electron heating to be available in ITER and this can be provided by RF heating. As also discussed in Section 2 and in [Helou 2023], ICH modelling for ITER, following the guidelines from experiments in ASDEX-Upgrade, shows that it can be optimized to provide up to 20 MW per antenna for W control with a small impact on the global W wall influx into the plasma. We note that these modelling results as well as those regarding the W wall influx in Section 5.1 are subject to uncertainties associated with assumptions on plasma transport in the far SOL and, thus, experimental confirmation in AFP is foreseen in the new baseline IRP [Part II: new baseline outline IRP], especially for H-mode scenarios. ECH can provide 20 MW for central heating per equatorial launcher (plus 27 MW from the Upper launchers for off-axis heating) without any direct effect on the W wall source since its absorption in the plasma is de-correlated from edge effects.

As risk mitigation strategy to minimize W wall influxes for the achievement of the AFP and DT-1 goals it is therefore proposed to modify the 2016 baseline ECH system to provide 40 MW of ECH in AFP and 67 MW for DT-1. In addition, 10 MW ICH will be installed in AFP in one antenna to be upgraded to 20 MW for exploitation in DT-1 following confirmation in AFP that the antenna can couple the required power with low impact on the W wall source. This will be the subject of dedicated experiments in AFP, for which experimental time is specifically allocated, with focus on H-mode plasma conditions with I_p = 5 – 7.5 MA.

We note that the ICH antenna in AFP will also provide the required capability for fuel removal tests and wall conditioning in AFP (and later in DT-1), as discussed in Section 3, using ICWC. Scaling from present ICWC experiments results in a coupled power to the plasma of 2 MW being required for effective ICWC application in ITER, as shown in Fig. 4-4. This implies that at least 5 MW ICWC power need to be available since the absorbed power by the plasma for ICWC is typically 40% of the injected power. For ICH tests in AFP a higher power level is beneficial and thus the choice of 10 MW for AFP is made [Helou 2023].

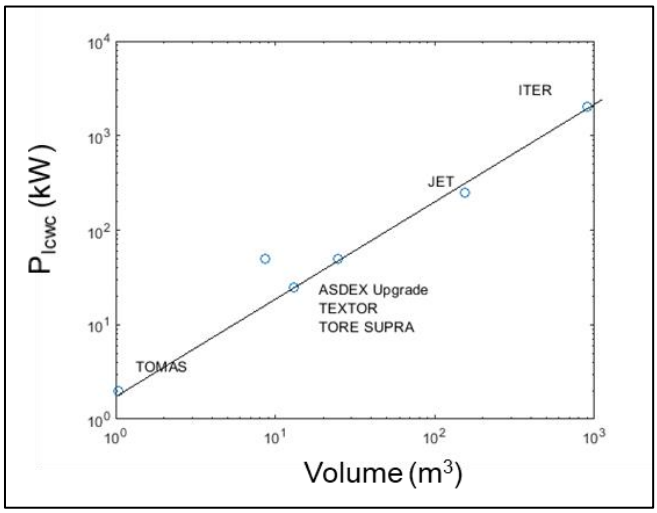

Figure 4-4. Plasma absorbed power for effective ICWC in present experiments showing its scaling with volume.

In the context of the heating mix choice for the new baseline, two specific aspects have been assessed by modelling studies for ITER. One is the impact of ECH power level on W density control and the second the impact of ion heating that can be provided by ICH (in addition to that from NBI) on the access to Q = 10 in ITER.

To assess the effect of central ECH heating, transport simulations for nominal Q = 10 plasmas with 33 MW NBI have been carried out for the main plasma with the JINTRAC code including the TGLF-SAT2 model for turbulent transport from the pedestal top up to ρ =0.05. The ECH power deposition profile is chosen so as to deposit 20-40 MW from equatorial launchers in the central part of the plasma and 10 MW off-axis for NTM control, with the upper launchers, as shown in Fig. 4-5. We note that this is an initial proof-of-principle study and more detailed analysis with accurately modelled ECH power deposition profiles will be carried out in the near future. The ECH central power level has been scanned in steps of 10 MW. Table 4-1 summarizes the heating mix for these studies.

P_{tot} (MW)	$P_{ECH}^{central}$ (MW)	$P_{ECH}^{off-axis}$ (MW)	P_{NBI} (MW)	Q
53	10	10	33	10.7
63	20	10	33	9.5
73	30	10	33	8.6
83	40	10	33	8.3

Table 4-1. Total power, central ECH power, off-axis power and resulting Q for ITER plasmas modelled with JINTRAC-TGLF-SAT2. The reference condition for 53 MW of total power has Q ~ 10.

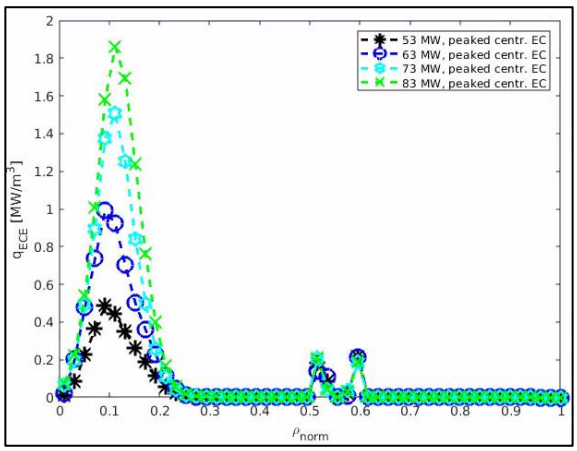

Figure 4-5. ECH power deposition profiles used for the assessment of ECH central power deposition effects on plasma transport.

The results of this study, compiled in Fig. 4-6, show that, for these plasma conditions, central ECH power at a level of 30-40 MW can have a significant impact on electron and ion transport and modify the density and temperature profiles in the central part of the plasma in a way that is favourable for W transport (weaker density gradients and stronger temperature gradients), if W transport were dominated by neoclassical effects. Both neoclassical and anomalous W transport are included in these simulations, with the result that increasing the central ECH power from 10 to 30 MW decreases the core W density. However, going beyond 30 MW leads to an increase again to levels similar to those of 10 MW. This is associated with a large change of the modelled anomalous diffusion and inwards pinch for W beyond 30 MW central ECH power.

Further studies and discussions with modelling experts are in progress to understand if this is physically meaningful or the result of numerical issues/inaccuracies of the turbulent transport model in this very central region of the plasma. Increasing the level of central ECH heating has thus been shown to decrease the W core density in these simulations but this comes at a cost in Q; in these studies the decrease in Q is in the range of 10-20%.

Further simulations to optimize the application of ECH (power level and deposition profile) in order to maximize the impact on W density with minimum impact on Q remain to be performed for ITER. This needs to be accompanied by an experimental programme on this issue together with the validation of the models applied to ITER in these experiments as discussed in [8YFSB3].

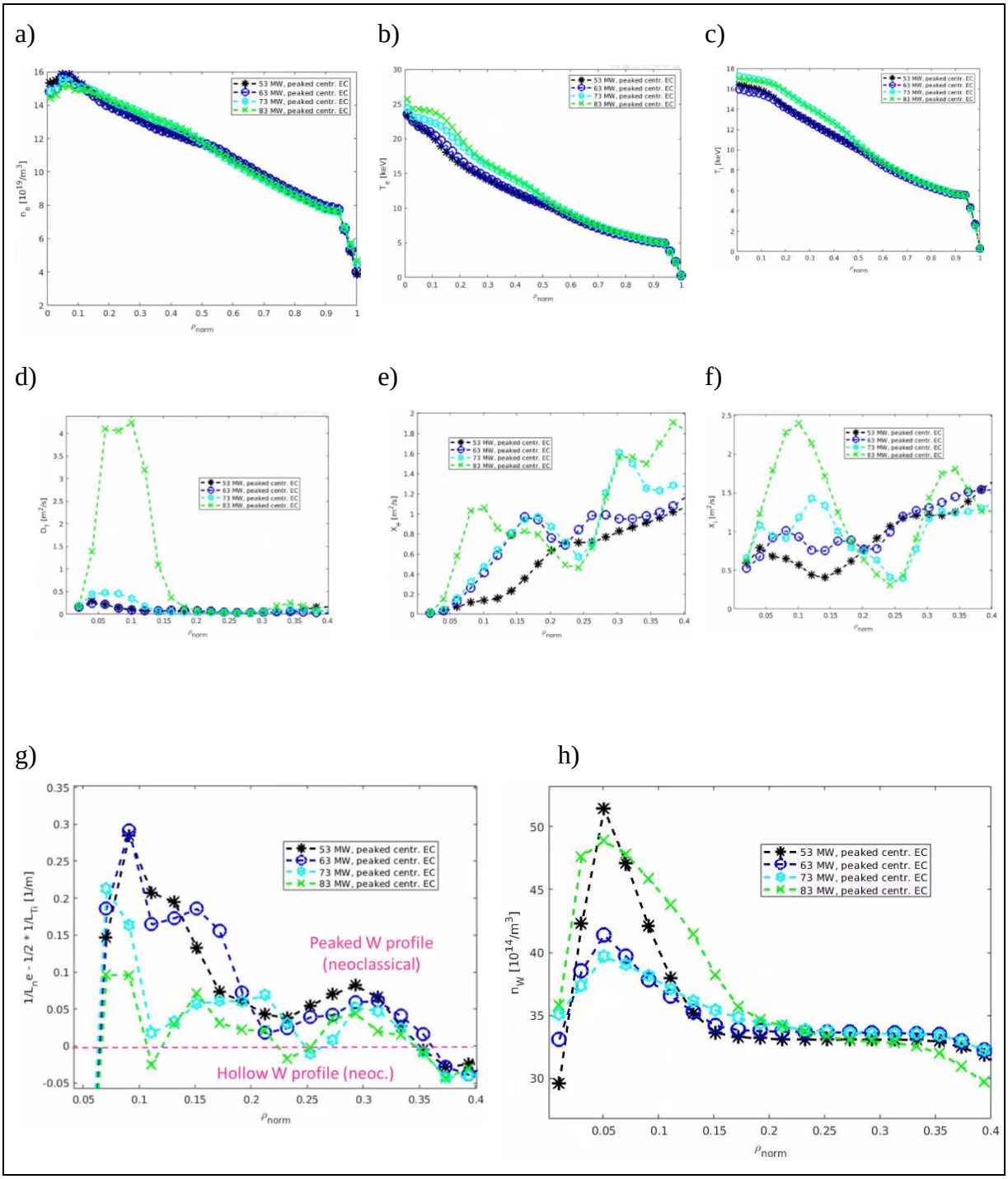

Fgure 4-6. ITER core plasma parameters from JINTRAC- including the TGLF-SAT-2 transport model for a scan of central ECH power from 10 to 40 MW, corresponding to a total injected power of 53 to 83 MW. a) Plasma density, b) Electron temperature, c) Ion temperature, d) Particle diffusion coefficient, e) Electron heat diffusion coefficient, f) Ion heat diffusion coefficient, g) Relation between density and ion temperature scale lengths determining the shape of the W density profile, if neoclassical transport is dominant, and h) Modelled W density profiles including both neoclassical and turbulent transport effects.

A study of the impact of the heating mix has been carried out for Q = 10 plasma conditions by varying the sharing of RF power between ECH and ICH for an initial 70 MW level of additional heating to access Q ~10 burning plasma conditions (including 33 MW NBI), assuming a 30% radiated power fraction. In these simulations, shown in Fig. 4-7, it is seen that access is similar for the cases explored in terms of access to the burning plasma conditions themselves. In terms of fusion power production, the case with highest ICH power produces ~10% more fusion power than that with NBI+ECH. This is consistent with previous studies [Wagner 2010] which showed an increase in Q ($\Delta Q < 1.5$) associated with the increased ion heating provided by ICH in ITER Q = 10 plasmas.

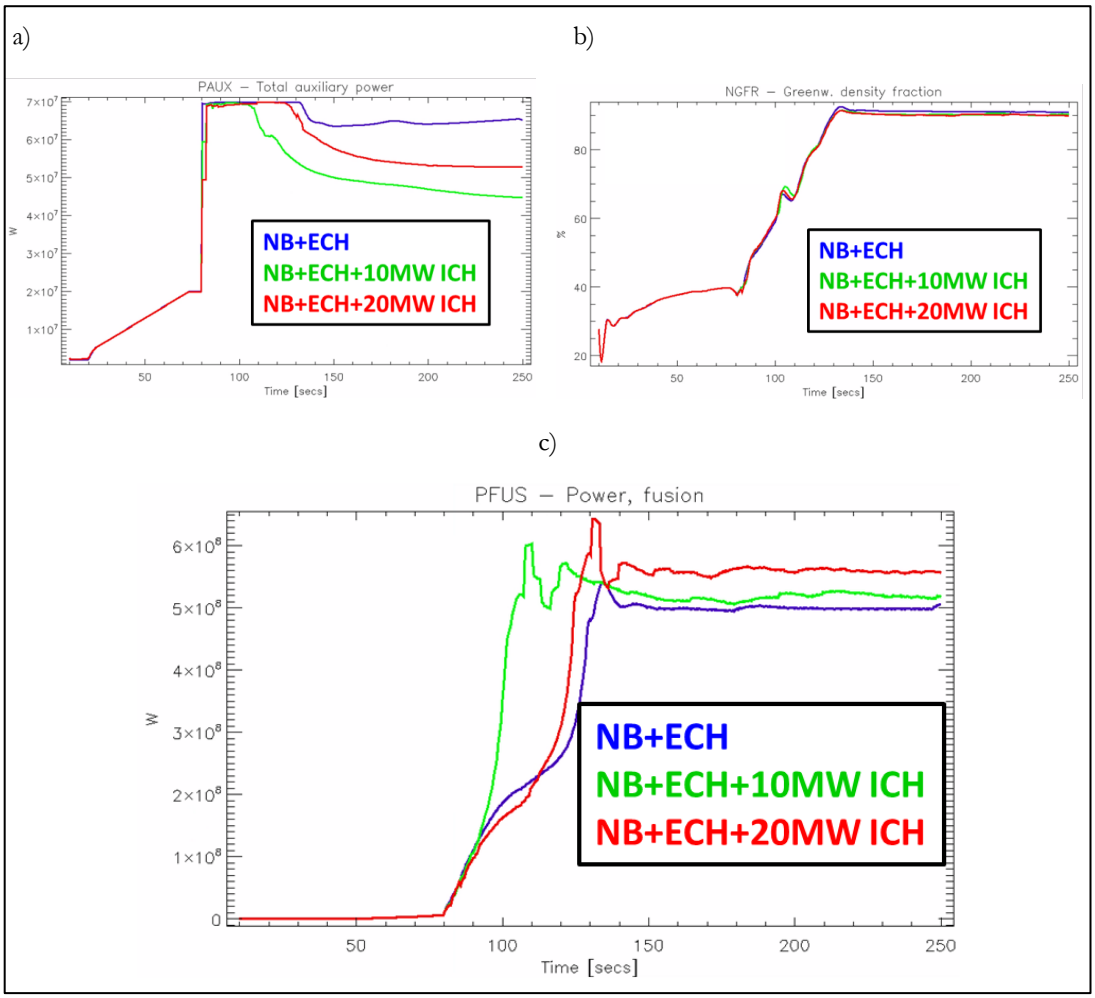

Figure 4-7. a) Additional heating power waveform to achieve Q ~ 10 in ITER 15 MA plasmas assuming that the core radiated power level is 30% of the total heating power (alpha + additional heating). b) Density waveform including the fastest rise to stationary burning conditions with robust access to Q ~ 10. c) Resulting fusion power in these simulations.

5. Evaluations of the impact of a W wall in ITER plasmas and risk mitigation measures

5.1 Impact on Q = 10 operation

The impact of the W wall source on ITER high Q operation has been quantified by JINTRAC simulations including core and SOL plasmas and plasma-wall interactions. At high Q, ELMs must be suppressed to avoid melting of the W divertor [Gunn 2017] and thus do not contribute to the W wall source. ELM suppression in JINTRAC is reproduced by means of the so-called continuous ELM model in which the pedestal transport coefficients are adjusted so as to obtain the values of pressure (density and temperature) expected from ideal MHD modelling.

Under these conditions without ELMs, the W wall source is generated by the impact of plasma ion flux (including impurities) and CXN wall fluxes. It is not technically possible to perform full integrated simulations including a proper description of the plasma-wall interactions with the main wall in JINTRAC; the edge simulation grid is restricted to the first field line that intercepts the wall, starting from the divertor area (target + baffle). Specific modelling studies of the wall source have therefore been carried out with the 2D version of the WallDYN code [Schmid 2015] for a selected set of edge plasma conditions for Q = 10 plasmas and single null magnetic configuration. The WallDYN simulations provide the W wall influx and the penetration of W up to the far-SOL region that can be modelled with JINTRAC. An effective W wall source has then been then used to reproduce the values of the W density at the edge of the modelled grid produced by WallDYN.

5.1.1 Evaluations of W wall source for Q = 10 plasmas

This source has been evaluated with WallDYN using plasma backgrounds previously utilized for Be wall erosion estimates [Khan 2019], with a neon (Ne) concentration of 1.8% at the separatrix, corresponding to a high seeding case. The total W gross erosion wall source ranges from 1.6×10^{19} to 2.6×10^{21} W atoms/s, depending on far-SOL assumptions; it is highest in the absence of SOL flows, concurrent with higher Ne fluxes to the wall. Evaluations have been previously carried out with similar plasma backgrounds and various erosion/deposition modelling assumptions [Eksaeva 2022]. Assuming no impurities to be present in the plasma, the gross erosion rate for the W wall in ITER is found to be more than 10^{-4} times lower than for Be walls i.e. in the range of 10^{19} W atoms/s (we note that Be gross erosion rates are in the range of $1.5\text{-}3.5 \times 10^{23}$ [Romanov 2022])). Including Ne impurity in the simulations increases the gross source by around an order of magnitude compared to that for pure plasmas. In this case, Ne sputtering is the main primordial source of W for single null plasmas [Eksaeva 2022].

In the present studies, WallDYN separates the W source for different processes: sputtering by Ne, by CXN and by W self-sputtering and considers a range of edge/SOL plasma parameters, with two typical examples shown in Fig. 5.1.1-1. The overall set of simulations and results is shown in Table 5.1.1-1; these include a range of assumptions regarding far-SOL profiles, SOL parallel flow and impact angles for ions impinging on the W. The expected gross wall source for Q = 10 plasma is in the range of $0.2\text{-}30 \times 10^{20}$ W atoms/s. From these overall results it can be already seen that, besides the impact angle dependence of the sputtering field, the value of

the assumed far-SOL temperature and flow play a major role in the resulting W source. The far-SOL flow strongly impacts the concentration of Ne in the SOL, which is found (as in Eksaeva 2022]) to be the main source for W sputtering, while the far-SOL temperature impacts the value of W sputtering by Ne and W self-sputtering.

Case/M_{SOL}	**$n_{Ne\text{-}SOL}$/ $n_{Ne\text{-}divertor}$**	**$T_{e\text{-}wall}$(eV)**	**Impact angle vs horiz. (°)**	$W_{source}(10^{20}s^{-1})$
00d:0	169	10	60	16.1
00d:0	169	10	90	4.2
01d:0.5	0.02	10	60	0.26
01d:0.5	0.02	10	90	0.16
00g:0	387	20	60	-
00g:0	387	20	90	26.3
01g:0.5	0.02	20	60	0.4
01g:0.5	0.02	20	90	0.25
00m:0	196	10	60	17.6
00m:0	196	10	90	4.38
01m:0.5	0.02	10	60	0.37
01m:0.5	0.02	10	90	0.24

Table 5.1.1-1. Summary of WallDYN calculations for the gross W source from sputtering by Ne ions, CXN and W self-sputtering for a range of ITER Q = 10 plasma backgrounds and far-SOL temperatures, ion flows and impact angles. For case 00g:0 with M_{SOL} = 0 and impact angle 60°, the simulations do not converge due to the large self-sputtering levels [Schmid 2023].

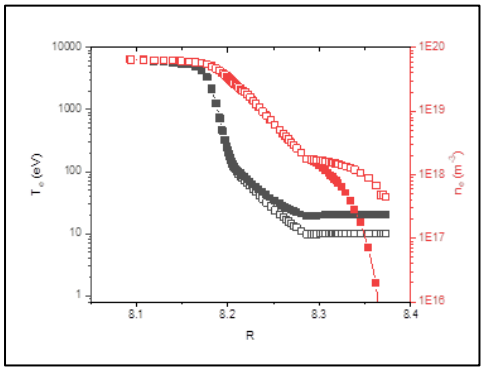

Figure 5.1.1-1. Outer midplane (OMP) n_e and T_e profiles including the far-SOL plasma extrapolations for ITER Q = 10, P_{SOL} = 100 MW, 1.8% Ne seeded plasma. Square edges: high far-SOL n_e ($v_\perp$ = 100m/s) (case 00g in Tab. 5.1.1-1) and low T_e (case 00g in Tab. 5.1.1-1). Filled squares: low far-SOL n_e ($v_\perp$= 30 m/s) and high T_e (case 00m in Tab. 5.1.1-1).

Table 5.1.1-2 provides a detailed breakdown of the WallDYN W sources for the two cases with high and low far-SOL density and low and high far SOL temperature, 00m and 00g respectively, shown in Fig. 5.1.1-1. These two cases cover a range of total wall source that spans 4.5-26.3x10^{20} W atom/s, including the largest value in Table 5.1.1-1.

Table 5.1.1-2 Summary of WallDYN calculated gross W source from sputtering by Ne ions, CXN and W self-sputtering for the ITER Q = 10 plasma backgrounds shown in Figure 5.1.1.-1. The last column combines EIRENE and DOUBLE-MC spectra to reflect the role of sputtering by neutrals in the energetic tail of the CXN distribution, as well as the energy and angular dependent W sputtering yield.

Case	**$W_{Ne}(10^{20}s^{-1})$**	**$W_{Self\text{-}sput}(10^{20}s^{-1})$**	**$W_{C\text{-}X<E>}(10^{20}s^{-1})$**	**$W_{C\text{-}X}^{max}(10^{20}s^{-1})$**
High far-SOL n_e and low T_e	3.04	1.27	0.073	0.8
Low far-SOL n_e and high T_e	6.83	19.5	0.0053	0.14

According to WallDYN, the contribution of CXN (4th column in Table 5.1.1.-2), obtained using the W sputtering yield corresponding to the average CXN energy and perpendicular impact, is negligible compared to that of Ne ions. This energy averaging scheme includes a dominant portion of neutrals below the sputtering threshold for W, which leads to an underestimated sputtering yield since the average particle energy obtained in this way is dominated by those at low energy. Therefore, the role of energetic neutrals in the tail of the CXN energy distribution has been re-assessed (Fig. 5.1.1.-2) by considering spectra from EIRENE for corresponding plasma backgrounds with the far-SOL plasmas used in these simulations [Khan 2019, Romazanov 2022], and also by using the DOUBLE-MC code [Babenko 2020].

The lower flux at higher energy in the EIRENE spectra is due to SOL screening which is absent in DOUBLE-MC code, since the latter does not include the SOL plasma in the evaluation of neutral wall fluxes. The last column of Table 5.1.1.-2, estimates the W source from the combined OMP spectra, taking the maximum CXN count at each energy bin, using the energy and angular dependent W sputtering yield, and conservatively applying it to the full main chamber wall surface area. As can be seen in Table 5.1.1.-2 the contribution from CXN to the W source increases by more than an order magnitude due to the high energy neutral tail. However, even with this increase, the dominance of the Ne-induced sputtered W source over CXN remains, with CXN contributing at most 20% of that due to Ne. Self-sputtering of W also plays a significant role, particularly when the far-SOL plasma temperature is higher.

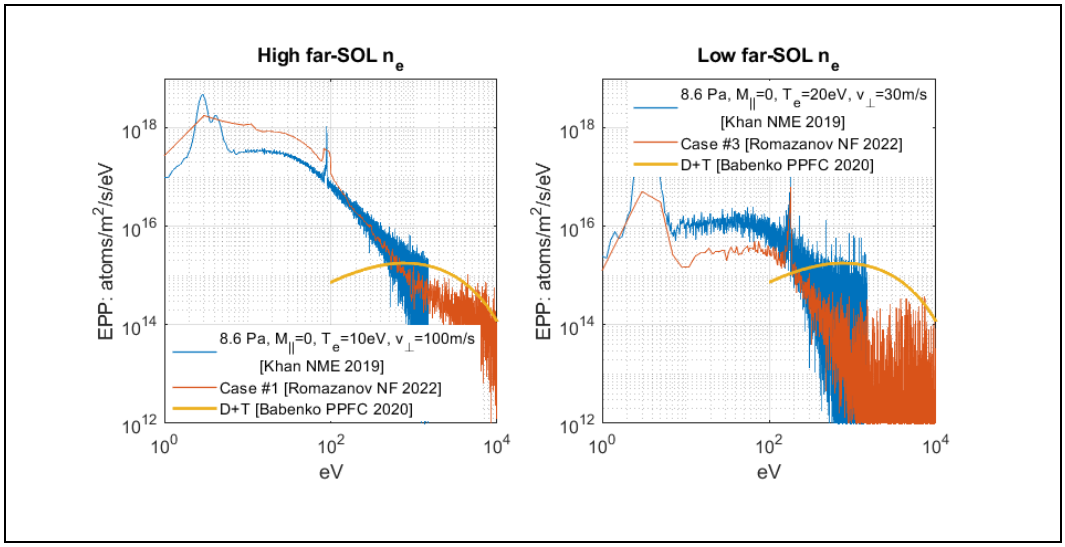

Figure 5.1.1-2. Comparison of Eirene and DOUBLE-MC CXN energy spectra for ITER Q = 10 plasma conditions.

A new set of edge plasma simulations has been started to expand these studies with higher fidelity self-consistent plasma solutions (using the SOLPS-ITER wide grid version) and a detailed and consistent description of the CXN fluxes to the wall. These need to be accompanied by dedicated experiments and model validation to ensure that the modelling of the W wall source for ITER is accurate, as described in [8YFSB3].

5.1.2 Integrated modelling of Q =10 plasmas with W divertor and wall source

To evaluate the effect of the W wall source on high Q operation, JINTRAC simulations have been carried out. As described above, JINTRAC cannot simulate the W wall source due to technical limitations of the grids used for the edge/SOL simulation module (EDGE2D-Eirene). An effective W wall source has therefore been implemented in JINTRAC which provides W atoms with typical energies of physically sputtered W at the edge of the computational grid (~9 cm from the separatrix at the OMP for the particular magnetic equilibrium used in the WallDYN calculations) within an angle of ~ +/45^o around the midplane. The magnitude of this effective source is then varied so as to obtain the values of the W density predicted by WALLDYN at the JINTRAC computational grid edge (see Fig. 5.1.2-1) and the impact of such effective source is then modelled, together with the W divertor source, in a self-consistent way.

As a conservative approach, it is assumed that there is no prompt-re-deposition either for the wall-injected W or for the W produced at the divertor. A comparison of the W density profiles obtained with WallDYN for a range of W source intensities and those from JINTRAC with the effective wall source is shown in Fig. 5.1.2-2. For JINTRAC a much smaller W wall source than for WallDYN needs to be used to obtain the same far SOL W density. This is because a significant fraction of the W produced at the wall (modelled by WallDYN) is ionized close to the wall and deposits locally before it can reach the ΔR_{sep} = 9 cm line. Thus, only a small part of the W wall flux (modelled by WallDYN) actually reaches the plasma region modelled by JINTRAC, which is consistent with previous modelling studies [Eksaeva 2022]. Note that while the maximum values of the far-SOL W density in JINTRAC and WallDYN are similar and have highest values at the LFS (R ≥ 6 m), the detailed shape of the profiles is different;

WALLDYN profiles have a significant up/down asymmetry at the LFS (see Fig. 5.1.2-1); this LHS/HFS asymmetry also exists, but is much smaller, in JINTRAC.

Increasing the effective W influx in JINTRAC beyond that corresponding to the maximum WallDYN influx increases further the far-SOL W density. For effective wall fluxes of ~10^{21} W atoms/s in JINTRAC, this eventually leads to a large W production from the divertor caused by self-sputtering and a large increase in the edge W density in the area near the outer divertor baffle, as shown in Fig. 5.1.2-3. This large W divertor production leads to an increased core radiation and a reduction of Q (see below). We note again that all our simulations are performed with zero W prompt re-deposition, which is extremely conservative for the conditions at the ITER divertor for Q = 10. Including prompt re-deposition under these conditions (probably >95% for the divertor) would significantly reduce the resulting W source into the ITER plasma.

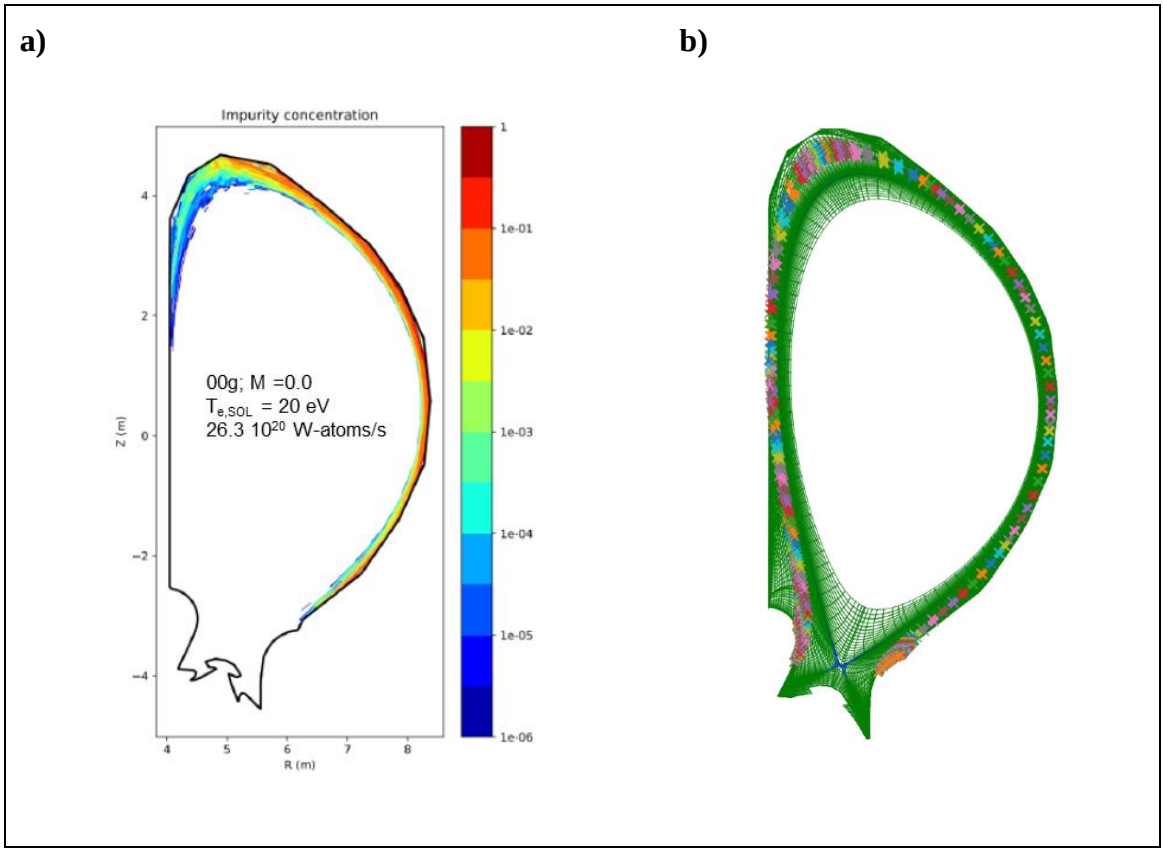

Figure 5.1.2-1. a) Edge W density from WALLDYN for the case in Table 5.1.1-1 with highest wall source and b) WALLDYN simulation grid.

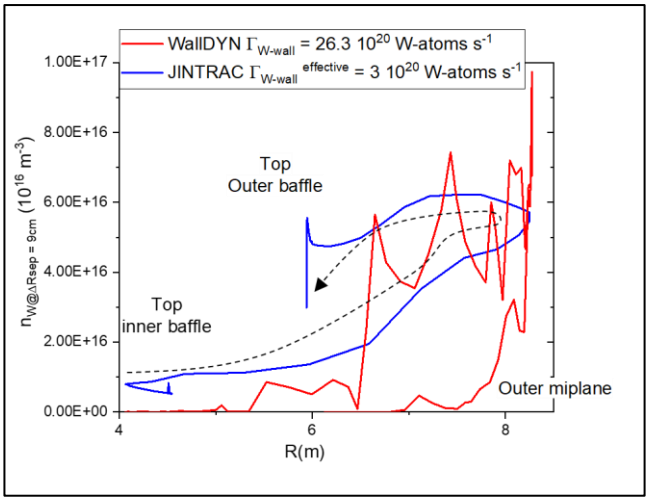

Figure 5.1.2-2. Far SOL (9 cm from the separatrix at the OMP field line) W density versus major radius for the WallDYN case with the highest wall flux in Tab. 5.1.1.-1 and for JINTRAC with an effective source roughly an order of magnitude lower. The dashed line shows the direction in which the major radius changes as the field line 9 cm from the separatrix travels from the inner to the outer divertor baffle.

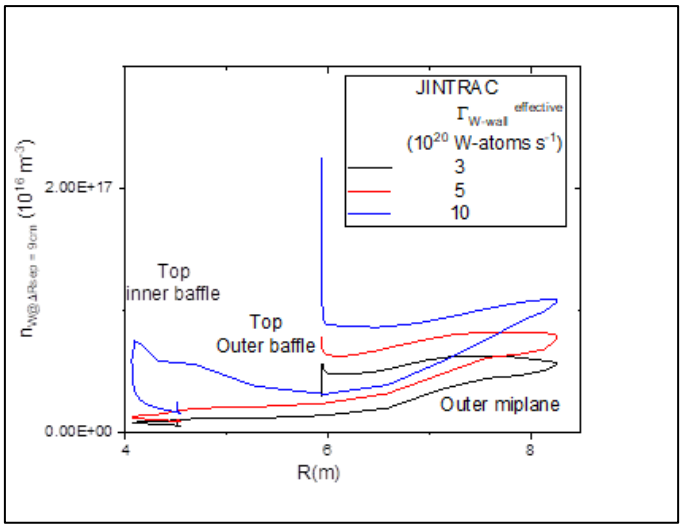

Figure 5.1.2-3. Far SOL (9 cm from the separatrix at the OMP field line) W density versus major radius from JINTRAC modelling with an effective source equal to that required to match the highest WallDYN W wall source ($26.3x10^{20}$ W-atoms/s in WallDYN is matched with $3x10^{20}s^{-1}$ W-atoms/s in JINTRAC), and for higher effective wall source values. Note the large increase of the edge SOL W density near the outer divertor caused by self-sputtering at highest value of the effective source.

The resulting consequences for high Q plasma operation in ITER modelled with JINTRAC are summarized in Fig. 5.1.2-4 showing that Q = 10 operation can be maintained up to the largest fluxes calculated by WallDYN of ~ $26x10^{20}$ W atoms/s (case 00g:0 in Table 5.1.1.-1). For higher effective JINTRAC W wall influxes (corresponding to real W wall influxes beyond those of WallDYN), a higher level of additional heating is required since core radiation increases to ~ 72 MW (51 MW from W) and the core W concentration reaches $5x10^{-5}$. The

JINTRAC effective source must be more than an order of magnitude smaller than that of WallDYN to match the average far-SOL W density, as shown in Fig. 5.1.2-5.

Given that Q =10 operation is compatible with effective JINTRAC wall sources up to ~ $5x10^{20}$ W-atoms/s, which correspond to WallDYN wall sources of $50x10^{20}$ W-atoms/s from the arguments above, and that the modelled values of the W wall source with WallDYN are $26x10^{20}$ W-atoms/s or lower, the risk to Q = 10 operation of W first wall armour on ITER is therefore considered to be medium/low, particularly also given that prompt re-deposition is neglected.

In these Q = 10 plasmas moderate W screening is found in the pedestal with the continuous ELM model (a factor ~ 3), which is most likely conservative and much smaller than that expected if neoclassical transport dominates W transport at the pedestal in ITER (a factor of larger than ~ 100), as shown in Fig. 5.1.2-6. This is a result of the assumptions of the continuous ELM model, in which the value of the anomalous diffusion coefficient is increased to achieve stationary plasma conditions; this value is applied to all plasma species, while the neoclassical pinch velocity for W is used for pedestal transport, which is conservative. We note that modelling of ITER edge plasmas with the SOLPS-ITER code for Q = 10 plasmas also shows a decrease of the Ne impurity concentration (from the separatrix to the pedestal top), confirming that ITER neoclassical impurity screening predictions are robust [Kaveeva 2020]. Again, here specific experiments on edge W transport in regimes with small/suppressed ELMs and validation of the models used for ITER are required to ensure that the modelling of the W edge transport in ITER is accurate, as described in [8YFSB3].

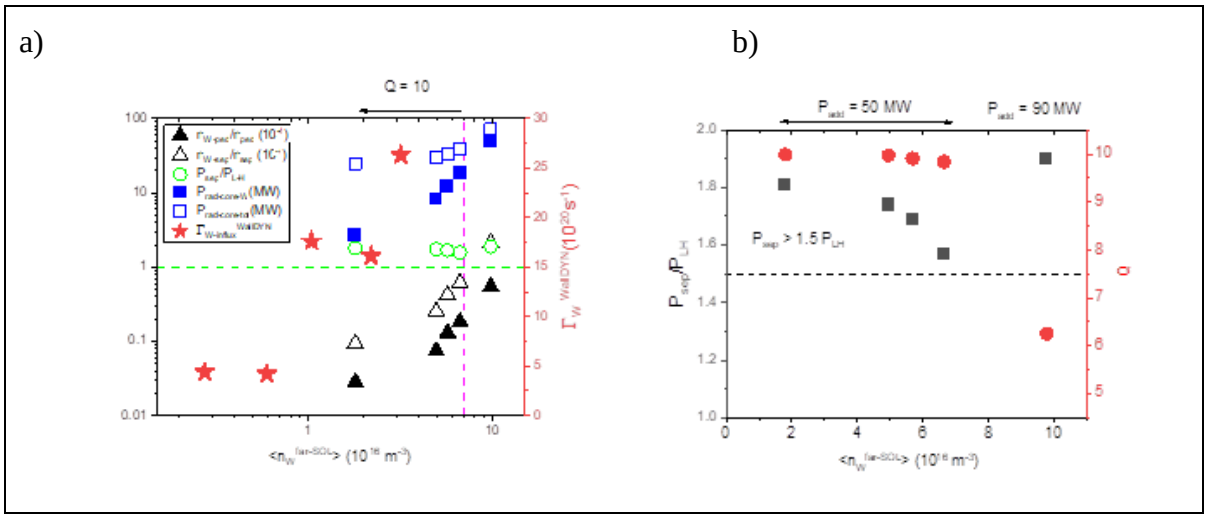

Figure 5.1.2-4. a) JINTRAC modelled W concentrations at the separatrix and pedestal top, core W and total radiation, margin of edge power flow above the L-H transition and WallDYN modelled fluxes versus average W density in the far-SOL for 15 MA/5.3 T DT plasmas with additional power heating levels of 50 MW (Q =10) and 90 MW for the highest W density value. b) Corresponding Q and margin of edge power flow above the L-H transition versus average W density in the far-SOL for the simulations in a).

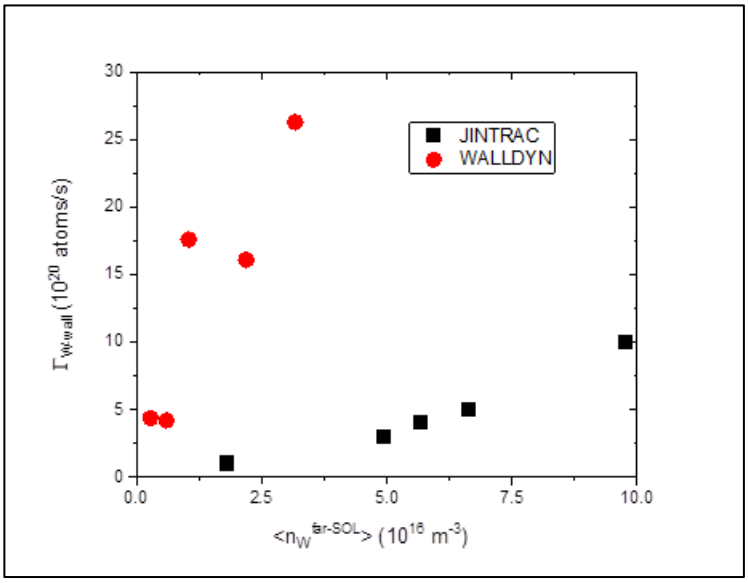

Figure 5.1.2-5. Modelled average W densities in the far-SOL versus effective W source (JINTRAC) and self-consistently modelled W source (WallDYN).

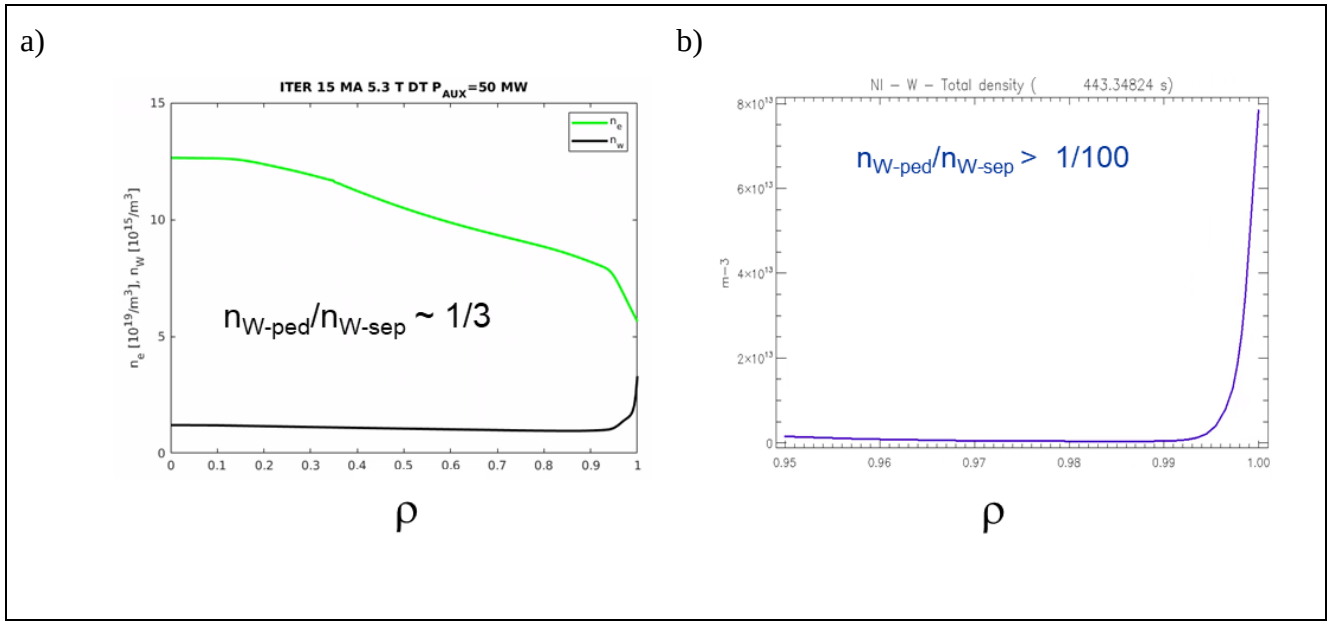

Figure 5.1.2-6. a) Electron and W densities for Q = 10 plasmas modelled with JINTRAC with the continuous ELM model and b) W density profile assuming that neoclassical physics dominates W transport in the pedestal.

If high levels of core W radiation were to materialize in ITER for high Q conditions (which does not seem compatible with the modelled W wall source levels), this would impact not only the achievable Qbut also the access to high Q. In ITER Q = 10 scenarios, the alpha heating needs to be built up in the initial H-mode access phase at low density so that it can sustain later the burning plasma in H-mode with Q = 10. A higher level of additional heating is, therefore, used in this access phase and is later reduced in the burning phase to maximize Q. To quantify the impact of the increased core radiation due to W on high Q access, a series of JINTRAC simulations have been performed with varying core radiation levels, as shown in Fig. 5.1.2-7.

For a radiative power level of 30% (the standard assumption for ITER Q = 10 plasmas), an auxiliary power level of 70 MW provides robust access to Q = 10 operation. This level of auxiliary power is higher with increasing radiation power level and, for 45% radiative power losses, 90 MW are required; consistent with Fig. 5.1.2-4. Under such conditions, the stationary burning phase Q is found in the range 6-7.

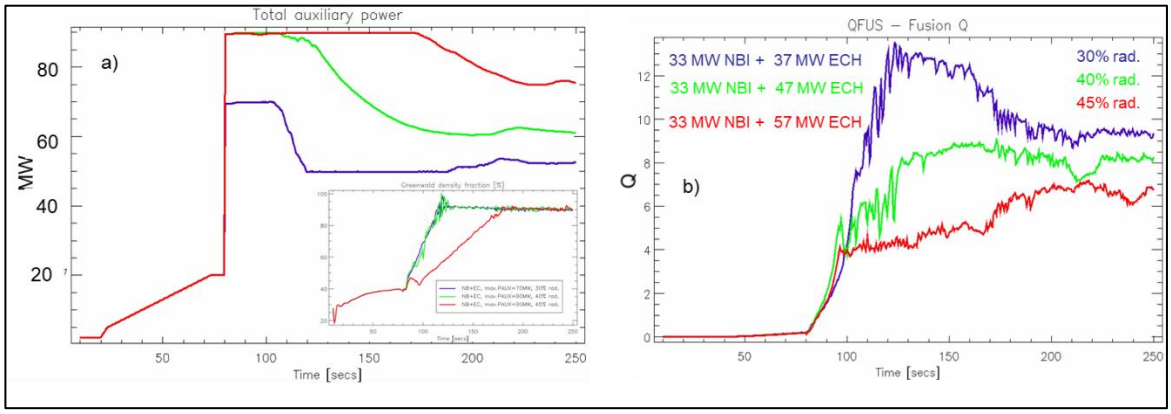

Figure 5.1.2-7. JINTRAC modelled access to high Q for 15 MA/5.3 T DT plasmas with a range of core radiative fractions: (Left) Auxiliary heating waveforms for access to high Q and plasma density evolution (in the insert); note that faster density ramps than those modelled would prevent access to high Q for the different cases. (Right) Evolution of Q for the access phase for different radiative fractions.

5.2 Impact on the limiter phase

Plasma start-up on limiters with W PFCs poses specific issues associated with W radiation, leading to radiative collapse of the early phase plasma. In the very early phase of the start-up, temperatures at the plasma edge can be high enough for W to be released by physical sputtering due to fuel ion impact. The sputtered neutrals can reach the confined plasma much more readily than in a diverted configuration and may be ionized to high charge states. Since the W self-sputtering yields can easily exceed unity for highly charged W ions accelerated to high energy in the plasma sheath, the plasma W concentration can rise very rapidly in the initial phase of the limiter start-up once some W sputtering occurs. The situation may be worsened by the presence of light impurities (e.g. oxygen) due to their higher W sputtering yields in comparison with hydrogen isotopes. Such impurities are likely to be present at some level in the residual ITER vacuum, even after initial wall conditioning before plasmas are attempted (this is often seen on present tokamaks). As discussed below, the plasma-W system is to a large extent self-regulatory since the high initial W release leads to high radiative losses, which in turn reduces the edge temperature and hence the sputtered influx. The issue is whether or not the plasma passes through this difficult early phase.

On present all-W devices, even without the use of wall passivation techniques (such as boronization – see Section 3), limiter start-up has proven possible on pure W surfaces, albeit requiring some optimization to allow adequate burn through. On ASDEX Upgrade, careful tailoring of the density and very early EC heating is a recipe which has been used successfully to achieve plasma start-up after a vent without boronization [Neu 2009] – see Fig. 5.2-1.

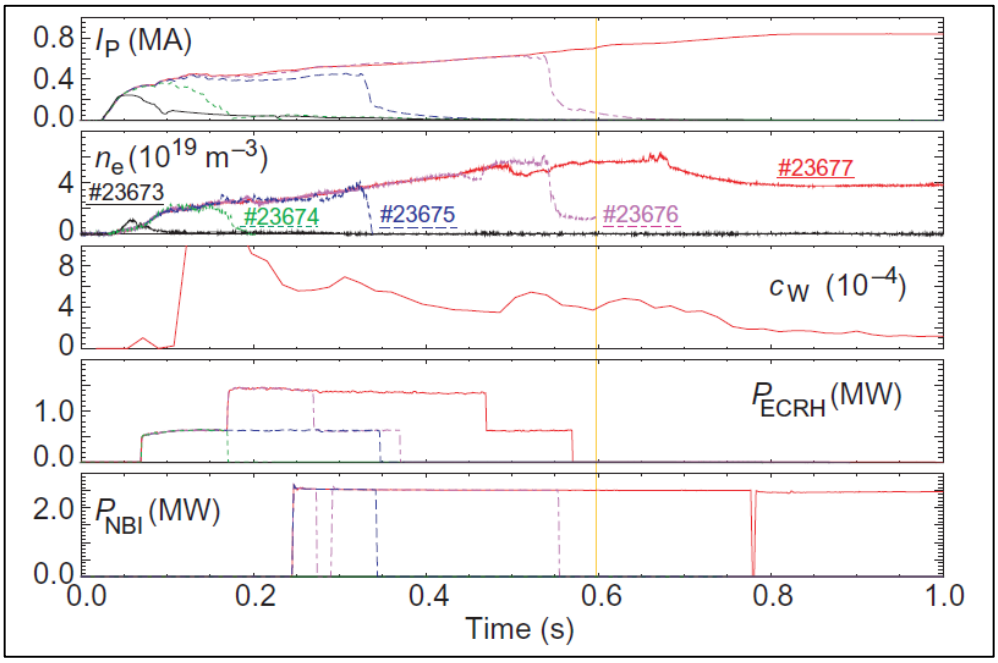

Figure 5.2-1. Time traces from restart attempts following a 2008 machine maintenance vent in the full-W ASDEX Upgrade. The deuterium plasma is ramped up on outboard W limiters, using early injection of ECH power, with NBI added from ~0.3 s. The transition to the divertor is performed as early as possible (t = 0.6 s). Five discharges were required to reach the pre-programmed I_p flattop and only 4 more to achieve the first H-mode plasmas. Note that the average W concentration (c_W) is shown only for the final discharge in the sequence [Neu 2009].

Scenario modelling for ITER has not historically closely examined the limiter start-up phase – this was not considered an issue in the case of a Be FW (as evidenced by the ease of plasma start-up in JET in the ITER-Like Wall). To study the impact of switching to W, a two-pronged modelling approach has been initiated, consisting of the usual time dependent DINA simulations, complemented by a plasma boundary simulation programme in which the SOLPS-ITER code has been applied to the limiter phase, including the sputtering and evolution of W. Such limiter simulations have not previously been attempted for ITER and, as far as is known, have never been performed with full inclusion of W sputtering for any device. Similarly, until now, DINA simulations had never previously been tried with W as the main wall material and some modifications of the code were required to include this new capability.

The DINA code has been the main workhorse for scenario simulations on ITER and is a particularly important tool for all aspects of magnetic control. It comprises a 2D free boundary plasma equilibrium solver and 1D model describing transport of the poloidal magnetic flux and the plasma temperatures (electrons and ions). The code simulations take into account eddy currents in the vacuum vessel, models of the power supplies, engineering limits imposed on the CS and PF coils, plasma-wall gaps and divertor strike points, as well as feedback and feedforward control of plasma current, position and shape.

It also contains a simplified description of the plasma-wall interaction in the limiter phases of current ramp-up, using zero-dimensional power balance to determine heat fluxes and plasma temperatures at the last closed flux surface (LCFS) and accounting for the double exponential

SOL heat flux profile scaling expected for inner wall limiter plasmas [Kocan 2015]. A sputtering model based on standard Eckstein yields is included, with a correction of the normal incidence yields to account for surface roughness and sheath straightening of ion orbits. Fuel and impurity ion sputtering (including self-sputtering) is accounted for, with a "screening factor" applied for W ingress into the confined plasma based on the results of the 2D SOLPS-ITER modelling (see below). The densities of all impurities with given ionization state are calculated on each magnetic surface assuming coronal equilibrium. Details may be found in Appendices A and B of [9CMZSM].

Fig. 5.2-2 compiles several key plasma signals from the initial 15 s (comprising the central column limiter ramp-up phase and the transition to divertor) of a first successful attempt to design a full end-to-end hydrogen L-mode scenario to 15 MA. Such a discharge, with a sufficiently long flattop duration, is an important goal of the AFP phase. The full scenario will be presented in the following section. The simulation starts with the same initial currents in all coils as in the standard DINA 15 MA DT scenario running on a Be FW (I_{CS3U} = −36 kA, I_{CS2U} = I_{CS2L} = I_{CS1} = −40 kA, I_{CS3L} = −42kA, magnetic field on CS coils < 13 T) [3T4JWP], producing a PF system magnetic flux of Ψ_{ext} = -116.2 Wb, followed by gas breakdown at t = 1.1 s, plasma initiation and I_p ramp-up.

The target density for the main limiter phase is $\langle n_e \rangle / n_{GW} \sim 0.5$, as a compromise between keeping boundary plasma temperatures low whilst avoiding disruptions. Such normalized density values seem consistent with the high end of values used in JET start-up plasmas (on Be PFCs). At breakdown, 0.5 MW of EC power is injected, ramping linearly to 2 MW at the end of the limiter phase with an assumed parabolic deposition profile. A small quantity of oxygen (O) impurity is introduced just after breakdown ($c_O = \langle n_O \rangle / \langle n_i \rangle = 2 \times 10^{-4} = \sim 0.02\%$), increasing the W sputter release and intending to simulate in an approximate way an unboronized start-up in the presence of some residual O in the background neutral pressure.

In common with the ASDEX Upgrade start-up phase measurements in Fig. 5.2-1, c_W peaks soon after breakdown, corresponding to the first interactions with the limiter surface when W sputtering begins and self-sputtering strongly increases the W atom influx. This is also reflected in the very high values of average W charge state, Z_W impacting the wall (the incoming ion energy, which determines the sputtering yield, is approximately $E_0 = 2T_i + 3ZT_e$). Beyond this point, the W ingress is sufficient to radiate almost all of the ohmic power for most of the limiter phase, decreasing the plasma edge temperature to the point at which the W influx decreases (due to a decrease in $T_{e,LCFS}$ and a reduction in Z_W at the LCFS) by enough to avoid radiative collapse given the additional P_{ECH}. At the transition to divertor configuration (t = 11 s, I_p ~3 MA, $c_W \sim 1.2 \times 10^{-4}$), the simple 1D sputtering model used in the limiter phase no longer applies and a value for c_W is simply fixed in the simulation. This will be discussed further in Section 5.3.

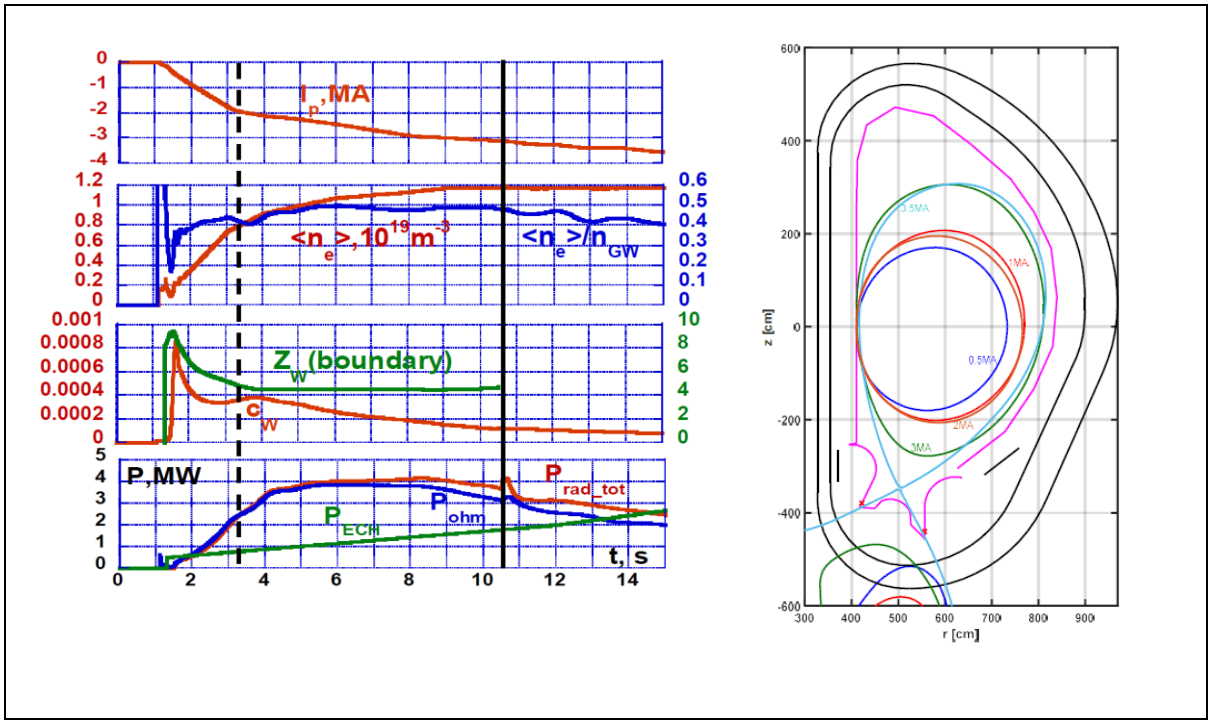

Figure 5.2-2: Left: key time traces from the first 15 s of a full DINA hydrogen 15 MA L-mode scenario. From top to bottom: I_p, volume averaged density and Greenwald fraction, averaged W concentration, $c_W = \langle n_W \rangle / \langle n_i \rangle$ and average W charge state at the LCFS, ECH, ohmic and radiated powers. Transition to divertor configuration at 11 s (marked by the vertical black full line). Time for which $I_p = 2$ MA is marked by the vertical dashed line and is the point used as reference for the SOLPS-ITER stationary limiter configuration simulations. Right: equilibrium reconstructions at various values of I_p (0.5, 1, 2, 3 and 3.5 MA)

In support of these preliminary DINA limiter phase scenarios, new attempts have been made to study W erosion and its impact on the limiter plasma using the SOLPS-ITER code package. As a starting point, the DINA magnetic equilibrium at t ~4 s (vertical dashed line in Fig. 5.2-2), corresponding to $I_p = 2$ MA and roughly 3 MW of ohmic and ECH power has been selected. Radial transport coefficients are assumed anomalous and constant throughout the core region ($D_{\perp,e,i} = 0.5$ m^{2}s^{-1} and $\chi_{\perp,e,i} = 1.25$ m^{2}s^{-1}), with radially varying coefficients in the SOL, designed to provide a double exponential parallel heat flux profile close to the scaling derived for ITER (for inner wall limiter plasmas) and on which basis the FWP toroidal shaping was chosen [Kocan 2015]. As mentioned above, the DINA boundary temperature is fixed according to the same scaling, but now in a pure 0D sense.

The SOLPS simulations account for atomic W and the first 20 ionization states (without charge bundling), the latter choice made on the basis that T_e on the innermost computational boundary is found to be several 100 eV, so that inclusion of high W charge states would not necessarily impact much the outcome. They would, however, significantly increase convergence times on what is already a roughly 5-6 week turnaround for a single case, even for these comparatively simple limiter plasmas.

A key difference between these DINA and SOLPS-ITER approaches is the absence of time dependence in the SOLPS runs, so that the solution converges to a stationary state appropriate

to only a single instant in the dynamic DINA simulations, but with the added benefit of a higher fidelity treatment of W radiation and plasma-surface interaction. In addition, by virtue of the 2D nature of the code, an estimate of the SOL screening factor for W atom penetration to the core is obtained, which can then be applied in the DINA simulation. At this preliminary stage, prompt re-deposition of W is not included – simple estimates show that it can be expected to be low for the SOL plasma conditions found in the simulations – but it is planned to include it in future code runs. Similarly, DINA simulations in which the plasma current is ramped in the limiter phase to a fixed value and then held constant over many particle confinement times will be performed to provide a more direct benchmark with SOLPS-ITER.

The first SOLPS runs attempted used a computational grid capturing only a small fraction of the core plasma (up to 12 cm inside the LCFS). A value of P_{SOL} = 2 MW, injected uniformly across the inner core boundary, is fixed in the code runs, ~30% lower than in the DINA example scenario of Fig. 5.5-2. These "narrow grid" simulations found very high W content (c_W ~10^{-3}), radiating ~75% of P_{SOL} in just the small core region covered by the original numerical grid. Moreover, the plasma density in these solutions is peaked close to the LCFS in the highly radiating region, decreasing towards the core, raising the question of whether or not the solution is artificially stabilized by the core boundary condition and would collapse if the density at the core interface were not fixed. To address this issue, a second round of simulations are being performed with the computational grid extended much further into the core. In addition, the H content is controlled in the new runs by puffing from the top of the machine and pumping in the divertor region, providing a self-consistent density evolution at the core boundary of the simulation domain.

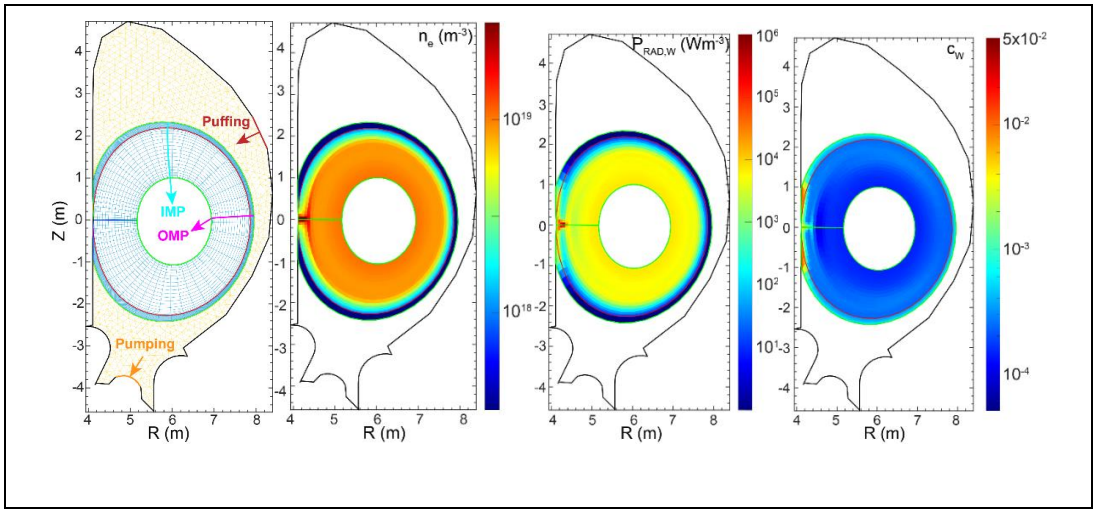

Figure 5.2-3: Selected output from one of the first converged SOLPS-ITER W inner wall limiter plasma simulations with numerical grid extending further into the core region. From left to right: simulation grid, based on magnetic equilibrium of the DINA scenario (Fig. 5.2.-2) at I_p = 2 MA, 2D distributions of n_e, total radiation from W and W concentration.

Several cases are running at the time of writing, covering different transport coefficient assumptions and values of P_{SOL}. Figure 5.2-3 compiles some key results from the simulation at P_{SOL} = 2 MW, for which the power balance is satisfied enough to be considered sufficiently

converged. The wider grid simulations confirm those of the early runs in finding that these stationary solutions are marginally stable from the power balance point of view with $P_{rad,W}$ ~1.7 MW out of the 2 MW injected (note that the W is by far the dominant radiator – hydrogenic emission accounts for only ~3% of $P_{rad,tot}$).

What is clear from the simulations is that the very strong dependence of the W self-sputtering yield on the edge plasma temperature results in a highly self-regulating plasma-limiter system. In steady state, it is ultimately drawn to an equilibrium in which, on average, the W sputtering yield corrected by the neutral assimilation reaches unity. Regarding the latter, the SOLPS simulations find assimilation factors (due to the geometry of the configuration) in the range 0.3 – 0.5. This provided guidance for the factor 0.5 used in the DINA limiter phase simulation described above. Since the effectiveness of W self-sputtering reduces rapidly below T_e ~ 10 eV, almost all of the input power must be radiated inside the LCFS by the W impurity to provide for such a temperature decrease.

As shown in Fig. 5.2-3, the W concentration profile is strongly peaked at the LCFS, flattening out in the core to c_W ~2 x 10^{-4}, which compares favourably with the DINA value of ~3.8 x 10^{-4} at 2 MA (Fig. 5.2-2), taking into account that this particular SOLPS run does not match the DINA P_{SOL}. At the innermost boundary of the SOLPS grid, the converged run finds T_e ~700 eV (not shown in Fig. 5.2-3), somewhat lower than DINA, but here the comparison is less meaningful given the different assumptions on how the power is deposited and the lower P_{SOL}. In contrast, SOLPS finds $n_{e,LFCS}$ ~ 2 x 10^{18} m^{-3} at the OMP LCFS, only ~25% lower than the DINA value at 2 MA. Across the core region of the simulation domain, n_e ~ 1 x 10^{19} m^{-3} in SOLPS, which again compares very favourably with the DINA volume averaged core density: $\langle n_e \rangle$ = 0.9 x 10^{19} m^{-3} at 2 MA. Similarly, the average core radiated power in DINA at this current (6.6 x 10^3 Wm^{-3}) is in very good agreement with the equivalent SOLPS value.

Overall, despite the very different simulation tools, the relatively good match between the two codes, at least at a single operating point, must be considered encouraging. The similarities between the much longer duration DINA simulated limiter phase for ITER and the behaviour seen on ASDEX Upgrade with W walls (duration of limiter ramp-up only ~0.5 s), provides some confidence that a window for high field side limiter ramp-up on W in ITER is possible. What is clear, however, from the narrow margins in power balance found in both SOLPS and DINA, is that this window may not be very large. Development of this first W limiter DINA scenario was significantly more challenging than for Be limiters and is very sensitive, for example, to temporal and spatial waveforms of the ECH power, the amount of initial light impurity and the plasma density evolution (gas puffing waveform). In this respect, it is similar to the experience of start-up on current full W devices without prior boronization.

Even if sustained ramp-up does turn out to be challenging, various mitigation routes have been proven useful on present experiments. For example, on WEST, reliable early current ramp-up (but beyond the limiter phase) is often associated with high levels of central plasma radiation (due to W), cooling the core region (resulting in hollow T_e profiles) and triggering MHD modes [Bucalossi 2022]. One recipe to overcome this is to use nitrogen injection, which induces an increase of plasma resistivity in the edge region, driving faster current diffusion and higher central ohmic heating. Dedicated control techniques, not presently foreseen, but easily

implemented in the ITER Plasma Control System, could also be introduced, such as the feedback scheme on the central electron temperature using the ECH power as actuator employed on ASDEX Upgrade [Hobirk 2023]. Measurements of radiated power along specific bolometer channels passing close to the limiter contact area controlling the torus gas feed could also be an option.

An important next step, in addition to the planned wider pursuit of the DINA and SOLPS simulations, including expanded sensitivity studies, is to validate the models against experiments on current full W tokamaks as described in [8YFSB3]. Discussions are underway with groups on ASDEX Upgrade and WEST to perform this benchmarking, both on existing data and in dedicated new experiments which can be specifically tailored to focus on the limiter phase. On smaller machines, this is always much shorter than is possible on ITER and is often not as well diagnosed as it might be for the purposes of model validation. Although this validation is important and will be done to refine our predictions for ITER, from the outcome of the discussions with WEST and ASDEX Upgrade experts, we expect that the limiter start-up part of the ITER scenarios with a W first wall might not be as critical as originally thought.

5.3 Impact on the L-mode diverted scenarios

The previous section has focused on the initial limiter ramp-up phase of hydrogen fuelled L-modes, demonstrating that even for the relatively long durations in this configuration required on ITER to develop robust magnetic control before the divertor is formed, start-up on W surfaces can in principle be achieved, even if this may be considerably more challenging compared with Be PFCs. Once the transition to divertor configuration is made, key questions for this scenario are the conditions under which 15 MA can be achieved, the possible total discharge and current flattop durations and the impact of ECH power. In particular, the overall discharge and flattop times and the fractions of input power radiated in the core and conducted to the edge are the most important quantities for design of the inertially cooled W PFCs proposed for the FW in AFP.

As mentioned in Section 5.2, the self-consistent description in DINA of W sputtering in the limiter phase is no longer applicable once the plasma diverts and here the average W concentration is simply prescribed. In this respect, as far as the divertor phase is concerned, from the point of view of DINA, the choice of hydrogenic isotope is largely irrelevant. There will be an impact in the limiter phase, since the energy threshold for W sputtering will be lower for D or T fuel ions, but this has not yet been assessed. In the hydrogen scenario so far obtained with successful limiter ramp-up, c_W is linearly reduced over 10 s from its value at X-point formation (1.2×10^{-4}) to 3×10^{-5}, where it remains fixed until the end of the discharge. The emphasis in the DINA study is on the design and simulation of an achievable end-to-end scenario from the point of view magnetic control, resistive and inductive flux consumption, etc., but with much lower fidelity regarding plasma transport and boundary coupling than is possible with the JINTRAC integrated model employed at IO. As discussed later in this section, time independent JINTRAC simulations are instead used to assess the impact of W concentration on the main plasma at various values of I_p (and thus also plasma density) in order to validate the DINA prescription for c_W.

The primary aim for this first AFP L-mode hydrogen scenario design is, for given target volume averaged density, to optimize the ramp-up to 15 MA to find the maximum flattop duration assuming the maximum ECH power (40 MW) available in AFP. This represents the worst case for conducted power to PFCs. In DINA scenario designs, $<n_e>/n_{GW}$ is also a prescribed parameter throughout the pulse; it is not evolved self-consistently. For the scenario described here (Figure 5.3-1), the density is reduced from its value at the end of the limiter phase ($<n_e>/n_{GW}$ ~0.5) to $<n_e>/n_{GW}$ ~0.3 during the same 10 s period over which the reduction in c_W is imposed. This target normalized density seems a reasonable lower limit in view of the avoidance of disruptions due to error fields. The simulation uses the standard assumption for most ITER DINA scenarios created to-date for the Be wall of noise in the dZ/dt diagnostic signal fixed at an RMS value of 0.6 ms^{-1} (used in feedback stabilization of plasma vertical displacements).

A selection of the more important time traces from this scenario is given in Fig. 5.3-1 – see [9CMZSM] for a detailed account. An important aspect to note is that these preliminary simulations have shown that current ramp-up scenarios maximizing the I_p flattop duration are limited by two factors. The first is the peak value of the magnetic field on the PF6 conductor, B_{PF6} for which, at 4.3 K, the engineering limit is 6.4 T if the coil current is less than 48 kA [33NHXN]. The second is the maximum vertical (axial) force, F_{gap5} acting across the central solenoid (CS) gap #5 (the gap between CSU3 and CSU2). The definition of this force and its limit, F_{gap5} < -26 MN, are given in [3LDS93]. For the scenario in Fig. 5.3.-1, the current ramp to 15 MA is close to optimum with regard to maximising the flattop duration. It takes place over 65 s, with the waveform of P_{ECH} linearly increasing from 2 MW at X-point formation to 15 MW 5 s after the start of the flattop. Parameters B_{PF6} = 5.9 T and F_{gap5} = -30 MN are both close to their engineering limits but with some margin, and the scenario stays within all other engineering constraints on the PF and CS coils.

The full 40 MW of ECH power is then injected throughout the flattop which extends to t = 160 s (duration at 15 MA = 95 s), when the CS1 coil current reaches 44 kA, just below the 45 kA engineering limit on this current. During this phase the power conducted to the boundary is P_{con} = 35 MW, with a total radiation of $P_{rad,tot}$ ~7.5 MW, (of which ~70% is due to W) and the core plasma temperatures reach $<T_e>$ ~5 keV, $<T_i>$ = 3.3 keV (Fig. 5.3-1, lower row). Subsequently, the controlled current ramp down in divertor configuration to ~1.6 MA requires 63 s for a total discharge duration of 223 s. Thus, despite the very high W radiative losses and strong plasma cooling in the limiter phase (Section 5.2), significant current flattop times are achievable in these L-mode plasmas at the nominal 15 MA. This is mostly a consequence of the fact that inductive, rather than resistive losses are the main drivers of flux consumption in the I_p ramp-up phase (see Fig. 5.3-1, top right).

At these low assumed flattop plasma densities ($<n_e>/n_{GW}$ ~0.3) and maximum available AFP heating power, total radiated powers at the maximum level (~20 MW) assumed by the AFP blanket design team cannot be achieved. The only way to substantially increase this radiation loss is to increase the plasma density, but this would come at the cost of significant reduction in flattop duration, or even inability to reach the 15 MA target if the W concentration is not

reduced accordingly. Further sensitivity studies for this scenario are required and are planned to assess the impact of different input assumptions (e.g. waveform of P_{ECH}, $<n_e>/n_{GW}$, c_W).

To investigate if the DINA assumptions regarding W contamination of the plasma are within the range of expectations, a series of fully integrated JINTRAC simulations with the TGLF-SAT2 transport model has been carried out for three plasma current/ECH heating power levels in the DINA scenario. The simulations consider W production from the divertor and an effective wall source with no prompt re-deposition of W included at either the divertor or the wall. The effective W wall source is scanned to determine the effect on the plasma. We note that, as described in Section 2, the ratio of the W wall source to the divertor source in experiments is ~ 10-20% and recall, from the simulations in Section 5.1, that using the same value for the effective wall source in JINTRAC as that of the realistically evaluated wall W source from WallDYN grossly overestimates the effects of the W wall source on the plasma. In this sense an effective W wall source of a value ~ 10-20% of the modelled W divertor source in JINTRAC is expected to be an extremely conservative assumption to account for the effects of the W wall in these plasmas.

The plasmas modelled with JINTRAC are DT (and not in hydrogen), since this will drive higher W sputtering and thus provides an upper estimate of the W effects. As a consequence of all the above assumptions, the W concentrations obtained are expected to be a very conservative estimate of those that are expected in ITER hydrogen plasmas.

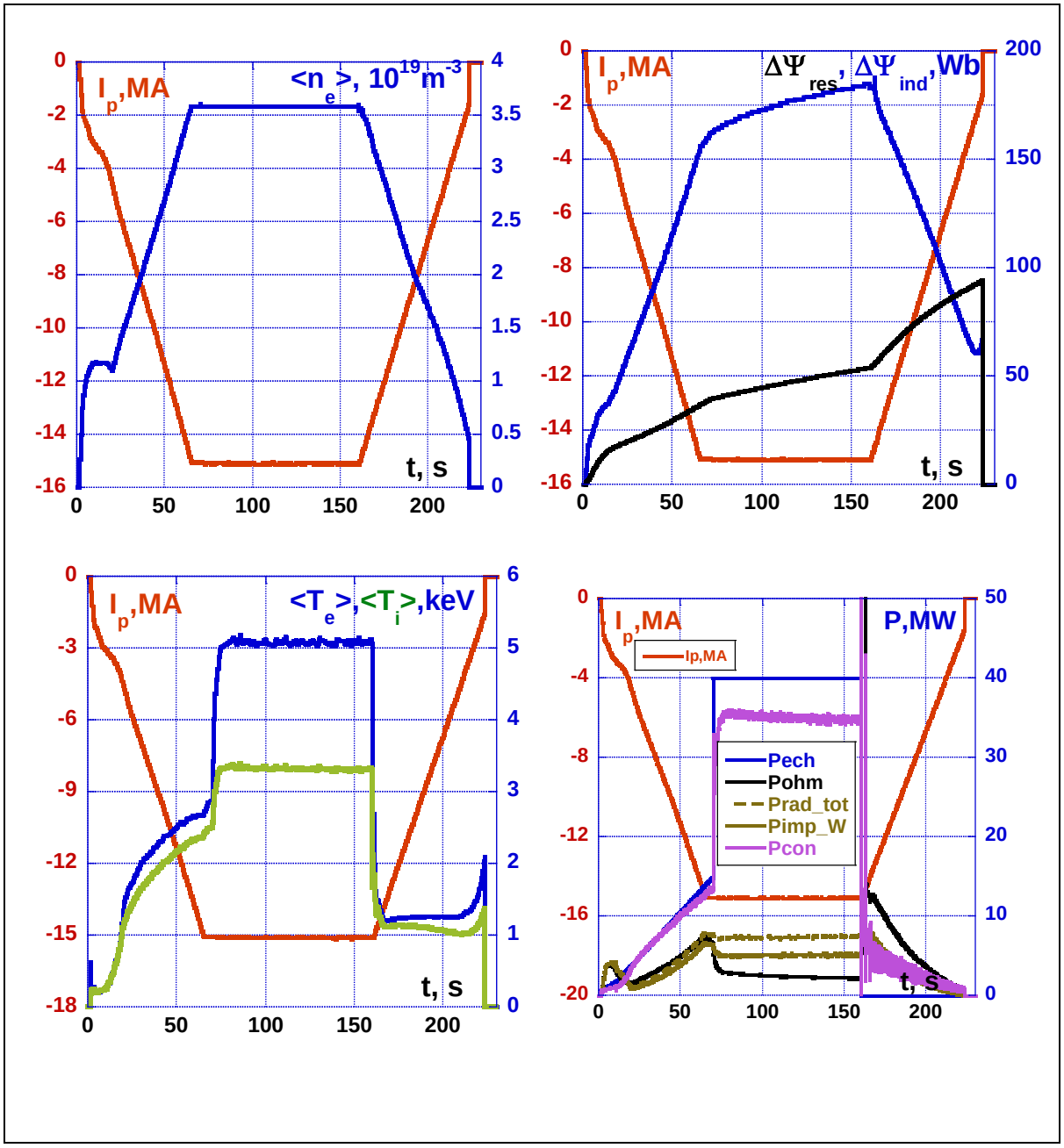

Figure 5.3-1. Selected time traces for a DINA end-to-end L-mode hydrogen scenario with 15 MA flattop and the maximum ECH power available in AFP. Clockwise from top left: I_p and volume averaged density, resistive and inductive poloidal magnetic flux losses, volume averaged plasma temperatures, input and radiated powers.

The specific conditions modelled by JINTRAC are: a) 5 MA, P_{ECH} = 5 MW, $\langle n_e \rangle$ = 0.3 n_{GW}; b) 10 MA, P_{ECH} = 10 MW, $\langle n_e \rangle$ = 0.3 n_{GW}; c) 15 MA, P_{ECH} = 40 MW, $\langle n_e \rangle$ = 0.5 n_{GW}. We note that with our very conservative modelling assumptions, and without the addition of Ne for divertor power dissipation, it is necessary to choose higher densities than 0.3 n_{GW} when simulating 15 MA with P_{ECH} = 40 MW to avoid excessive core radiation from W.

The results of the simulations for low W wall source levels are shown in Fig. 5.3.-2 with temperatures similar to those in the DINA simulations being achieved. Regarding divertor parameters, these plasmas maintain a high ion temperature across most of the divertor target,

and the divertor power flux remains under 10 MWm^{-2}. The resulting core W concentrations and radiated power fractions for the range of wall W sources studied is shown in Fig. 5.3-3. For values of the ratio of the wall W-flux to the divertor flux of 10- 20%, the W concentration is in the range of 3-4x10^{-5} for the plasmas with $\langle n_e \rangle = 0.3\ n_{GW}$. For the 15 MA plasma with higher plasma density, the W concentration is expected to remain at much lower values (simulations are on-going at the time of writing). In all cases, the core radiated power fraction remains under 40%, with the 15 MA plasma having the lowest radiated fraction, consistent with the DINA simulations.

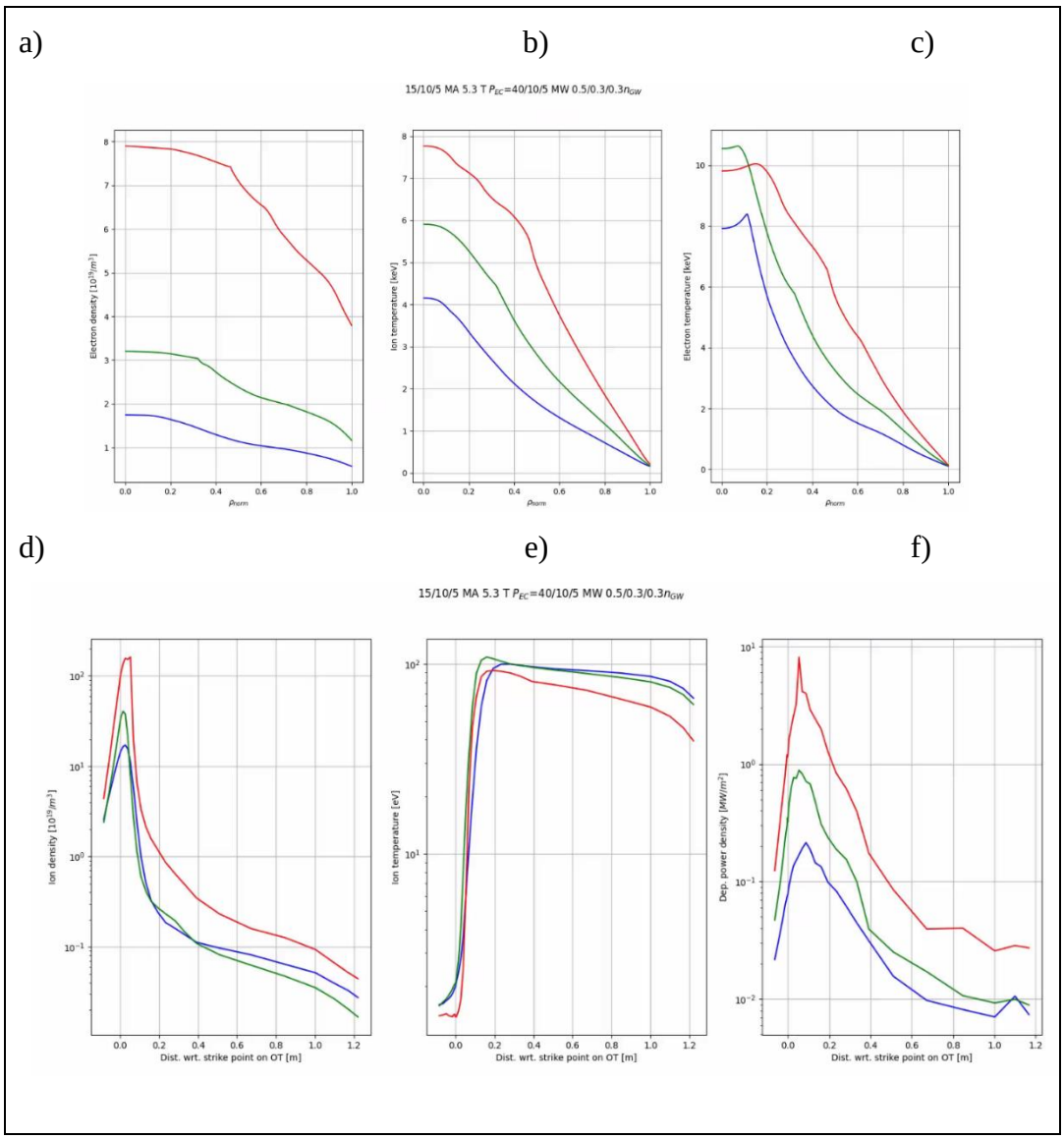

Figure 5.3-2. Plasma parameters from JINTRAC integrated modelling for: 5 MA, P_{ECH} = 5 MW, $\langle n_e \rangle = 0.3\ n_{GW}$ (blue), 10 MA, P_{ECH} = 10 MW, $\langle n_e \rangle = 0.3\ n_{GW}$; (green) and 15 MA, P_{ECH} = 40 MW, $\langle n_e \rangle = 0.5\ n_{GW}$ (red). a) Plasma density, b) Electron temperature, c) Ion temperature, d) Ion density at the outer divertor target, e) Ion temperature at the outer divertor target and f) Power flux to the outer divertor target.

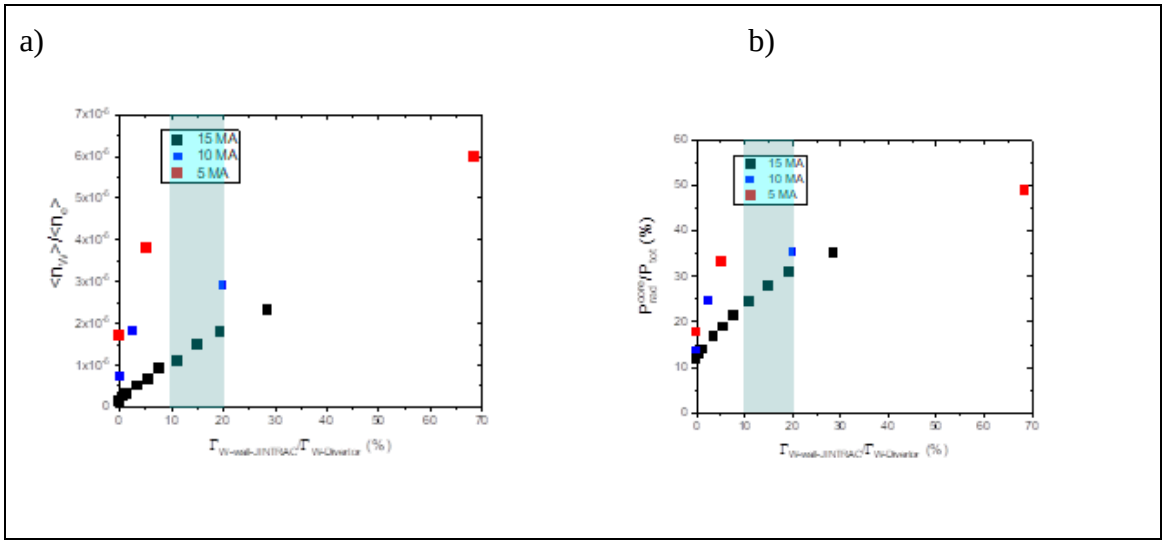

Figure 5.3-3. a) Core W concentration and b) Ratio of core radiated power to total heating power versus the ratio of the effective W wall source to the divertor source in JINTRAC. The cyan shaded region indicate the values for this ratio found in experiment. Note that the effective source overestimates the effect of the W wall source on the plasma for similar values to those of a self-consistently calculated wall source.

These JINTRAC simulations, although, due to their conservative nature, not producing identical results to the assumptions in DINA regarding core W concentration, show that the assumption made in the DINA L-mode scenario design can be taken a solid basis for the evaluation of the 15 MA hydrogen scenario in AFP. Again, here experiments on W production and transport in L-modes accompanied by modelling would be needed to ensure the accuracy of the predictions of these models for ITER.

5.4 Impact on low current H-mode operation

Initial H-mode operation in ITER will start from low levels of plasma current ($I_p \leq 5$ MA) to avoid melting of the W divertor by uncontrolled ELMs [Gunn 2017]. As discussed in Section 2, present experiments show that for ELMy H-modes, the W source is dominated by sputtering during ELMs when the plasma temperature at the edge is low or the distance between separatrix and W wall is large [Dux 2009, Huber 2020]. Tungsten produced by ELM interactions with main chamber PFCs is much more effective in contaminating the core plasma than that produced at the divertor.

To determine the effect of an ELM dominated W source on initial H-mode operation, two approaches have been followed. One is to evaluate the gross divertor W source due to ELMs from SOLPS simulations [Dux 2017] and, on this basis, evaluate an equivalent W influx from the wall into the plasma and model the consequences of such an ELM-averaged W flux on H-mode performance. In this approach the W source from the PFCs into the plasma is given by:

$$\Gamma_W^{\text{ELM-averaged}} = (1\text{-}f_{\text{div,redep}})\Gamma_{W,\text{divertor}}^{\text{no-redep}} + \Gamma_{W,\text{divertor}}^{\text{no-redep}}/10 \qquad (5.4\text{-}1)$$

where the first term corresponds to the effective W divertor source and the second term corresponds to the W wall source. The resulting ELM-averaged W influx is shown in Fig. 5.4-1 for a range of assumptions regarding the edge power flow and the fraction of W promptly

redeposited at the divertor during ELMs. We note that the divertor prompt re-deposition fraction is found to be larger than 95% in present experiments [Brezinsek 2019].

The impact of the resulting wall source on initial H-mode operation has been evaluated with JINTRAC by introducing an effective W wall source (with typical energies of physically sputtered W) whose magnitude has been varied. The results of these modelling studies are shown in Fig. 5.4-2. We note that for W wall sources corresponding to the largest values, the ELM-averaged W wall influx has a detrimental effect on H-mode sustainment. These critical values of W wall sources are comparable to those corresponding to the wall and the divertor together evaluated from Eq. 5.4-1. The modelling results from [Dux 2017] thus imply that the effect of ELM-averaged W influxes on initial ITER H-mode operation will not be a concern, provided that very low ELM frequencies are avoided. This requires that robust schemes for ELM control be available when such H-mode experiments are performed in ITER. We note that modelling of the ELM-averaged W influxes across the separatrix following a similar approach and using ASTRA to evaluate the impact of these fluxes on the core plasma leads to very similar conclusions.

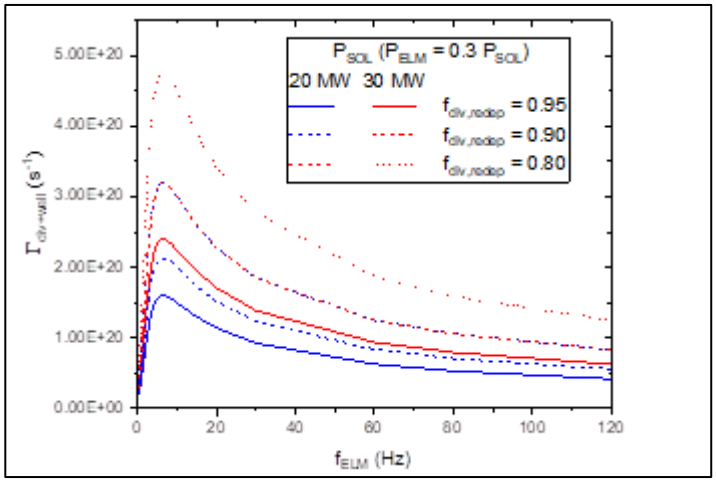

Figure 5.4-1. Modelled ELM-averaged W influx into the plasma from the divertor and the main wall versus ELM frequency for typical edge power levels of initial H-mode operation in ITER and a range of assumptions regarding prompt divertor re-deposition. The W influx is calculated by applying Eq. 5.4-1 to the modelling results for the gross W source in [Dux 2017].

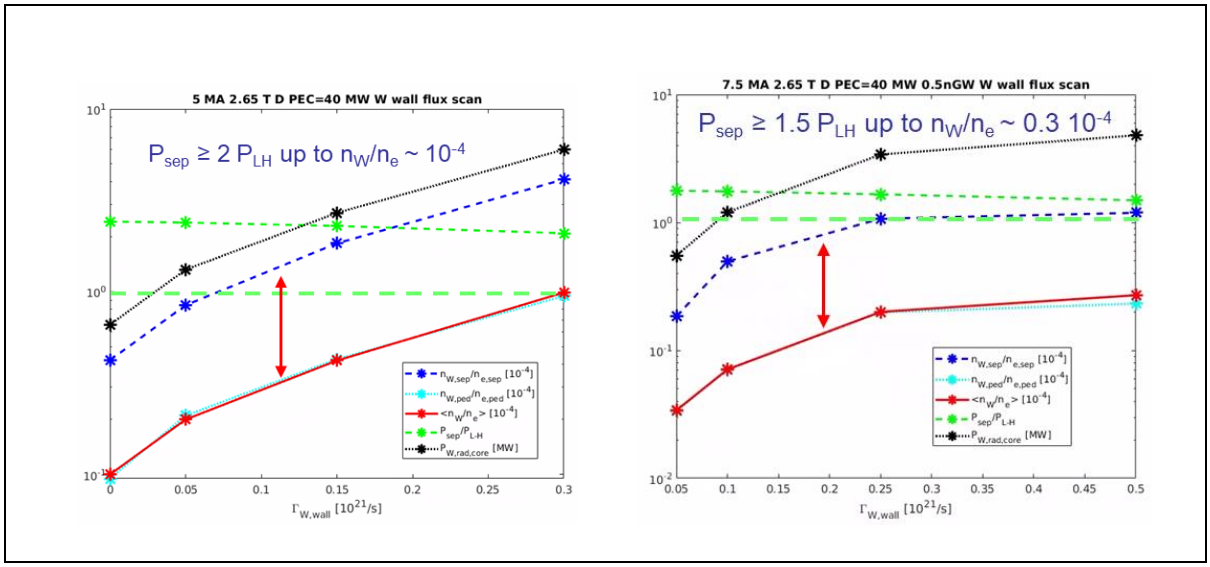

Figure 5.4-2. Modelled W concentrations at the separatrix, pedestal top, core plasma, core W radiation and margin of the edge power flow to the L-H transition versus ELM-averaged W wall source for: a) 5 MA/2.65 T $<n_e> = 0.5\ n_{GW}$ and b) 7.5 MA/2.65 T $<n_e> = 0.5\ n_{GW}$ DD H-mode plasmas with $P_{ECH} = 40$ MW. The red double-headed arrows show the difference between separatrix W concentration (in blue) and core/pedestal W concentration (in cyan/red) due to W screening in the pedestal.

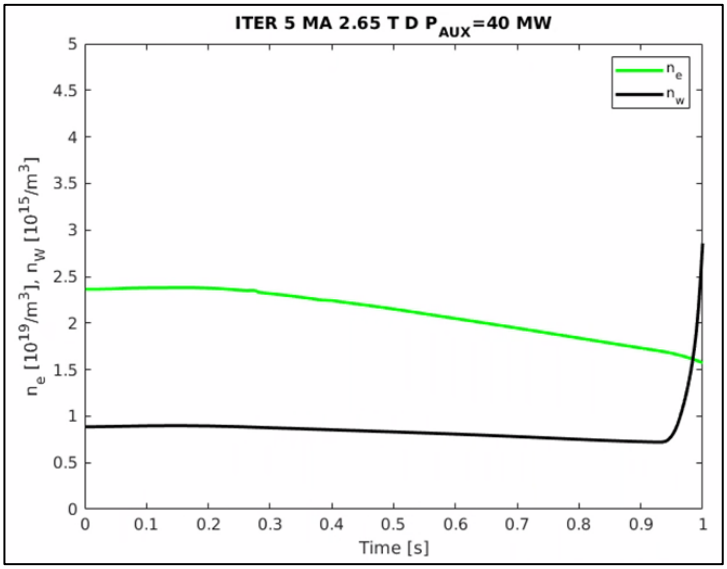

Figure 5.4-3. Modelled electron and W density profiles for a 5 MA/2.65 T $<n_e> = 0.5\ n_{GW}$ DD H-mode plasma with $P_{ECH} = 40$ MW showing the effective neoclassical screening for W provided by the pedestal plasma with $n_{sep}/n_{GW} = 0.4$.

The reason for the resilience of these initial H-modes to wall W influxes comes from the effective screening of W at the pedestal plasma due to neoclassical transport effects, as shown in Fig. 5.4-3, and the high value of the electron temperature (~ 20 keV due to poor electron ion thermal coupling and large ion heat transport) that maintain the W radiation loss under 10 MW in these low density plasmas, even for the significant W concentrations of ~ 10^{-4} for $I_p = 5$ MA.

As mentioned in Section 2, the screening effects were identified in previous studies for ITER [Dux 2014] and have been recently confirmed at JET.

The second approach followed to evaluate the effect of W influxes driven by ELMs is to perform full ELM-resolved JINTRAC simulations of the effective W influx from the divertor into the plasma and double its magnitude to mock-up the effect on the W wall source. The results of such an approach for a 5 MA/2.65 T DD H-mode with $\langle n_e \rangle = 0.5\ n_{GW}$ and $P_{ECH} = 40$ MW assuming an 80% level of prompt re-deposition at the divertor and a wall source similar to the divertor source, are shown in Fig. 5.4-4. For these conditions, the level of radiation in the core plasma remains low (18% of P_{tot}). However, the instantaneous level of core plasma radiation during the ELM is much larger (18 MW). If this exceeds 25 MW, it can trigger an H-L transition for these plasmas. This reinforces the need for appropriate ELM control schemes to be available when these initial H-mode experiments are performed in ITER in AFP.

We note that the capability to perform integrated modelling studies with a self-consistently generated W source from the divertor and the wall is not presently available. Thus, approximations such as those detailed above are required and this introduces unavoidable uncertainties in the ITER simulations.

To cope with uncertainties in the evaluation of the W wall source and screening by the pedestal plasma in the initial AFP H-mode operation, a risk mitigation strategy has been developed. This is based on the development of "high-clearance" H-mode plasma scenarios, in which the distance from the plasma separatrix to the wall is increased. This has been performed following two approaches: in the first, the overall distance from the separatrix to the wall has been increased, whilst in the second, the distance to the outer wall separatrix has been increased at the expense of reducing it elsewhere. The latter is guided by the experimental observation in [Dux 2009] that the W source from the LFS wall is more effective in contaminating the core plasma than from the HFS, consistent with ELMs being a key driver for the main chamber W source, as we expect for low I_p H-modes in ITER. The resulting plasma configurations are shown in Fig. 5.4-5 for 5 MA/2.65 T H-mode plasmas with $P_{ECH} = 40$ MW.

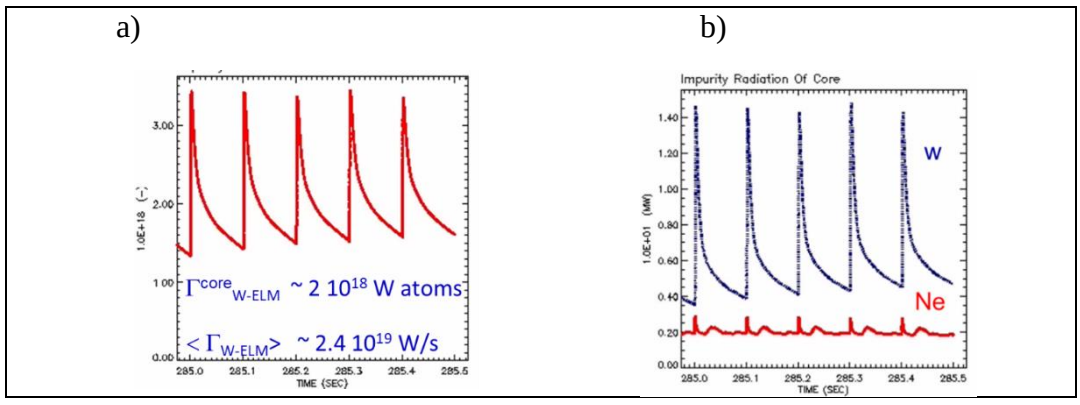

Figure 5.4-4. JINTRAC ELM-resolved W modelling for a 5 MA/2.65 T $\langle n_e \rangle = 0.5\ n_{GW}$ 40 MW ECH heated DD H-mode plasma with 1 MJ ELMs and $f_{ELM} = 10$ Hz. The W divertor source is evaluated assuming an 80% prompt re-deposition fraction and the wall source is assumed to be similar to the effective divertor W source. a) ELM-resolved W influx into the core plasma and b) ELM-resolved core plasma radiation from W and Ne.

With increasing distance to the outer wall, the vertical stability of the plasma worsens and there are increasing demands on the VS3 in-vessel coils to maintain the plasma vertically stable. For the standard assumption of noise in the dZ/dt diagnostic signal fixed at an RMS value of 0.6 ms^{-1}, the VS3 design limits imply that plasma elongation and triangularity cannot be maintained at the reference values for large outer wall clearances with acceptable vertical stability control through the H-mode scenario. Higher elongations and triangularities would be possible, close to the reference values, if the dZ/dt signal noise can be reduced to 0.2 ms^{-1} [Lukash 2017].

The reduction of elongation and triangularity for high wall-clearance impacts the pedestal plasma characteristics (lower pedestal pressures) as shown in Fig. 5.4-6. If the plasma densities are kept as per the reference case, this will lead to lower pedestal temperatures and worse screening for high clearance configurations. The specific requirements for ELM control in these high clearance configurations have been quantified in [Part II: new baseline outline IRP] and shown to be feasible with the ITER ELM control coil system with some minor tuning of the plasma current for each clearance.

The large wall clearance is expected to have a significant impact on the core W levels. This effect can be quantified in a relative way by extrapolation of the ASDEX Upgrade observations with a physics-based scaling. As shown in Fig. 2-8, the core W concentration in ASDEX Upgrade increases by a factor of ~ 2-3 when the gap to the outer wall is reduced from 8 to 4 cm. The physics-based scaling uses the validated model in [Pitts 2007], which relates the ratio of the ELM energy flux to the wall ($\Delta W_{ELM,wall}$) to the total ELM wall+divertor flux (ΔW_{ELM}) with the normalized ELM energy loss ($\Delta W_{ELM}/W_{ped}$) and the ratio of the distance of the wall to the device dimensions ($-\Delta R_{wall}/R$). We then further assume that the ELM W wall source is proportional to the ELM wall energy flux such that:

$$\Gamma_{W\text{-}ELM,wall}/\Gamma_{W\text{-}ELM} \sim \Delta W_{ELM,wall}/\Delta W_{ELM} \sim \exp\left[-\Delta R_{wall}/R\,(\Delta W_{ELM}/W_{ped})^{-1/2}\right] \quad (5.4\text{-}2)$$

This leads to ΔR_{wall} = 15 - 30 cm in ITER producing similar relative ELM W wall to divertor fluxes as those in ASDEX Upgrade with 4 - 8 cm for the same $\Delta W_{ELM}/W_{ped}$. On this basis plasmas with an outer wall clearance $\Delta R_{wall} \geq 30$ cm should have a very low wall contribution to core W contamination and thus provide an effective means to develop H-mode scenarios at low current with low risks regarding the impact of W wall fluxes in the IRP.

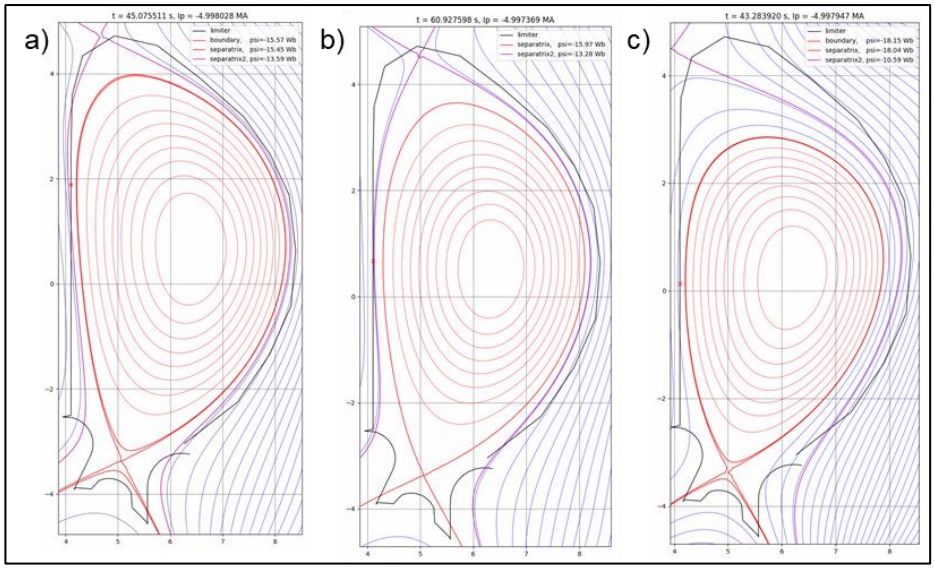

Figure 5.4-5. Plasma configurations for DINA 5 MA/2.65 T $<n_e>$ = 0.5 n_{GW}, P_{ECH} = 40 MW, DD H-mode plasma scenarios: a) reference baseline configuration, b) increased overall wall clearance (15 cm at the outer midplane) configuration and c) 45 cm outer gap configuration.

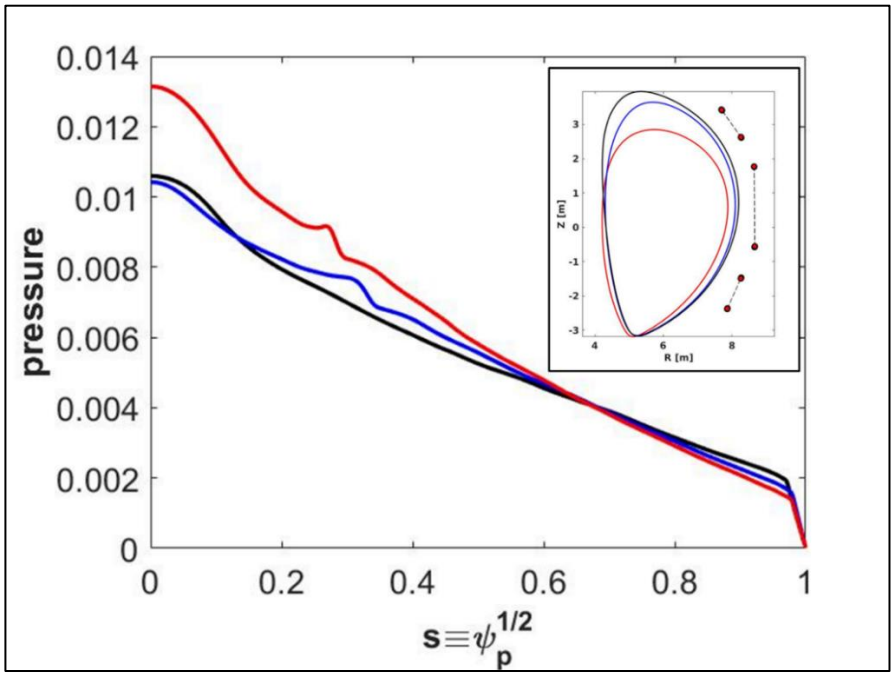

Figure 5.4-6. Plasma pressure profiles modelled with JINTRAC including edge MHD plasma stability modelling for the three DD H-mode plasma scenarios in Fig. 5.4-5.: 5 MA/2.65 = 0.5 n_{GW} with P_{ECH} = 40 MW and varying wall clearance (the corresponding separatrices are shown in the inset).

Specific experiments on the impact of ELMs on the wall and divertor sources and edge W transport and quantification of the effect of wall clearance on W plasma contamination accompanied by the validation of the models used for ITER are required to ensure that the modelling for ITER initial H-mode operation is accurate, as described in [8YFSB3].

5.5 Disruption load impact on the W wall

Disruptions and VDE induced heat loads have a major impact on the PFC lifetime and are one of the principal drivers of the need for an effective DMS. It is therefore essential to avoid, as far as possible, unmitigated disruptions and to commission the DMS as soon as possible in the IRP to ensure effective mitigation before operation with high plasma current and energy is attempted. Effective disruption mitigation needs to simultaneously meet the requirements for mitigation of the TQ, CQ and RE loads. However, the specific choice for material injection which maximizes the mitigation of one load can lead to an increase in the other (especially RE production). This can potentially cause single event failure of PFCs (i.e. water leak caused by RE impact or large electromagnetic loads following extensive FWP melting).

In this context, as shown in Fig. 5.5-1, the high melting point of W opens a wider operational space than Be in terms of I_p/W_{plasma} within which melting is avoided during the TQ and CQ.

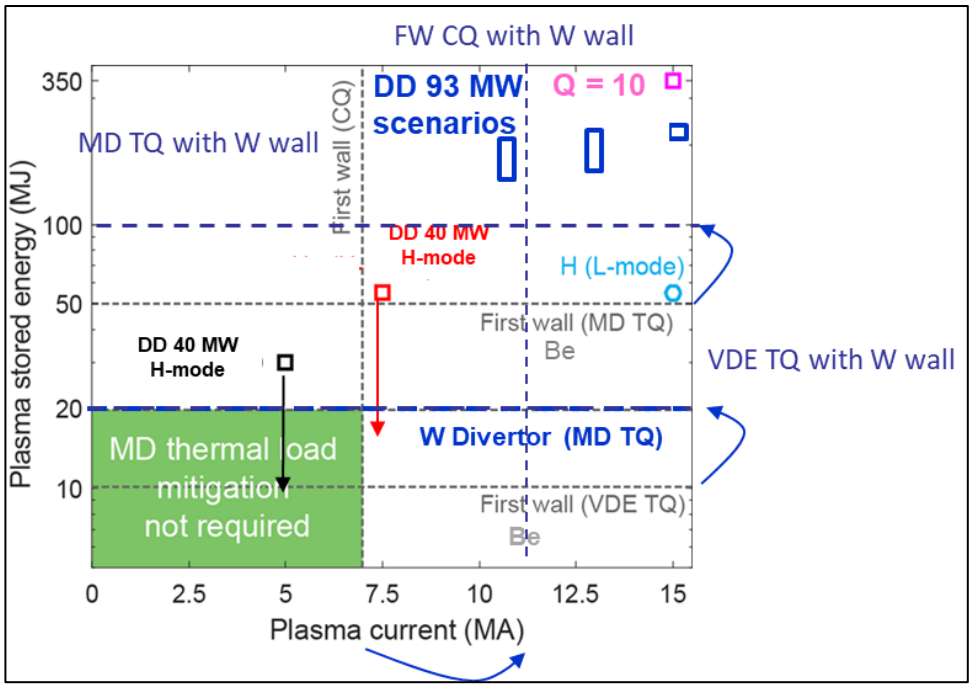

Figure 5.5-1. ITER operational space over which disruption mitigation is required from the point of view of transient thermal load induced PFC melting (for larger values of I_p/W_{plasma} than vertical/horizontal dashed lines melting occurs without mitigation). The operational space for unmitigated disruption loads widens (blue arrows) when changing the FW material from Be to W. Several key Research Plan plasma target milestones for AFP and DT-1 are also indicated, together with the expected degradation of plasma energy before the disruption for H-mode plasmas. Runaway electrons are not included.

Regarding first the thermal loads, switching to W essentially removes the major issues with regard to TQ-induced melting on the FW, even at the highest stored energies, since degradation of plasma performance is expected in advance of the TQ for H-mode discharges. In this case, the unmitigated CQ phase is of the greatest concern. A detailed analysis using the DINA-SMITER-MEMOS-U code workflow of the CQ-induced loads has been made for Be FW components in [Coburn 2022] for the CQ phase of VDE's and major disruptions for both

upward and downward quenches. Under worst case conditions (highest I_p, lowest P_{rad} levels and largest stored poloidal magnetic energy), Be melting and melt motion is severe on the upper FW panels (FWP) and occurs to a lesser extent on the lower, outer FWP rows. Preliminary analysis using the same workflow with W replacing Be finds that, even given the much higher melting temperature of W compared with Be, surface melting will still occur on the upper FWPs under worse case conditions for upward going quenches at 15 MA, but is absent for the lower FWPs for downward events (Fig. 5.5-2). By scaling the magnetic energy and τ_{CQ} with plasma current ($\tau_{CQ} \propto I_p^{1/2}$ and $E_{CQ} \propto I_p^2$) and assuming the same DINA equilibrium trajectory for the 15 MA upward going VDE CQ's, a provisional assessment with the same workflow finds that melting on W upper FWPs would be expected to begin for I_p in the range 11-12 MA. In [Coburn 2022], fairly substantial melting occurs on Be already at I_p = 7.5 MA.

The MEMOS-U calculations for the worst case with W at 15 MA find maximum erosion depths of ~0.4 mm, a factor of ~7 lower than for Be under the same CQ loads, which is a major gain with regard to the ability of FWPs to tolerate a limited number of events. Whilst the principal reason for the reduced erosion depth is the much higher melt temperature of W, it is also in part due to the modified melt motion, where, in the case of W, Lorentz forces on the melt layer are driven by the balance between strong thermionic electron current emission from the heated surface and halo current carrying the heat flux. For Be, thermionic emission is essentially absent, and the melt motion is determined only by the halo current. For both materials, once melting and melt motion occurs, the melt displacement will be sufficient for the melt layer to bridge over some of the toroidal gaps between poloidally adjacent fingers on the actively cooled FWPs. If this bridging also leads to gap filling, such that fingers are electrically connected, and depending on where this takes place, significant eddy currents can circulate in the FWPs even for follow-up disruptions whose CQ has been mitigated. The associated electromagnetic forces can be very large (in some cases exceeding by many factors the design verification load) and can cause mechanical failure of the panels in single events. This was already identified as an issue for Be FWPs in 2021.

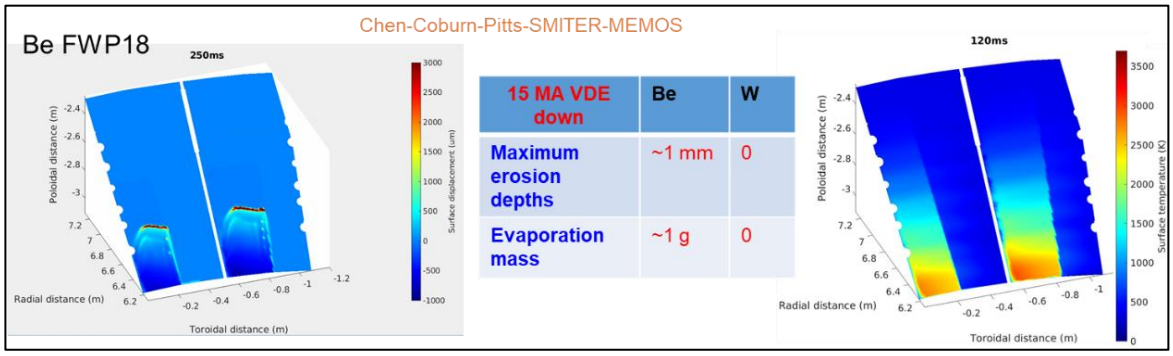

Figure 5.5-2. FWP erosion under 15 MA unmitigated downward going VDEs with Be and W as armour material simulated with the DINA-SMITER-MEMOS-U workflow. The erosion depth in Be is ~ 1 mm while the W panel does not melt.

A key point in the context of this gap filling is that for the typical upward going CQ on ITER, the strongest heat loads are expected on FWP#8 and here melting over large areas is predicted for both Be and W. However, whilst melting is also significant on FWP#9 for Be, the heat loads are low enough for melting to be avoided on most of the surface for a W panel. This is

important because the smaller size of FWP #8 (shorter toroidal finger length) and the differences in magnetic fields local to the panel during the quench, mean that the peak moments on FWP fingers are nearly two orders of magnitude higher on FWP #9 than on neighbouring FWP #8 [9E6W92]. This implies that for W, even with gap bridging on FWP#8, the peak moments will remain acceptable on those panels and will remain very low on FWP#9 since melting will not occur. This implies that the possibility of failure of these W FWPs as a consequence of unmitigated (or insufficiently mitigated) disruptions/VDEs is significantly reduced compared to Be.

Independently of the impact of gap filling, an outstanding question is whether it will occur at all on ITER with W PFCs. For the case of Be, gap filling has already been seen clearly on JET as a result of upward going VDE loads [Jepu 2019], albeit for gaps narrower than those foreseen on the ITER FWP's. Very recent experiments designed specifically to address gap bridging and infiltration for W material have been performed on ASDEX Upgrade [Ratynskaia 2023]. Under the conditions of this experiment (repeated ELM-induced transient melting on specially engineered samples exposed in the outer divertor), poor wetting and weak attachment of re-solidified melt were observed (and confirmed by melt modelling), including the wetting of inner gap walls (thus no gap infiltration). This is a consequence of re-solidification, which prevents the melt from revolving around the corners by modification of the sharp edge topology.

The apparent contradiction with the Be observations on JET emphasizes how the details of gap wetting are sensitive to melt speed, pool depth, lifetime and the liquid metal and wall temperatures. Further experiments will shortly be executed on WEST in which shallow and slow melt pools will be generated close to W divertor gap edges to assist in the understanding of near-gap dynamics of sustained pools. New simulations are also planned capable of resolving small scale dynamics in the gap vicinity. If these were to confirm the lower likelihood of gap bridging for W compared to Be under large disruption loads in ITER, this would further enhance the resilience of FWP # 8 and #9 to electromagnetic loads following unmitigated events discussed above.

Returning to the modelling of macroscopic CQ-induced melting on the ITER FWP's, although the MEMOS-U calculations are unique in accounting both for the 3D nature of the plasma wetted area and the time varying magnetic equilibrium of the quenching plasma (based on DINA simulations of the CQ phase), they do not take proper account of the important phenomenon of vapour shielding. An attempt was made to include the shield effect in the Be melt modelling of [Coburn 2022], but this was highly approximate, based on shielding coefficients derived from 1D Particle-in-Cell simulations. These coefficients are not available for W. Even if they were, the reduction in Be surface melt thickness due to shielding found in [Coburn 2022], was only ~30% at most for the worst case of the 15 MA upward going VDE CQ. The effect should be much stronger when properly taking into account the (at least) 2D nature of the shield dynamics and under conditions of severe surface vaporization once boiling temperatures are reached.

To study this, new simulations have been performed with the TOKES code [Landman 2009], which includes a reasonably well benchmarked vapour shielding model [Pestchanyi 2017] and

operates in 2D. Unlike the MEMOS-U simulations, however, TOKES cannot yet follow the CQ equilibrium evolution and, given the 2D nature, is unable to account for the reduced wetted areas for heat loads introduced by the 3D FWP shaping. It thus assumes that the equilibrium is fixed in time from the first point at which significant heat flux is deposited in limiter configuration on the upper FWP's using the same upward going, 15 MA, 5.3 T VDE DINA simulations as those adopted for the MEMOS-U studies. Thereafter, the TOKES model assumes that the total magnetic energy which should be dissipated during the CQ is stored as ion thermal energy in the core and is then transferred to the electrons via equipartition, at a rate which is adjusted to provide appropriate low electron temperatures in the halo region and fits the value of τ_{CQ} found in the DINA simulation. The e-folding length, λ_q, of the heat flux at the outer midplane of the halo is approximately matched to the values used in [Coburn 2022] by adjusting plasma transport coefficients in the halo. Simulations have been performed with and without vapour shielding, for varying λ_q, E_{CQ} and τ_{CQ} (corresponding to I_p = 7.5, 10.0, 12.5 and 15 MA) with the latter two quantities varied using the same scalings from the 15 MA case as in the MEMOS-U runs (see above). The details will be reported in [Pitts 2023] and only a brief summary is given here.

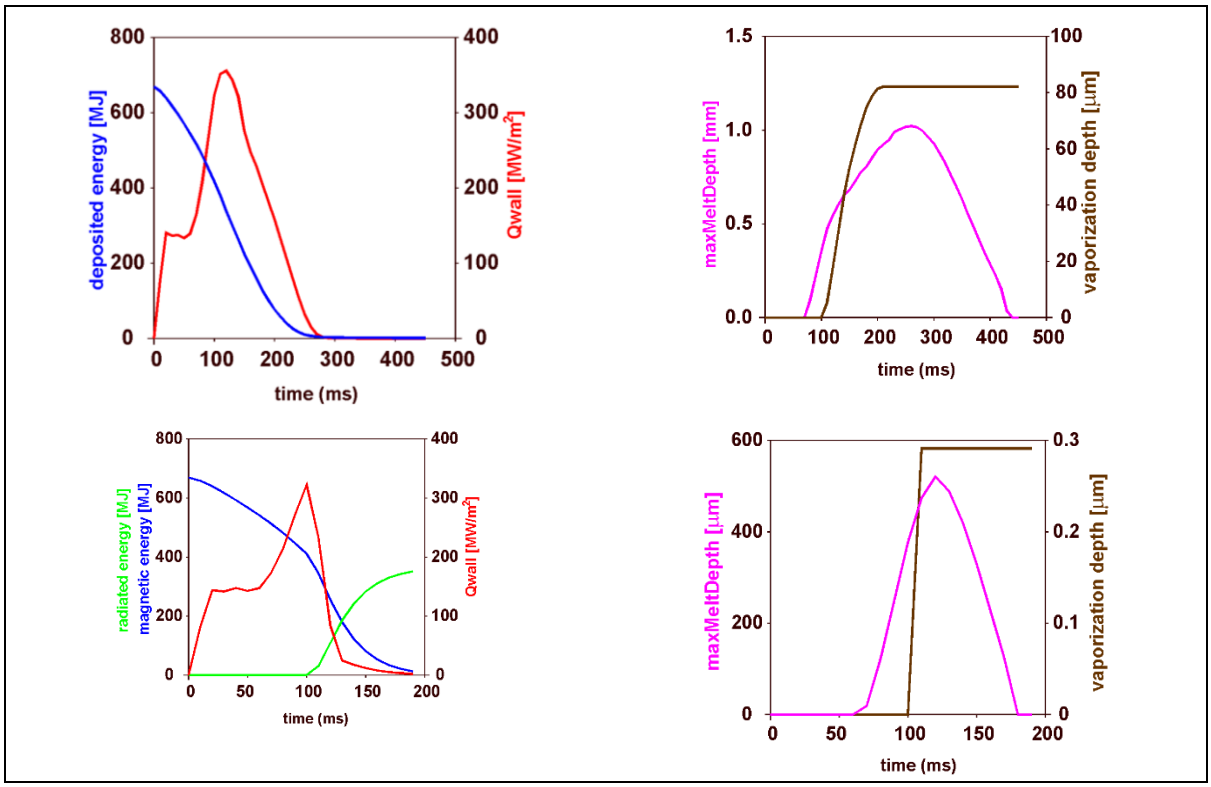

Figure 5.5-3. TOKES simulations of W melt and vaporization depth for the same 15 MA upward going VDE studied for Be in [Coburn 2022]. Without (upper row) and with (lower row) vapour shielding. E_{CQ} = 670 MJ, τ_{CQ} = 250 ms, λ_q = 3.5 cm. The simulations are carried through to complete resolidification.

For Be PFCs and roughly equivalent input parameters to the MEMOS-U study in [Coburn 2022] for the worst 15 MA VDE case without shielding, TOKES finds a peak melt depth of ~1.2 mm, roughly consistent with (but lower than) the MEMOS-U result (~2.8 mm). This can

be considered reasonable agreement given that MEMOS-U accounts for melt motion and more focused (3D) wetted areas. In contrast, because the shielding is more accurately accounted for in TOKES, predicted worst case peak melt depths with shielding activated are much lower in Be (~0.3 mm) than found in the MEMOS-U simulations (~2 mm). For the lower I_p case at 7.5 MA, in which the Be vaporization temperature is not reached and there is thus no vapour shielding benefit, an even better agreement is found compared to the unshielded 15 MA case. Here, TOKES finds peak melt depths of ~0.24 mm, compared with ~0.25 mm for the MEMOS-U equivalent case. This high level of agreement must be to some extent considered fortuitous.

For W, Fig. 5.5-3 compiles TOKES results with and without shielding for the 15 MA worst case upward going VDE. Shielding reduces the peak melt depth by ~factor 2, the vaporization depth by more than 2 orders of magnitude, the melt duration by nearly a factor 3 (this also significantly decreases the time over which melt motion can occur) and ~50% of the magnetic energy is radiated by the shield near the FWPs. With decreasing, λ_q, the shielding becomes ever more efficient (not shown). Note that the peak melt depths of ~1 mm and ~0.5 mm for this worst case without and with shielding respectively, compares favourably with the ~0.4 mm found with MEMOS-U for the same 15 MA case without shielding.

As I_p is decreased in the simulations, the shield strength is drastically reduced because the W vaporization temperature is not reached. Vaporization begins only for the 12.5 MA simulation, and in this case only ~14% of E_{CQ} is radiated. Tungsten melting still occurs at I_p = 10 MA, with a peak melt depth of 0.4 mm and a melt duration of ~160 ms, comparable to the 15 MA worst case with shielding. No melting is found at 7.5 MA. An important conclusion is thus that unmitigated CQ's at lower current on W (and Be) can generate similar melting and melt durations to events at higher current, where shielding is effective.

It is important to point out that all of the unmitigated disruption melt calculations performed to date (thus using MEMOS-U and TOKES) must be considered only approximate given their reliance on the 2D DINA disruption simulations. In reality, the CQ phase is expected to be an extremely time and spatially variable event, with significant MHD activity and a complex 3D heat deposition pattern with strong filamentary nature [Artola 2023]. The assumption of a 2D equilibrium with an essentially smooth envelope of energy deposition, leading to global surface melting with well-defined wetted area, will thus likely be a rather conservative picture. More realistic time and spatial heat deposition patterns are starting to become available through new 3D JOREK simulations and could be eventually used as input to more refined melt estimates.

In addition to thermal loads during the CQ and TQ, runaway electrons (RE) can be produced during unmitigated disruptions or during the process of optimizing the DMS for disruption mitigation itself. Tungsten is more effective in stopping the RE and this concentrates the energy deposited by RE and increases the temperature at the W/Cu interface with the cooling channel compared to the case with Be PFCs. We note that the W/Cu bond is much more resilient than that of Be/Cu and, thus, this higher temperature does not necessarily imply an earlier failure of the W/Cu bond compared to that of Be/Cu. The effect of the more concentrated runaway loads in W can be countered by thickening of the W armour layer on the first wall, as shown in Fig. 5.5-4 derived from simulations using the DINA-SMITER-GEANT4-MEMOS workflow [Chen 2022]. Since W can reach higher surface temperatures, it can provide the same stationary power

flux exhaust with larger thickness than Be. Studies are ongoing to assess how such a thickness increase may be incorporated in the current FWP design and optimized for both RE energy deposition and stationary power handling, noting that, because the RE's are expected to be deposited only in the apex regions of the panels, the W thickening need not be necessarily deployed everywhere on the panel surface.

On the basis of the modelling studies discussed above, the use of W as material for the FWPs in ITER significantly reduces the risk of FWP damage due to thermal loads during the TQ and CQ as well as that of failure due to electromagnetic loads following unmitigated or insufficiently mitigated major disruptions and VDEs. For RE loads, the higher melting of W allows for the optimization of the FWP W thickness to increase their resilience to RE loads to match and exceed that of the Be panels.

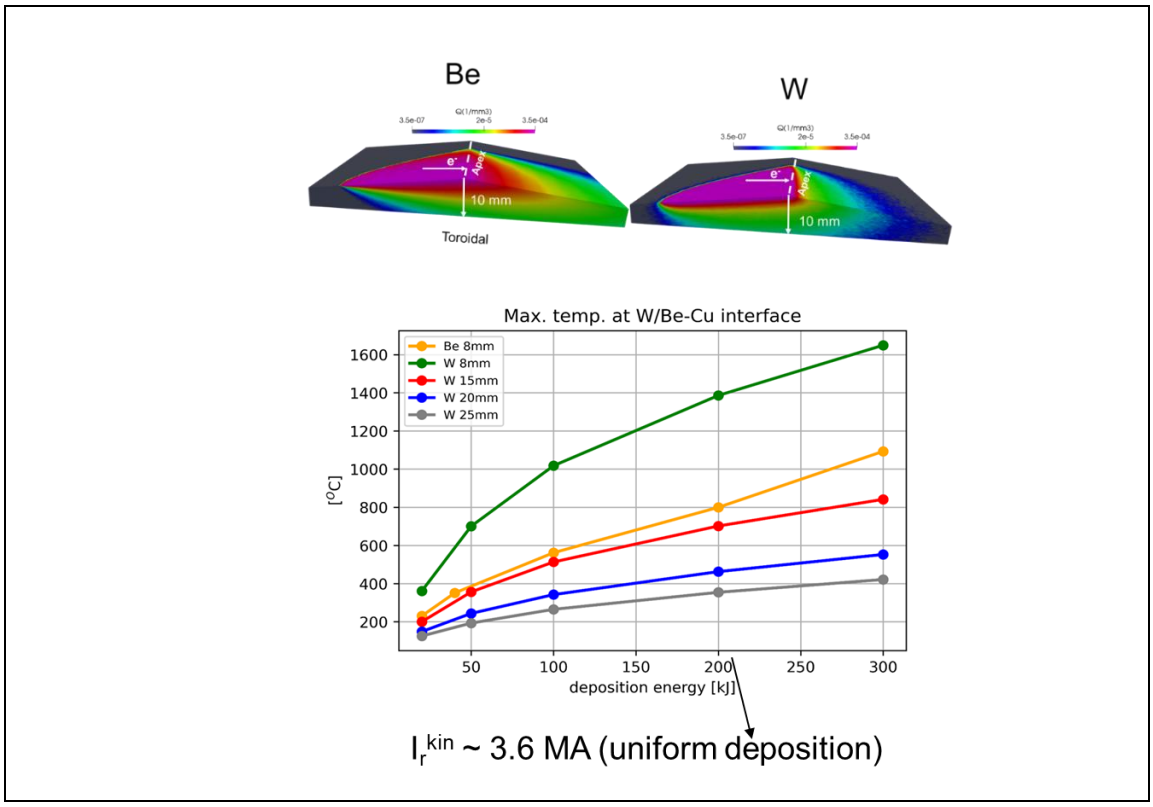

Figure 5.5-4. (Upper) Modelled heat loads on a Be and a W FWP apex. (Lower) Temperature at the Be/W-Cu cooling channel interface for the reference Be thickness of 8 mm and for a range of W thicknesses versus energy deposited per first wall apex (there are two apexes per FWP in ITER). A 200 kJ RE deposition per apex corresponds to the kinetic energy of a runaway plasma with 3.6 MA, assuming uniform deposition across the apexes of the impacted FWPs.

6. Summary and Conclusions

This report quantifies the impact that the change of wall material from Be to W has on the achievement of ITER's AFP and DT-1 goals and how the risks that the W wall poses are mitigated with new ancillary systems and improved designs that are included in the baseline. From the evaluations carried out thus far we conclude:

a) The risks to the demonstration of high Q operation are low and effectively mitigated by the additional heating power level (100 MW) and mix (33 MW NBI and 67 MW ECH and a later installation of 20 MW ICH in DT-1). The risk to Q = 10 operation remains low/medium since the W wall influxes that would prevent this are much higher than those presently evaluated, although significant uncertainties remain with regard to the evaluation of these influxes.

b) A boronization system in ITER based on GDC can provide the required vacuum conditions for plasma operation by reducing the residual impurity content that can impact negatively the start-up phase of the plasma discharge, particularly when limited on the W FWPs. If it is eventually required because W influxes for high Q operation are much larger than those evaluated here, a boron powder dropper could be used to cover the plasma exposed areas of the W FWPs with boron, thus ensuring the achievement of Q = 10. Note that because of the associated T retention, the use of such boron dropper would be limited to a restricted set of discharges.

c) The introduction of boron causes increased T retention compared to that expected from W alone and this can be significant in ITER if boronization is applied on a regular basis (i.e. every two weeks). To remove the retained T in DT-1, ICWC is needed together with specific operational time. We note that before DT-1 the system must have been already fully demonstrated and, thus, the need to be installed before AFP.

d) In addition to ICWC, the flexibility that the ICH system provides is of advantage, although not essential, to the execution of the DT-1 plan. It is thus recommended that a one antenna 20 MW ICH system is maintained in the new baseline for DT-1. The increase of power to 20 MW will follow the confirmation of the expected coupling and low impact on the W wall source in dedicated AFP experiments with a power of 10 MW.

e) The impact of a W wall in the limiter phase and in the development of initial scenarios has been quantified and found significant, but still allowing viable development paths for such scenarios. Of particular interest is the limiter phase of ITER scenarios, for which a high level of optimization of plasma parameters will be required (density, applied ECH heating power, etc.). This is well aligned with present operational experience in all-W tokamaks.

f) The use of W as first wall material decreases significantly most of the risks associated with loads during the TQ and CQ of disruptions and VDEs. While disruption mitigation will be required on a routine basis for high current and high Q ITER operation, the increased resilience of W to such loads reduces the risk of damage to FWPs resulting from events in which the DMS fails altogether, or in which the levels of mitigation requested are not achieved. In addition, modification of the FWP design to increase its thickness in areas were runaway electrons deposit their energy can increase their resilience to RE loads beyond that of the previous baseline Be panels.

To refine the assessments on which these conclusions are based requires dedicated experiments on present full-W devices supported by modelling. This will allow the validation and refinement of the models used to predict ITER plasmas, thus increasing confidence in these predictions. An initial list of the highest priority topics for R&D related to the use of a W wall in ITER are described in [8YFSB3]. This document has been provided to the ITPA

Coordinating Committee to guide the research in the ITER Members fusion research institutes to support the new ITER baseline.

7. References

[Kallenbach 2009] A. Kallenbach et al 2009 Nucl. Fusion 49 045007

[Martin 2008] Y R Martin et al 2008 J. Phys.: Conf. Ser. 123 012033

[Schweinzer 2016] J. Schweinzer et al 2016 Nucl. Fusion 56 106007

[Ryter 2013] F. Ryter et al 2013 Nucl. Fusion 53 113003

[Joffrin 2014] E. Joffrin et al 2014 Nucl. Fusion 54 013011

[Angioni 2017] C. Angioni et al 2017 Nucl. Fusion 57 056015

[Bobkov 2010] Vl.V. Bobkov et al 2010 Nucl. Fusion 50 035004

[Bobkov 2017] V Bobkov et al 2017 Plasma Phys. Control. Fusion 59 014022

[Wukitch 2013] S.J. Wukitch et al Phys. Plasmas 20, 056117 (2013)

[Helou 2023] W. Helou, et al., et al., Proc. 29th IAEA Fusion Energy Conference, London, UK, 2023. Paper PD/P9.

[Angioni 2021] C. Angioni, Plasma Phys. Control. Fusion 63 073001

[Manas 2022] P. Manas, et al., EPS 2022 conference

[Dux 2011] R. Dux et al 2011 Nucl. Fusion 51 053002

[Dux 2009] R. Dux, et al, Journal of Nuclear Materials 390–391 (2009) 858

[Pütterich 2011] T. Pütterich et al., Journal of Nuclear Materials 415 (2011) S334

[Field 2023] A.R. Field et al 2023 Nucl. Fusion 63 016028

[Loarte 2015] A. Loarte, et al., Physics of Plasmas 22, 056117 (2015)

[Manas 2021] P Manas et al, IAEA Fusion Energy Conference, 2021, France

[Yang 2020] X. Yang et al 2020 Nucl. Fusion 60 086012

[Fajardo 2022] D Fajardo et al 2022 Plasma Phys. Control. Fusion 64 055017

[Angioni 2014] C. Angioni et al 2014 Nucl. Fusion 54 083028

[Loarte 2016] A Loarte et al, IAEA Fusion Energy Conference, 2016, USA

[Reynolds-Barredo 2020] J.M. Reynolds-Barredo et al 2020 Nucl. Fusion 60 086017

[Pitts 2019] R.A. Pitts, et al., Nuclear Materials and Energy 20 (2019) 100696

[Dux 2014] R Dux et al 2014 Plasma Phys. Control. Fusion 56 124003

[Dux 2017] R. Dux, et al, Nuclear Materials and Energy 12 (2017) 28

[van Vugt 2019] D.C. van Vugt, et al., Phys. Plasmas 26, 042508 (2019)

[Winter 1990] J. Winter, et al., Journal of Nuclear Materials 176 & 177 (1990) 14

[Winter 1989] J. Winter, et al., Journal of Nuclear Materials Volumes 162–164 713

[9ATR8M] Wall conditioning by particulate injection from multiple devices (9ATR8M)

[Li 1999] J. Li etal 1999 Nucl. Fusion 39 973

[Gao 2009] X. Gao, et al., Journal of Nuclear Materials 390–391 (2009) 864

[Bucalossi 2022] J. Bucalossi et al 2022 Nucl. Fusion 62 042007

[Liu 2007] H Q Liu et al 2007 Plasma Phys. Control. Fusion 49 995

[Buzhinskij 1997] O. I. Buzhinskij and Y. M. Semenets (1997) Fusion Technology 32, 1

[Hong 2011] S.-H. Hong et al., Journal of Nuclear Materials 415 (2011) S1050

[Ennaceur 2000] M.M. Ennaceur, et al., Journal of Nuclear Materials 280 (2000) 33

[ITR-19-004] ITER Vacuum Handbook (ITR-19-004)

[Schmid 2023] K. Schmid, ITER Scientist Fellow, private communication

[Yoshikawa 2009] A Yoshikawa, Journal of Nuclear Materials 386–388 (2009) 367–370

[Matveev 2023] D. Matveev et al 2023 Nucl. Fusion 63 112014

[Wauters 2022] T Wauters et al 2022 Phys. Scr. 97 044001

[Park NF 63 2023] J.-S. Park et al., 2023 Nucl. Fusion 63 076027

[de la Cal PPCF 2006] E. de la Cal, Plasma Phys. Control. Fusion 48 (2006) 1455

[Lopez 2023] Data by Daniel López-Rodríguez, TOMAS team LPP-ERM/KMS

[96SPT4] Optimal number of anodes and gas feed points for boronization on ITER (96SPT4)

[Hagelaar 2014] G J M Hagelaar et al Plasma Phys. Control. Fusion 57 (2015) 025008

[Kogut 2014] D Kogut et al Plasma Phys. Control. Fusion 57 (2015) 025009

[Dibon 2021] M. Dibon, et al, Fusion Engineering and Design 165 (2021) 112233

[Saidoh 1993] M. Saidoh, et al., Fusion Engineering and Design 22 271 (1993) 271-275

[8YFSB3] Open issues in the new ITER baseline with a W wall for Q = 10 operation that require experimental assessment (8YFSB3)

[Part II: new baseline Outline IRP] Part II of this technical report

[Loarte 2021] A. Loarte et al 2021 Nucl. Fusion 61 076012

[Righi 1999] E. Righi et al, 1999 Nucl. Fusion 39 309

[Solano 2023] E.R. Solano et al 2023 Nucl. Fusion 63 112011

[Hillesheim 2018] J. Hillesheim et al, 2018 IAEA Fusion Energy Conf., India

[Binkenmeier 2023] G Birkenmeier et al 2023 Plasma Phys. Control. Fusion 65 054001

[Angioni 2023] C. Angioni et al 2023 Nucl. Fusion 63 126035 2023

[Schmidtmayr 2018] M. Schmidtmayr, et al 2018 Nucl. Fusion 58 056003

[Loarte 2016] A Loarte et al, IAEA Fusion Energy Conference, 2016, USA

[Wagner 2010] F Wagner et al, 2010 Plasma Phys. Control. Fusion 52 124044

[Gunn 2017] J.P. Gunn et al 2017 Nucl. Fusion 57 046025

[Schmid 2015] K Schmid et al Journal of Nuclear Materials 463 (2015) 66

[Eksaeva 2022] A. Eksaeva et al 2022 Phys. Scr. 97 014001

[Romazanov 2022] J. Romazanov et al 2022 Nucl. Fusion 62 036011

[Babenko 2020] P Yu Babenko et al 2020 Plasma Phys. Control. Fusion 62 045020

[Neu 2009] R. Neu et al., Phys. Scr. T138 (2009) 014038

[Kocan 2015] M. Kocan et al., Nucl. Fusion 55 (2015) 033019

[9CMZSM] A. A. Kavin et al, Preliminary results of design and simulation of 15MA hydrogen L-mode scenario with tungsten inboard limiter start-up using the DINA code (9CMZSM)

[3T4JWP] A. A. Kavin et al., 15 MA DT scenario satisfying new constraints on electromagnetic forces acting on Central Solenoid (3T4JWP)

[Hobirk 2023] J. Hobirk, Max-Planck Institut für Plasmaphysik, private communication

[33NHXN] Data for study of ITER plasma magnetic control (33NHXN)

[3LDS93] Limits on vertical (axial) forces acting on CS (3LDS93)

[Huber 2020] A. Huber, et al, Nuclear Materials and Energy 25 (2020) 100859

[Brezinsek 2019] S. Brezinsek et al 2019 Nucl. Fusion 59 096035

[Kaveeva 2020] E. Kaveeva et al 2020 Nucl. Fusion 60 046019

[Lukash 2017] V.E. Lukash 44th EPS Conference, 2017, United Kingdom

[Pitts 2007] R.A. Pitts et al 2007 Nucl. Fusion 47 1437

[9E6W92] Assessment of EM loads on blanket FWs 08 and 09 in case of extensive electrical shorting between fingers - Be and W tiles configurations

[Coburn 2022] J. Coburn et al 2022 Nucl. Fusion 62 016001

[Jepu 2019] I. Jepu et al. 2022 Nucl. Fusion 59 086009

[Ratynskaia 2023] “Metallic melt transport across castellated tiles”, submitted to Nuc. Fusion

[Landman 2009] Tokamak Code TOKES: models and Implementation, Forschungszentrum Karlsruhe report FZKA-7496 (2009)

[Pestchanyi 2017] S. Pestchanyi et al., Fus. Eng. Des. 124 (2017) 401

[Pitts 2023] R. A. Pitts et al., “TOKES simulations of first wall and divertor damage during unmitigated disruptions on ITER”, Proc. 29th IAEA Fusion Energy Conference, London, UK, 2023.

[Artola 2023] J. Artola et al., “Modelling of vertical displacement events in tokamaks: status and challenges ahead”, presented at 49th EPS Conference, Bordeaux, France, July 2023, paper I1.104. Submitted for publication in Plasma Phys. Control. Fusion.

[Chen 2022] L. Chen, et al., 25th Plasma Surface Interactions Conference, 2022 (7TUA3N).

Part II: Outline of the New Baseline Proposed Operation and Research Plan

Executive Summary

An outline of the ITER new baseline Operation and Research Plan is presented including the foreseen machine configuration, overall experimental strategy, key technical and experimental activities including those specifically target at risk retirement/mitigation. Preliminary time allocation for some of the activities is made on the basis of previous evaluations for the 2016 baseline ITER Research Plan and further follow-up studies in 2021-2023.

1. Introduction

The new baseline ITER Research Plan (NB-IRP) aims at demonstrating the Q = 10 Project Specification goal [Project Specification] within a reduced neutron fluence (~ 1% of the final Project Specification) minimizing technical and scientific risks as far as possible. It aims to represent a realistic plan to achieve the goals, i.e. not the best technically achievable strategy followed for the development of the 2016 staged approached baseline (2016-IRP), and to gradually retire risks to the achievement of the goal during execution.

The NB-IRP contains both the integrated commissioning phases preceding plasma operation as well as the plasma operational phases, as shown in Fig. 1-1. These are namely:

a) Integrated Commissioning I (IntCom-I) following completion of first (pre-AFP) machine assembly. This is divided into two parts including a First Plasma demonstration between them. Note that the specifications of the NB-FP need to be defined and they may not be the same as those for the 2016-FP;

b) Augmented First Plasma (AFP) including DD operation;

c) Integrated Commissioning II (IntCom-II) following completion of second (post-AFP) machine assembly;

d) DT-1 with up to 5 operational FPO campaigns (including 16 months of plasma operation and 8 months of shutdown and integrated commissioning) to the achievement of the Q = 10 goal, and;

e) A DT-2 phase with several operational FPO campaigns up to the achievement of the Project Specification goals including 16 months of plasma operation and 8 months of shutdown and integrated commissioning.

Note that between the end of DT-1 and the start of DT-2 there will be an additional assembly and an integrated commissioning phase whose details remain to be defined. These will depend not only on the DT-2 goals but also on the outcome of the DT-1 results on the possible upgrades required to meet these goals, as well as the licencing requirements to meet the DT-2 goals. The NB-IRP is represented in a schematic way in Fig. 1-1.

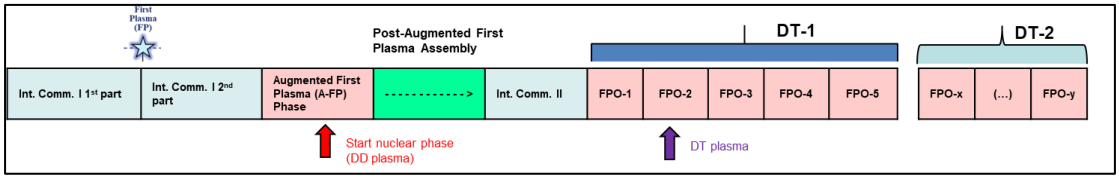

Figure 1-1. Schematic of the NB-IRP showing the integrated commissioning phases (in cyan with NB-FP at the end of the first part of IntComm I) and the operational campaigns (in red) for the various phases (AFP, DT-1 and DT-2). For completeness the post-AFP assembly phase, not part of the IRP is shown (in green).

2. Overview and rationale of the new baseline Research Plan and associated hardware configuration

In the NB-IRP, the scientific exploitation of ITER up to the achievement of the Project Specification goals is divided into three main phases: Augmented First Plasma, DT-1 and DT-2, each of which is preceded by an assembly and integrated commissioning phase. As mentioned above, the first two integrated commissioning phases are included in the IRP since they are intrinsically associated to the tokamak and ancillaries configurations that are required to demonstrate the AFP and DT-1 goals. The one for DT-2 is not included since there are uncertainties on the final configuration required.

The overall rationale of the NB-IRP is similar to that of the 2016-IRP with some important new scenario development elements, some of which result from the lessons learnt from the 2016-IRP and subsequent research:

- H-mode operation is explored as early as possible in DD plasmas. This and the increase of ECH power in AFP avoids the restricted operational space identified for H and He plasmas with W PFCs and the need for 1.8 T operation and the risks/additional hardware (gyrotrons) that this may entail (no ECH assisted start-up).
- Division of the DT programme into two phases: DT-1 programme focused on the achievement of the Q = 10 with low neutron fluence (~1% of the final Project Specification goal) and the DT-2 programme to address the remaining fusion power goals. The need to develop the DT-1 programme with low fluence impacts the strategy to develop the DT scenarios starting from DD, which is enabled by a higher level of additional heating power than in the 2016-IRP for the start of DD/DT operations.
- To develop, as far as possible, a realistic plan where risks are planned to be retired gradually with minimum impact on the programme. This is unlike the best technically achievable plan required for the 2016-IRP. These considerations can impact the time allocated to specific research activities in the NB-IRP compared to the 2016-IRP but also the machine and ancillary configuration required to achieve scientific objectives that are intrinsic to both IRPs. These goals and the associated machine and ancillary configuration for each operational phase are summarized below.

2.1 Augmented First Plasma

The main overall objective of this phase is to start ITER plasma operation and to minimize/retire risks for later NB-IRP phases. Key specific sub-objectives of this phase are:

- To commission control and protection systems with plasma up to 15 MA/5.3 T;
- To demonstrate disruption mitigation up to 15 MA/5.3 T;
- To develop plasma scenarios up to 15 MA/5.3 T in L-mode;
- To develop plasma scenarios up to, at least, 5 MA/2.65 T in H-mode with deuterium (DD) plasmas.
- To achieve these objectives the ITER device will be equipped with the following systems in this phase:
- A W first wall with inertially cooled in-vessel components.
- The water cooled W divertor;
- 40 MW of ECH heating from one equatorial and four upper launchers;
- 10 MW of ICH heating to demonstrate ICWC and to test ICH heating in a W environment;
- The Disruption Mitigation System;
- 4 pellet injectors for plasma fuelling and ELM control;
- The complete set of in-vessel coils and power supplies for both the Vertical Stability and ELM control coils;
- A large set of plasma diagnostics to provide the measurements required for plasma control and physics assessments;
- A boronization system to deposit boron films by glow discharge cleaning.

The main risks to be retired/mitigated in this phase concern those related to the commissioning of the control and protection systems with plasma and to disruption mitigation commissioning and demonstration. These can potentially lead to damage of the first wall components due to excessive power fluxes. Its impact on operation is minimized by using inertially cooled components for the areas where such damage is more likely thus avoiding water leaks. Other risks that will be retired/mitigated in this phase are those associated with water cooled W divertor operation (tests to ~10 MWm^{-2} will be carried out) and plasma operation with a W wall, in particular, those related to H-mode scenarios and ELM control for which DD plasmas are considered.

A successful completion of the AFP phase will demonstrate that ITER can reliably operate at its maximum plasma current and field (in L-mode) and in H-mode at reduced levels (5-7.5 MA/2.65 T) in DD plasmas marking the start of nuclear operation.

2.2DT-1

The main overall objective of this phase is to demonstrate routine Q = 10 operation with P_{fusion} = 500 MW and, at least 300 s burn, within a total neutron fluence of ~ 3 10^{25} neutrons. Key specific sub-objectives of this phase are:

- To commission control and protection systems with plasma up to Q = 10;
- To demonstrate disruption mitigation up to Q = 10;
- To develop plasma scenarios in DT up to 15 MA/5.3 T in H-mode (or lower current levels if Q = 10 can be demonstrated at those levels);

- To study the physics of burning plasmas and their integration with an all-W plasma facing component configuration;
- To address specific issues for the TBM development programme, including high repetition operation with $P_{fusion} \geq 250$ MW.

To achieve these objectives the ITER device will be equipped with the following systems in this phase:

- Fully water cooled W first wall and divertor;
- 67 MW of ECH heating from two equatorial and four upper launchers;
- 20 MW MW of ICH heating for ICWC and for ICH heating in a W environment (following successful tests in AFP with 10 MW);
- 33 MW of Neutral Beam Heating;
- The Disruption Mitigation System;
- 6 pellet injectors for plasma fuelling and ELM control;
- The complete set of in-vessel coils and power supplies for both the Vertical Stability and ELM control coils;
- A large set of plasma diagnostics to provide the measurements required for plasma control and physics assessments for DT burning plasmas;
- A boronization system to deposit boron films by glow discharge cleaning;
- Two ports equipped the first set of 4 test blanket modules (TBMs).

The main risks to be retired/mitigated in this phase concern those related to the commissioning of the control and protection systems with DT plasmas and to disruption mitigation commissioning and demonstration in DT plasmas up to (not all values to be achieved simultaneously) the highest: a) additional heating power into the plasma (~ 120 MW), b) fusion power (500 MW), c) plasma energies (350 MJ) and d) plasma currents (15 MA) that will be achieved in ITER. Note that in DT-2 the value of the fusion power could be increased up to 700 MW and plasma operation beyond 15 MA might be possible following the required authorization based on demonstration of acceptable loads on the vacuum vessel, as foreseen in the ITER INB creation decree [ITER INB Decree 2012].

To mitigate the consequences of the disruption risks associated with the presence of T in the plasma materializing while commissioning the DMS, a specific experimental time is allocated in hydrogen plasmas in the FPO-1 campaign. Other risks that will be retired/mitigated in this phase, based on progress in AFP, are those associated to DT plasma operation with a W wall, in particular, those related to H-mode scenarios, ELM control and plasma-wall interaction aspects with safety implications, namely in-vessel T retention and dust production.

A successful completion of the DT-1 phase will demonstrate that ITER can achieve burning plasmas with dominant alpha heating and that all required scenario integration and control issues can be maintained over time scales of 100’s of seconds. Besides a wealth of new knowledge on reactor scale DT plasmas and burning plasma physics, as successful DT-1 will provide key information on the required upgrades to the ancillaries in order to demonstrate the

DT-2 goals, as defined in the Project Specification and substantiated in the Project Requirements [Project Requirements].

2.3 DT-2

The main overall objective of this phase is to demonstrate routine operation in all ITER reference high Q scenarios addressing burning plasma physics, scenario integration issues and nuclear technology R&D, as defined in the Project Specifications and substantiated in the Project Requirements, up to the achievement of the Project Specification fluence goal. Some key specific sub-objectives of this phase can be defined with precision, while others related to R&D with focus on future demonstration reactors are subject to the experimental findings in the DT-1 and DT-2 phase themselves, as well as to the details of the licence to operate in DT-2:

- To commission control and protection systems required for the two Q = 5 ITER scenarios (long pulse and steady-state) to sustain high Q operation over their nominal burn lengths (1000s and 3000s, respectively);
- To develop long plasma scenarios in DT to, at least, Q = 5 for their nominal burn lengths (1000s and 3000s, respectively) and demonstrate the required current-drive capabilities;
- To study the physics of high Q plasmas, including current-drive and enhanced H-mode confinement, and their integration with an all-W plasma facing component configuration over timescales of ~ 1000's.
- To complete the TBM research and development programme;
- To explore the physics, integration and control aspects of Q > 10 plasmas up to 700 MW of fusion power;
- To address technology and plasma scenario development, control and integration issues for future DEMO reactors, such as: a) the determination of the minimum set of diagnostics and actuators required for high Q operation, b) the determination of the required heating and current drive mix, c) demonstration of the increased core radiation as solution to the power exhaust problem in DT plasmas, etc.

To achieve these objectives the ITER device will be equipped with the following systems in this phase:

- Fully water cooled W first wall and divertor;
- 67 MW of ECH heating from two equatorial and four upper launchers;
- 20 MW of ICH heating for ICWC and for ICH heating in a W environment;
- 50 MW of Neutral Beam Heating;
- The Disruption Mitigation System;
- 6 pellet injectors for plasma fuelling and ELM control;
- The complete set of in-vessel coils and power supplies for both the Vertical Stability and ELM control coils;
- A complete set of plasma diagnostics to provide the measurements required for plasma control and physics assessments for DT burning plasmas;

- A boronization system to deposit boron films by glow discharge cleaning;
- Two ports equipped the first set of 4 test blanket modules (TBMs).

The main risks to be retired/mitigated in this phase concern those related to the commissioning of the control and protection systems with DT plasmas and operation at high Q over very long timescales of 1000's of seconds. Of specific importance in this phase are the risks associated with high fast ion losses and inefficient current drive since these can impact the sustainment of high Q scenarios over very long timescales.

A successful completion of the DT-2 phase will demonstrate all ITER scientific and technical goals as per the Project Specification: "The goal of ITER is to demonstrate the scientific and technological feasibility of fusion power for peaceful purposes" and will provide a solid basis for the engineering and physics basis of future nuclear fusion reactors.

3. Integrated Commissioning I and Augmented First Plasma Phase

3.1 Integrated Commissioning II

The integrated commissioning phase follows the system commissioning phase when systems and services are commissioned individually. Once this commissioning is finalised, the systems are declared ready for integrated operations and the integrated commissioning phase can commence.

The Integrated Commissioning-I (IntCom-I) phase aims at preparing the tokamak for plasma operation and at demonstrating that the plant systems required for the AFP experimental programme perform as expected. This phase starts with the closure of the cryostat lid and its main objectives are to:

- Demonstrate no leaks (air, water, He, etc.) in the cryostat and vacuum vessel;
- Achieve the vacuum vessel base pressure to enable plasma operation;
- Achieve the cryostat base pressure to enable Magnets energisation;
- Perform wall conditioning for reduction of impurities necessary for plasma operation;
- Perform the magnets energisation to full performance;
- Commission all safety and protection functions required;
- Commission/calibrate diagnostics;
- Demonstrate conventional control of the plant and systems;
- Demonstrate that the plant operates in a secure and safe way (protection and safety functions as required for this phase);
- Demonstration of the integration of all systems contributing to NB-FP demonstration
- First Plasma demonstration (NB-FP).

Note that the specifications for NB-FP need to be developed and they may not necessarily coincide with those of the 2016-FP.

The machine configuration for IntCom-I will have temporary inertially cooled W plasma facing components, the shield blocks and the W divertor. The IVC coils will also be installed, ready for commissioning. Pressure tests of the first wall and divertor cooling system and flow balance, if required, will be performed during this phase in preparation for the AFP phase where

we already expect significant power fluxes on the divertor and wall. A NB-FP will be performed at B_T = 2.65 T or 5.3 T that will show the capability to execute basic tokamak plasma operation. In Int.Com-I superconducting coils will be energised to full current (TF will reach B_T = 5.3 T) and other commissioning activities will be completed such as for the ICH, DMS, etc. The following major activities are to be executed during IntComm-I:

Main magnet commissioning: In addition to the Magnets HV tests, the Paschen tests for the Magnets are also planned for this phase. Two sets of tests are being considered: (1) with the coils at room temperature (similar to those done at JT60-SA) and (2) with the coils at cryogenic temperature. At this stage, the plan for these tests is still being developed and 1 month is assigned to each test. This duration does not take into account the need for repairs as a result of these tests.

Wall and vacuum conditioning: The strategy for wall conditioning includes the specific need for boronisation as an O getter with W PFCs in AFP. The wall conditioning sequence (baking + GDC in H) is performed after cooldown to achieve the necessary wall conditions for A-FP attempt. This may require the use of the boronisation process (foreseen to be performed with the GDC system in H, He and D) which needs to be tested beforehand.

The ICH antenna will be available for the purpose of ICWC to be developed during AFP. Hence, the baking of the ICH antenna is to be performed during Int-Com-I in parallel with the wall conditioning activity but the completion of commissioning of the antenna (matching configuration, multi-pactoring, etc.) will be performed in AFP.

Key system operations commissioning in preparation for plasma operation: In parallel with the commissioning of pulsed systems (ECH, ICH, GIS, FPIS and the superconducting coils (except the TF coils)), the functionality of the pulse schedule and the control through PCS will be demonstrated. Protection and Safety functions (CIS, CSS) will be commissioned as required.

The following systems will be commissioned during IntCom-I in parallel with the major activities as much as possible. For some activities the commissioning might continue during the AFP phase:

- IVC coils (ELM and VS3) – Dedicated time for the commissioning is included in the schedule.
- ECH launchers (40MW of power installed) – The commissioning of the ECH system will be performed prior to integrated commissioning, i.e. during system commissioning, followed by a phase of plasma commissioning during AFP.
- ICH system (10 power installed for ICWC and ICH tests) – commissioned up to the matching of the antenna impedance. The commissioning for demonstration of power injection into the VV will be performed during the AFP phase.
- DMS – commissioning to be performed in parallel with a major activity
- Four Fuelling Pellet injectors – commissioning to be performed in parallel.
- Diagnostics – most of the commissioning activities such as calibration and alignment are performed before integrated commissioning during the assembly phase. If required to be performed during IC these are assumed to be possible in parallel with any major

activity. The dry runs required by some diagnostics to finalise their commissioning will be performed in parallel with the phase “Preparation for Plasma”. The commissioning of specific diagnostics such as magnetics is performed in parallel with the systems required for their commissioning, i.e., the magnetics commissioning is performed in parallel with the Magnets.

- Tritium Plant – Commissioning of the Gas compound for di-borane supply, the fuel processing system for exhaust connected to the definitive stack and the SQRS system for recycling of DD and trace T.

The Int-Com-I commissioning targets for AFP are listed in Table 3.1-1.

System	Targets
Vacuum	VV base pressure ~10^{-5}Pa VV Leak rate 10^{-7}Pam^3/s (or higher if still ok for FP demonstration) Cryostat base pressure ~10^{-4}Pa
Cryo-systems	Cryopumps at cryogenic temperature Superconducting Magnets at 4.5K Thermal Shields at 80K
TF coils	5.3T demonstrated. TF@2.65T for start of AFP
Plasma current	Demonstrate first plasma initiation at 2.65T
Diagnostics	Available and calibrated w/o plasma
ICH	Matching configuration performed ready for multipactoring and voltage increase in AFP (~65 days)
ECH	Available for breakdown assist
GIS	Available
Pellet injector	4 pellet injectors available when required for plasma operation
DMS	DMS injectors functional when required for plasma operation
Plasma Operation	Tokamak ready for plasma operation (AFP)
CIS functions	As required
CSS functions	As required
Boronisation	Boronisation Diborane

Table 3.1-1. Commissioning targets for start of AFP

3.2 Augmented First Plasma

The Augmented First Plasma phase has similar overall objectives to those of the PFPO-1 [PFPO-1] and PFPO-2 [PFPO-2] phases of the 2016-IRP. There, are however, key differences between the AFP NB-IRP phase and the PFPO1+PFPO-2 2016-IRP phases both in tokamak + ancillaries configuration beyond the choice of wall material (compared to 2016-IRP PFPO-2) and in the experimental programme. Most of these major differences are targeted to the mitigation and retirement of risks in a more efficient way than in the 2016-IRP:

- The heating mix which is optimized for operation with a W wall. This includes 40 MW ECH and 10 MW ICH, for tests;
- The inclusion of DD plasma operation (up to a total fluence of 1.5 10^{20} neutrons) while maintaining in-person access for assembly post-AFP. This allows early H-mode operational experience in a more robust way and easier to transfer to DT, compared to H/He plasmas and impacts the required additional heating power level and the length of the DD campaign;
- The use of inertially-cooled wall first panels/limiters to minimize the impact of damage by plasma operation during this phase.

Other smaller differences between AFP and the original PFPO-1 + PFPO-2 concern:

- The foreseen diagnostic set, which does not include active charge-exchange diagnostics, since neutral beams injectors will not be available;
- The increase of commissioning time for diagnostics with plasma to account for the need of plasma current reversal to commission the diamagnetic loop;
- The increase of the time for some ECH commissioning activities with plasma to account for the increased level of power/gyrotrons in AFP;
- A reduction of the time for ICH commissioning with plasma given the fact that only one antenna is included in the baseline;
- The target duration of the high heating diverted phase (P_{ECH} = 40 MW) to 50s compared to 100s in PFPO-2. The length of this phase is limited by the power handling capability of the inertially cooled components and 50s is the design guideline for high levels of core radiation. For lower radiation levels this duration will be determined by the capability of the ECH system to sustain pulses longer than 50 s in AFP;
- The need for boronization to achieve low impurity vacuum conditions required for operation with a W wall.

We note that the time required and the need for some of these activities were already identified in the context of the work done in 2022 to optimize the 2016 IRP and staged approach baseline schedule.

For the time allocation, the same principle followed for the development of the 2016 IRP is adopted:

- ITER operations are divided into two-weeks blocks with twelve days of two shifts/day dedicated to the experimental exploitation followed by two-days of short maintenance in which boronization by GDC can be applied, when needed;

- Completion of commissioning activities that may not have been fully completed by IntCom-I will be carried out in parallel with the experimental programme, when the affected system is not required or its commissioning does not impact plasma operation, or during the night shift and short maintenance days, when required for operations or when commissioning is not compatible with operations;
- It is assumed that on average 13 pulses per two shifts/day contribute to the IRP. This does not mean that all the pulses achieve the targeted objectives but that the measurements acquired are of appropriate quality for the progress of the IRP. The difference between the theoretical maximum number of pulses in two-shifts of 32 (one pulse every 30 minutes) and 13 pulses comes from the estimated availability of ITER systems, operational time lost to recover from disruptions/application of the DMS, failed start-ups, plasma discharges that are too short to contribute to the IRP, etc. These are the same assumptions as in the 2016 IRP.

It should be noted that, as adopted for the 2016 IRP, the allocation of time for commissioning time for systems with plasma (e.g. pellets, ECH and ICH) concerns dedicated plasma discharges (in operational days) to the commissioning of these systems. In addition to this, it is expected that significant commissioning of the systems will take place parasitically to plasma operations (e.g. by having some part of the discharge for tests) not interfering with the main goals of the experimental programme, as it is the case in present fusion experiments.

The total time required for the achievement of the AFP goals is presently estimated to be 670 operational days, which corresponds to 26 months of operation. This includes 10 days reserved at the end of the campaign for tests of the coils with Nb_3Sn conductors to monitor degradation, if needed.

A short description of the activities of the outline AFP plan and their logic is provided below.

- Plasma start-up and limiter phase optimization

Based on the NB-FP scenario used for demonstration during IntCom-I, AFP will commence with the optimization of plasma start-up and limiter phase at 2.65T. Later in the AFP campaign also start-up at higher fields than 2.65 T will be developed. During the initial phase of AFP, plasma operation will be limited on the W protective elements and this poses specific challenges related to plasma-wall interactions and resulting plasma radiation that may not be addressed in the NB-FP IntCom-I demonstration, if this remains limited to very low plasma currents (i.e. demonstration of hydrogen ionization but not of burn-through with W limiters). While plasma start-up and limiter phases have been demonstrated in many tokamaks operating with W wall PFCs, the W influx during this phase can lead to large radiative losses and to the radiative collapse of the plasma discharge. Optimization of the plasma density/low-Z radiation levels, ECH heating power level, etc., is used in present experiments to overcome these issues and these approached will be explored in AFP. Specific time is, thus, reserved in the AFP campaign to perform this optimization in ITER.

- Plasma scenario development and basic control

These activities concern the commissioning with plasma of the basic schemes for plasma control (plasma shape and position, vertical stability, etc.) and the development of L-mode

scenarios up to 15 MA/5.3 T. The expansion of the operational space in L-mode will be performed in steps and sequential with the availability of the systems required (e.g. diagnostics, ECH). The commissioning of these systems is interleaved with scenario development with specific dedicated time (see below) and also parasitic time in parallel with the experimental programme.

The AFP L-mode development programme contains the following blocks:

1. Development of L-mode plasmas in hydrogen and deuterium up to 7.5 MA/2.65 T and 40 MW of ECH.
2. Development of L-mode plasmas in hydrogen up to 15 MA/5.3 T and 40 MW of ECH.

The two blocks will not be implemented consecutively since DD H-mode experiments will be carried out once the capability to operate at 7.5 MA/2.65 T with 40 MW of ECH is demonstrated. This allows the decay of radiation levels after DD operation, to enable hands-on work inside the vessel after AFP, while the second phase of L-mode development takes place. We note that the 2016-IRP included hydrogen and helium L-mode development up to 7.5 MA/2.65 T; in AFP the helium development is substituted by deuterium which is more alike hydrogen than helium.

The successful execution of this programme should retire the risks associated with basic plasma control up to 15 MA/5.3 T in L-mode plasmas with a W wall and divertor. The choice of inertially cooled protective elements for the wall) facilitates retiring these risks without major consequences for the experimental programme (i.e. in-vessel water leak from the first wall). We note that the expected power loads in the divertor during this phase can reach up to 10 MWm^{-2}. While these loads are sufficient to assess the performance of the divertor targets for power exhaust they are unlikely to exceed its design capabilities.

- Disruption Management

This set of experiments will be interleaved with scenario development and aim at: a) validation of disruptions loads (chiefly electromagnetic loads to the vacuum vessel and in-vessel components), b) commissioning and optimization of disruption prediction and detection and c) commissioning and optimization of disruption mitigation. The experiments will cover the range of scenarios in AFP, namely L-mode plasmas in hydrogen up to 15 MA/5.3 T with 40 MW of ECH power and deuterium H-mode plasmas up to, at least 5 MA (target 7.5 MA)/2.65 T with 40 MW of ECH.

The successful execution of this programme should either retire risks associated with disruptions and disruption mitigation or consolidate the first steps towards their retirement:

- Regarding disruption load validation it is expected to obtain measurements of disruption loads up to L-mode plasma current levels that avoid melting of the first wall and divertor during the current quench vertical displacement of the plasma. For upwards vertical movements, this is evaluated to be ~ 11 MA for the W wall. A comparison of such loads between L-mode and H-mode will be performed in the current range of 5-7.5 MA. Obtaining measurements of disruption loads up to a current as close as possible to 15 MA ensures a good validation of the disruption and electromagnetic mechanical

models of the VV; this was limited to < 7 MA for a Be wall to avoid melting. We note that for upwards VDEs, since the plasma will interact with inertially cooled components, end of campaign experiments could be performed with I_p > 11 MA in which melting of such components could be considered, if the foreseen loads are acceptable and such additional experiments are required to refine load validation.

- Regarding disruption prediction and detection it is expected to validate models to predict disruptions in order to develop avoidance operational strategies. Similarly, the models to detect disruptions, required for an efficient application of the DMS will be validated and used. Both these activities should minimize the occurrence of disruptions and enhance the mitigation of its effects over the range of scenarios developed in AFP.
- Regarding disruption mitigation it is expected that the risks associated with disruption mitigation will be retired for the scenarios explored in AFP, namely hydrogen L-mode plasmas up to 15 MA/5.3 T with 40 MW ECH power and 5-7.5 MA/2.65 T in deuterium H-modes with 40 MW of ECH power. This will be done without compromising the water cooled divertor and with no significant impact to the experimental programme. To achieve it, the in-vessel vertical stability coils will be used to ensure that the plasma moves upwards following the application of DMS so that the energy that is not radiated during the current quench due to non-optimized disruption mitigation and/or formation of runaway electrons is deposited on the inertially cooled ones. This cannot be guaranteed in ITER by passive means since, as shown in Fig. 3.2-1, the plasma can drift upwards or downwards towards the divertor during the CQ depending on the degree of l_i flattening during the TQ and the rate of current decay in the CQ. Ensuring that the plasma moves upwards onto the inertially cooled W wall components, requires the voltages in the in-vessel vertical stability coils to increase to its maximum value 10-25 ms in advance of the current quench, as shown in Fig. 3.2-2. Such anticipation can be ensured for the DMS commissioning experiments themselves and does not appear to be very challenging for the activation of the DMS by disruption detection schemes; for ITER's DMS a warning time of 50 ms is foreseen in its design.

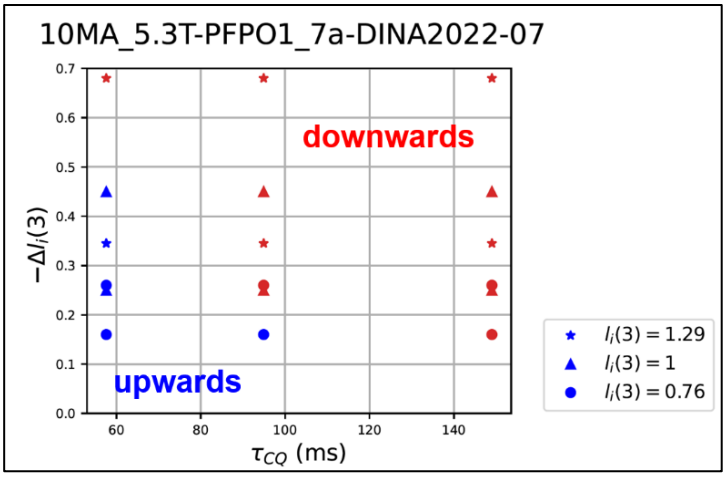

Figure 3.2-1. Plasma movement direction modelled by JOREK following the TQ for a 10 MA/5.3 T L-mode depending on the plasma l_i, the change of l_i at the TQ and the CQ time.

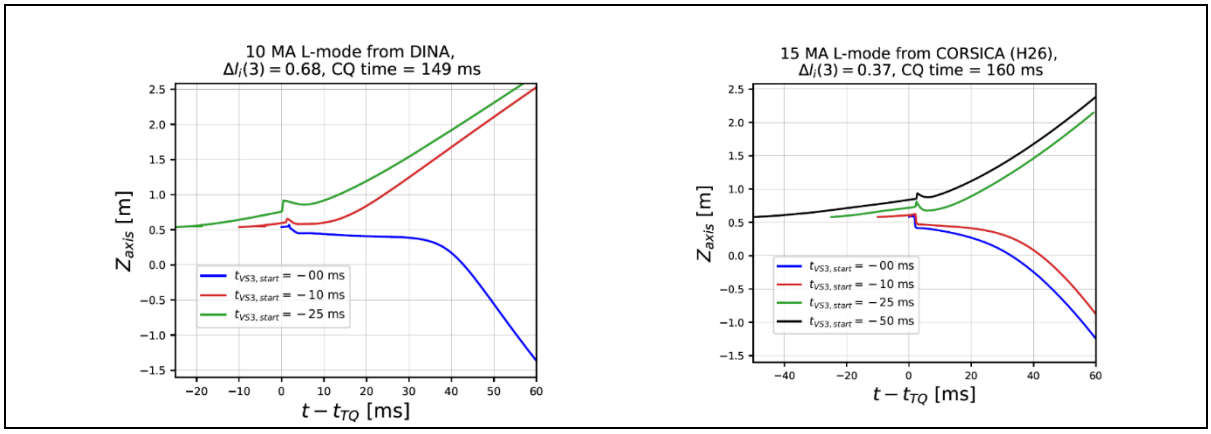

Figure 3.2-2. Plasma movement direction modelled by JOREK including the application of maximum voltage to the VS3 system to promote upwards movement of the plasma during the CQ: a) 10 MA/5.3 T L-mode plasma, b) 15 MA/5.3 T L-mode plasma. Note that t = 0 corresponds to the TQ and the start of the CQ.

Of particular importance (and difficulty) is the mitigation of TQ and CQ disruption loads by the DMS while avoiding runaways to be generated, as well as the mitigation of runaway loads once runaways are formed. In this respect, the tests of the DMS RE mitigation function in AFP should be as complete as possible regarding the processes that dominate RE formation in DT-1, to effectively retire as far as possible such risks in AFP, namely the runaway avalanche gain and the initial runaway seed. The first factor can be thoroughly explored by extending disruption mitigation to 15 MA plasmas, since the runaway avalanche gain scales as $G_{RE} \sim \exp(I_p)$. For the second factor, the main runaway seed mechanisms for DT-1 are expected to be hot-tail, tritium beta decay and Compton electrons [Martín-Solís 2017]. The last two mechanisms are exclusively relevant to T-containing plasmas and with high fusion power production and cannot, therefore, be addressed in AFP. However, the hot-tail mechanism is driven by hot-electrons that remain in the plasma after the TQ. This can be conclusively explored in AFP by applying disruption mitigation to plasmas with electron temperatures similar to those expected in high Q plasmas in DT-1, namely central electron temperatures ~ 20 keV. These can be achieved by high ECH power heating of hydrogen L-mode plasmas at 15 MA, or lower current H-mode plasmas in deuterium as shown in Fig. 3.2-4. Optimization of the DMS for disruption mitigation of 7.5 MA/2.65 T H-mode DD plasmas and with 15 MA/5.3 T in L-mode can thus be carried out to assess the RE mitigation function of the DMS with a high Q relevant hot-tail seed in AFP and retire this risk.

Simulations with the DREAM code framework [Hoppe 2021] of disruption mitigation in 7.5 MA/2.65 T AFP DD H-mode plasmas show that, depending on the timescale of the TQ and the degree of penetration of the shattered pellet shards into the plasma before they trigger the TQ, the optimum injection of shattered pellets for disruption mitigation and minimum RE production varies, as shown in Fig. 3.2-3. This, together with the inertially cooled in-vessel components and displacement of the plasma upwards during the current quench mentioned above, allows the optimization of the DMS mitigation strategy in AFP (SPI configuration, pellet composition, etc.) to obtain favorable TQ conditions for RE avoidance and, thus, retire

the hot tail RE risk for DT-1, while avoiding a major impact to the subsequent experimental program (e.g. a water leak).

As shown above, compared to the 2016-IRP the major differences in the area of disruption management in the NB-IRP compared to the 2016-IRP do not concern the foreseen activities and objectives in AFP compared to PFPO-1+PFPO-2 in 2016-IRP but the significant increase in certainty that these can be achieved without major impact to the operational campaign (e.g. a water leak) because of the use of W as first wall material and the installation of inertially cooled components on the wall which is subject to the largest thermal and runaway loads.

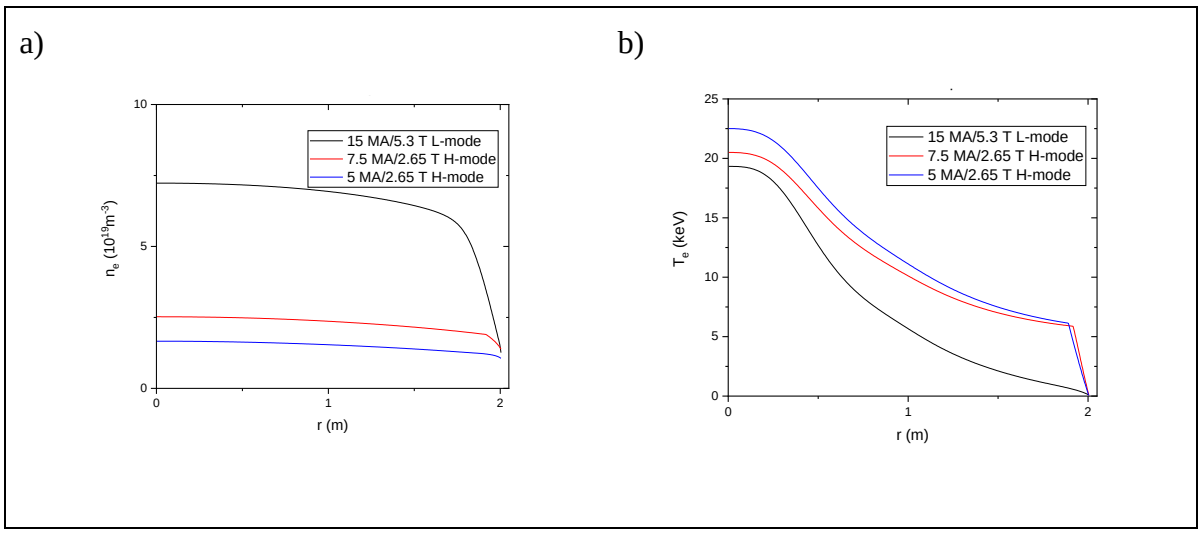

Figure 3.2-3. AFP 5 MA/2.65 T, 7.5 MA/2.65 T DD H-mode plasmas and 15 MA/5.3 T L-mode plasmas with 40 MW ECH: a) Density profiles modelled with ASTRA and b) Electron temperature profiles modelled with ASTRA.

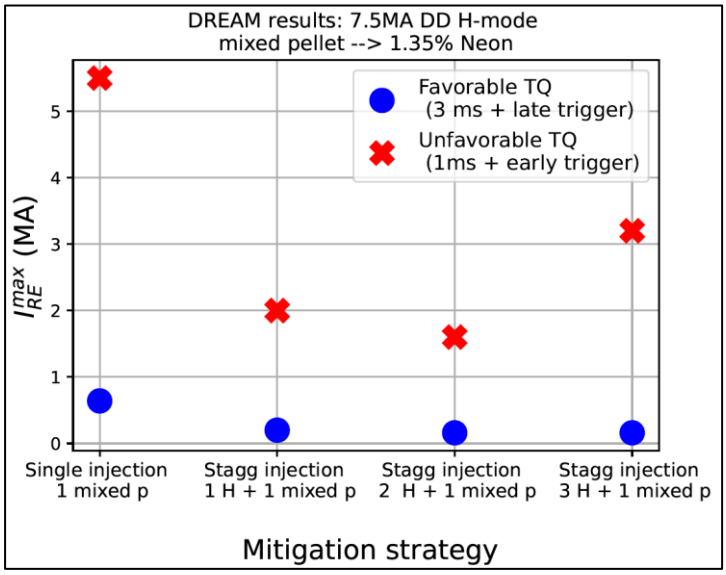

Figure 3.2-4. RE produced by the application of DMS to an AFP 7.5 MA/2.65 T DD H-mode plasma with 40 MW ECH depending on the TQ time and the triggering of the TQ by the shattered pellet injection (late TQ trigger = higher penetration of shards into the plasma when

the TQ is triggered and early trigger = the TQ is triggered when shards arrive at the q = 2 surface). The mitigation strategy considers four cases: a) a single pellet with H_2+Ne mix, b) an initial H_2 pellet followed by one pellet with H_2+Ne mix, c) two H_2 pellets followed by one pellet with H_2+Ne mix and d) three H_2 pellets followed by one pellet with H_2+Ne mix.

- Commissioning of auxiliary systems

The foreseen activities follow closely those identified in the 2016-IRP for the ECH system (adjusted to the increased number of gyrotrons) and the ICH system and the diagnostic systems. Note that for ICH this includes the studies of coupling in hydrogen L-mode and deuterium H-mode plasmas as well as assessments of the resulting W contamination of the main plasma due to ICH-generated impurities from the W wall, the latter was not considered in the 2016-IRP.

Another important difference with respect to the 2016-IRP, concerns the increased time allocation to the activities relative to the reversal of the plasma current. The activities to commission diagnostic with plasma include operation with I_p in the counter-clockwise direction, to be compared with the reference I_p clockwise direction, which is possible for plasma discharges limited on the high field side (HFS) first wall panels. This is required for the calibration of the Diamagnetic Loop (55.AF), to obtain the coupling between the plasma current and the diamagnetic loop, which is necessary for the calculation of the plasma stored energy and beta, and the time allocated to it was not accounted for correctly before.

Since all power supply circuit components (converters, DC busbars, make switches, FDUs) for PF and CS coils are four quadrants operational (bi-directional current), the only changes that need to be made to the coils power supplies concern the Switching Network Units for PF1, PF6 and all CS modules. This is foreseen in the design of the SNUs through changes in the connection of mechanical links. The change of these links is evaluated to require 1 day per change of I_p direction, including measurements of contact resistance on the re-connected mechanical links. In addition, it is required to re-commission the PCS, CIS and CSS to operate with reversed I_p, to establish plasma operation with HFS limiter plasmas with reversed I_p and to perform a range of plasma discharges up to the maximum current compatible with the power handling capabilities of the HFS FWPs. This has to be followed by the inverse sequence to re-stablish operation with the reference I_p clockwise direction. Since this will be the first time that such reversed I_p operation will be performed at ITER, on the basis of similar experience in existing tokamaks, the above sequence is evaluated to require three weeks. Therefore, the overall time allocated to all activities related to diagnostic commissioning with plasma in the AFP is 24 operational days which corresponds to 4 weeks.

- Commissioning of advanced control functions

This includes a wide range of activities such as error field identification and control, kinetic control, development of termination scenarios, exception handling, shared actuator management, etc. In general the activities are similar to those previously identified for PFPO-1+PFPO-2 in the 2016-IRP but have to be adjusted to the machine configuration considered for AFP in NB-IRP (e.g. ECH + ICH only). This implies that some activities such as error field identification and correction with TBMs, NBI shine-through protection, etc., have to be carried over to DT-1.

- Divertor and PWI studies

This includes activities related to the characterization of limiter and divertor power loads, the development of control schemes for divertor power loads, the characterization of disruption thermal loads as well as activities related to wall cleaning and fuel retention. In general the activities are similar to those previously identified for PFPO-1+PFPO-2 in the 2016-IRP but have to be adjusted to the fact that the high field side limiters are inertially cooled and that the wall material is W with boron being applied to improve vacuum conditions. Of particular importance in these studies will be the change over from hydrogen to deuterium for H-mode experiments and back to hydrogen. This will enable the first accurate determination of in-vessel fuel retention and removal effectiveness in an all-W ITER environment, the validation of the Tritium Monitor measurements, and will provide the initial confirmation of the basis for the evaluations of tritium retention in DT-1. Similarly, all along the AFP campaign, measurements of dust production will be done with the Dust Monitor supported by erosion measurements and the analysis of first wall samples after the AFP campaign.

- H-mode studies at 2.65 T

This includes the development of H-mode scenarios in deuterium plasmas with up to 40 MW of ECH at 2.65 T and a plasma current ~ 5 - 7.5 MA. The experiments will identify the H-mode threshold and of the power required to operate in Type I ELMy H-mode with high pedestal pressure for currents up to 5 MA and its further expansion to 7.5 MA. The choice of 5 MA as the initial target for the plasma current level is because up to this current level melting of the divertor monoblock edges by ELMs is not expected. Once the 5 MA H-mode scenarios are developed, or if needed for its development, ELM control by pellet injection and by 3-D fields will be applied. This is expected to be required in the subsequent steps to 7. 5 MA.

If it is found that the impact of wall generated W influxes is significant in such H-mode plasmas, the development of such scenarios could start with a large wall clearance that is gradually reduced as described in Part I: Consequences of Changing First Wall Material in ITER]. H-mode scenarios at these low current levels can be maintained stable at large wall clearances with the use of the in-vessel vertical stability coils. Modelling of ELM control by 3-D fields shows that a similar level of X-point displacement (which is experimentally correlated with large ELM mitigation/suppression) can be maintained as the wall clearance is increased i the current level in the ELM control coils is double. This should be possible since the expected level of current in the ELM control coils for ELM suppression scales with the plasma current and the coils are designed for 90 kAt operation at 15 MA. In addition, the value of the plasma current needs to be tuned to ensure that the q_{95} falls within the windows that provide maximum X-point displacement for each wall clearance, as shown in Fig. 3.2-5 (namely 4.7 MA for the configuration with large outer gap, 4.9 MA for the configuration with increased overall clearance and that with the nominal ITER separatrix for 15 MA Q = 10 operation). We note that the development of such H-mode scenarios with large outer gaps to the wall is only possible with ECH heating, since ICH coupling with such large distances between the plasma and the antenna is expected to be very poor.

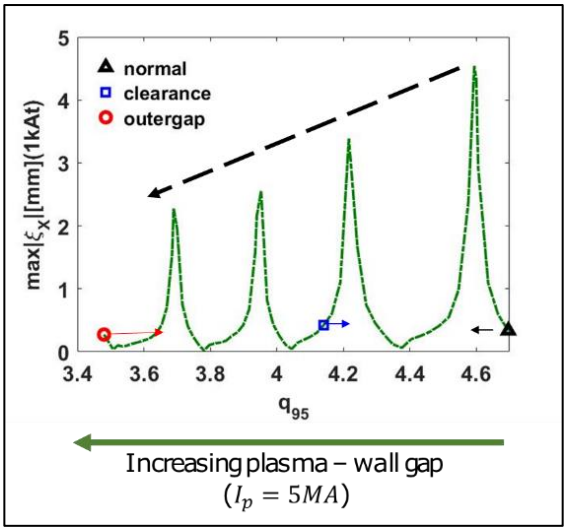

Figure 3.2-5. Modelled X-point response in mm per kAt in the ELM control coils showing the change in q_{95} of the resonant windows when the wall clearance is increased. A reduction of a factor of 2 is found from the nominal configuration to that with an outer wall gap of 45 cm.

The duration of these experiments is estimated to be ~ 3 operational months. In these months the total neutron production will be limited to 1.5 10^{20} neutrons to allow in-vessel access for post-AFP, after decaying for ~ 8 months of further hydrogen experiments. This production rate and the operational time is found to be consistent since the neutron production in these ECH heated H-modes is low because of the low ion temperature that results from the low equipartition and also from the increased turbulence with $T_e >> T_i$ identified already for 2016-IRP PFPO-1 H-modes [Loarte 2021], as shown in Fig. 3.2-6.

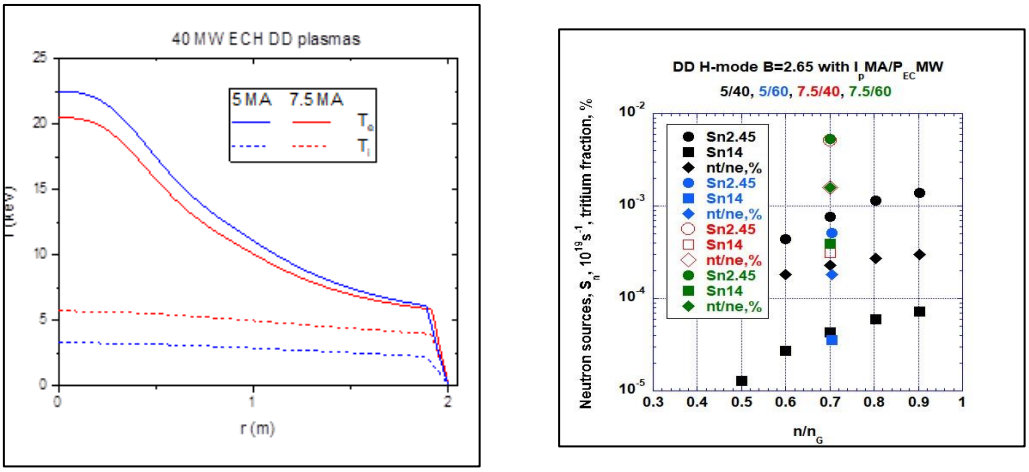

Figure 3.2-6. (Left). Electron and ion temperature profiles for two DD H-modes heated with 40 MW ECH and <ne> = 0.5 n_{GW} with plasma currents of 5 and 7.5 MA. (Right) Modelled neutron production (DD, DT) and T production rates for DD H-mode plasmas with 40/60 MW ECH.

4. Integrated Commissioning II, DT-1 and DT-2

4.1 Integrated Commissioning I

Similar to IntCom-I, this phase follows the assembly phase II (AP-II, post-AFP) where the new installed systems will be commissioned with services and declared ready for operations. This phase starts with the end of the AP-II phase and its main objectives are to:

- Demonstrate no leaks (air, water, He, etc.) in the cryostat and vacuum vessel;
- Achieve the vacuum vessel base pressure to enable plasma operation;
- Achieve the cryostat base pressure to enable Magnets energisation;
- Perform wall conditioning for reduction of impurities necessary for plasma operation;
- Perform the magnets energisation to full performance;
- Commission all safety and protection functions required;
- Commission/calibrate diagnostics;
- Commission the additional heating systems, ready for plasma commissioning;
- Demonstrate conventional control of the plant and systems;
- Demonstrate that the plant operates in a secure and safe way (protection and safety functions as required for this phase).

The water-cooled First Wall (FW) panels will be installed in AP-II and new systems are available such as HNB in H, diagnostics, one more ECH equatorial launcher, etc. The commissioning of the additional heating systems (HNB and ICH) is rather lengthy and it will require good co-ordination between all the phases (assembly, system commissioning, integrated commissioning and possibly, plasma operation). In this plan, the re-commissioning of ICWC will be performed during the STM days (2 days every two weeks of operation).

In parallel with the commissioning of HNB, the functionality of the pulse schedule and the control through PCS will be demonstrated. Protection and Safety functions (CIS, CSS) will be commissioned as required.

In addition to all systems to be re-commissioned from IntCom-I, the following new systems available will be commissioned:

- TBS – the commissioning activities for the TBS system are included, but their commissioning plan is not yet known in detail. For the purpose of preparing the schedule below, the commissioning of the TBSs is divided into three phases with *Baking of the VV* serving as the pivot activity. These phases are represented as a time interval limited by specific activities, which ensures that the TBS commissioning does not become the critical path for the integrated commissioning activities. It is expected that most activities related to the TBS system can be performed in parallel with the activities identified and thus have no impact on the schedule duration. However, confirmation of this expectation and the definition of the required length for the TBS integrated commissioning activities depends on the detailed design and commissioning requirements of the TBS.

- Diagnostics – most of the commissioning activities such as calibration and alignment are performed before integrated commissioning during the assembly phase. If required to be performed during IC these are assumed to be possible in parallel with any major activity. The dry runs required by some diagnostics to finalise their commissioning will be performed in parallel with the phase "Preparation for Plasma". The commissioning of specific diagnostics such as magnetics is performed in parallel with the systems required for their commissioning, i.e., the magnetics commissioning is performed in parallel with the Magnets.
- ECH (67MW of power installed) –. Similar to IntCom-I, the commissioning of the ECH system will be performed prior to integrated commissioning, i.e. during system commissioning, followed by a phase of plasma commissioning during DT-1.
- ICH (upgrade to 20MW of heating power in DT-1) – Fully commissioned, ready for plasma commissioning in DT-1 to the available power.
- HNB 1 and 2 – The HNB HV tests are performed during the assembly phase. The HNB commissioning to full voltage will be performed in H ready for plasma commissioning in DT-1.
- Protection and safety functions are commissioned as required.

The commissioning targets for DT-1 are listed in Table 4.1-1.

System	**Targets**
Vacuum	VV base pressure ~10^{-5}Pa VV Leak rate 10^{-7}Pam^3/s (or higher if still ok for FP demonstration) Cryostat base pressure ~10^{-4}Pa
Cryo-systems	Cryopumps at cryogenic temperature Superconducting Magnets at 4.5K Thermal Shields at 80K HNB cryopumps at cryogenic temperature
TF coils	5.3T demonstrated (at 2.65T to start DT-1)
Plasma current	No requirement
Diagnostics	Available and calibrated w/o plasma (list available)
ICH	Ready for commissioning with plasma
ECH	Available for breakdown assist and commissioning with plasma
GIS	Available

Pellet injector	Available
DMS	All DMS injectors functional
Plasma Operation	Dry runs in preparation for plasma, pulse schedule available, PCS ready for plasma
CIS functions	As required (functions TBD)
CSS functions	As required (functions TBD)
Boronisation	Boronisation Diborane
HNB	Ready for plasma commissioning in DT-1 (H)

Table 4.1-1. Commissioning targets for start of DT-1

4.2 DT-1

The objective of DT-1 is the demonstration of reproducible Q = 10 operation for burn times of, at least, 300 s as per the Project Specification within a total neutron fluence of ~ 3 10^{25} neutrons. The objective of DT-1 itself is similar to that of the FPO-1 plus the initial part of the FPO-2 campaign in the 2016-IRP. However, there are significant differences regarding the configuration of the ITER tokamak and ancillaries. These, as well as the neutron fluence budget, lead to the NB-IRP deviating considerably from the 2016-IRP.

Concerning ITER tokamak configuration for DT-1 the following points need to be considered:

- The complete water cooled W first wall will be operational for the first time in DT-1;
- The ICH antenna will be upgraded to 20 MW in DT-1, following confirmation of acceptable impact on W impurity contamination, thus providing the capability for high power ICH heating for DT-1 plasmas;
- The ECH system will be upgraded to 67 MW in DT-1 with an additional equatorial launcher (20 MW) and 7 MW additional MW in the upper launchers;
- TBMs will be installed in two ports for the first time;
- The diagnostic set will be increased significantly to include those based on active charge exchange as well as those required for the control of DT-1 plasmas and the experimental programme.

These, together with the retirement of the risks related to the RE associated with tritium operation, call for an operational period in hydrogen to be included at the beginning of FPO-1. This is followed by the development of DD and DT H-mode scenarios to the demonstration of the Q = 10 goal.

Since the Q = 10 goal has to be demonstrated with a relatively low total neutron fluence, the development of H-mode scenarios from those demonstrated in AFP (5-7.5 MA) up to Q = 10 is foreseen to be carried out in DD plasmas first and then in DT, starting from low levels of T (~ 10 %) up to the optimum DT mix for high fusion power (~ 50%). This is enabled by the higher level of heating power (33 MW of NBI, 67 MW of ECH and 20 MW of ICH assuming

this level of power will be available in the initial campaigns of DT-1). It is expected to be able to operate DD H-modes up to 12.5 MA for heating power levels of ~ 100 MW.

The operational ranges for DD and DT H-mode plasmas have been evaluated using the experimental guidance for H-mode sustainment ($P_{sep} \geq 1.5\ P_{LH}$ and $0.25 \leq P_{rad}^{core}/P_{heat} \leq 0.5$), including the isotopic effect of T on the L-H transition, as shown in Fig. 4.2-1; more details can be found in [Part I: Consequences of Changing First Wall Material in ITER].

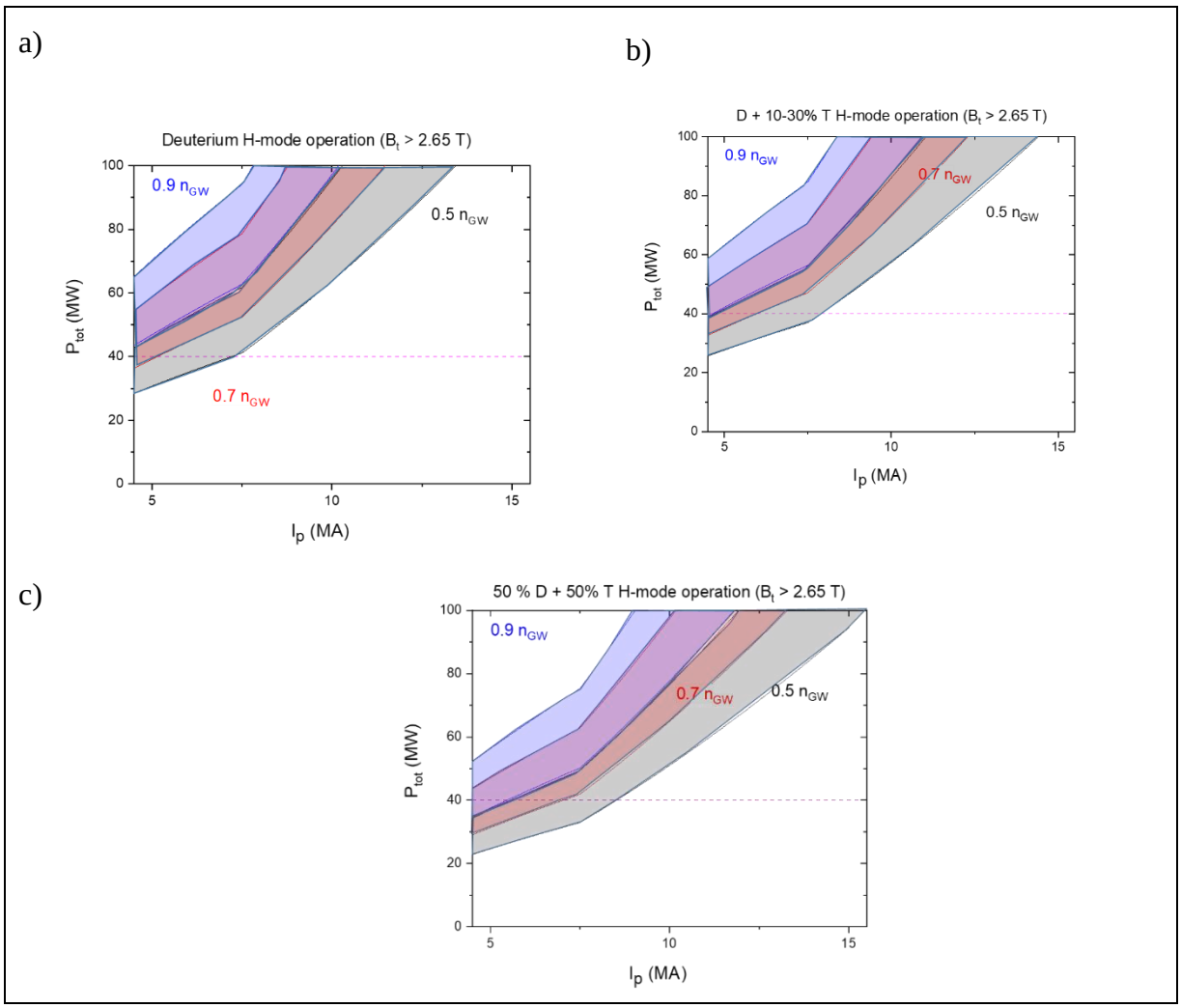

Figure 4.2-1. H-mode operational range (a, b, s) for DD, D+10-30% T and 50% D – 50% T plasmas and a range of operational densities and total plasma heating power including additional heating + alpha heating for DT plasmas.

The foreseen path to develop DD and DT H-modes is similar to that assumed for L- and H-mode development in the 2016-IRP. Namely, starting from 5.0-7.5 MA plasmas to follow a step ladder of plasma current and field increases while remaining for the most part in a range of $q_{95} = 3 – 4$.

Each DT-1 campaign has 16 months of operation. As for AFP, operations are divided into two-weeks blocks with twelve days of two shifts/day dedicated to the experimental exploitation followed by two-days of short maintenance in which boronization by GDC can be applied,

when needed. It is also assumed that on average on average 13 pulses per two-shift day contribute to the NB-IRP as it was also assumed for the 2016-IRP.

We describe below the logic for the strategy that the NB-IRP will follow to demonstrate the goals of the DT-1 campaign while the details of how this will be done from FPO-2 onwards remain to be elaborated.

The development of H-modes scenarios in DT-1 is guided by the need to optimize the neutron fluence for the achievement of each step in the path to Q = 10, to minimize risks to the achievement of the Q = 10 goal and to achieve this goal as early as possible. To this end the following expansion of the H-mode operational space (in terms of plasma currents and toroidal field) is foreseen, where each scenario is first developed in DD plasmas and this is followed by the DT development starting from ~ 10 % T level up to maximum fusion power (~ 50% T).

The development for DD and DT plasmas to Q = 10 is expected to follow one of the two paths summarized in Table 4.2-1 depending on the level of confinement enhancement beyond H-mode observed within the range q_{95} = 3-4. If a significant confinement enhancement beyond H-mode (typically, H_{98} ~ 1.5) is observed within the range q_{95} ~ 3.5 - 4, with the potential to demonstrate the Q = 10 project goal at I_p < 15 MA, the path described in Table 4.2-1.b will be followed.
As part of the DT development and, following it if required, specific plasma operation and fuel removal activities will be implemented to ensure that the residual level of in-vessel T remains under 1% (required for low neutron production in the follow-up DD plasmas). This has been recently demonstrated after the JET DTE2 experiment with Be-wall deposits and W [Matveev 2023] and a similar operational strategy is proposed for ITER with full-W PFCs and boronization. The advantages of such approach are:

- DD H-mode plasmas in ITER can achieve plasma characteristics which are similar to those in DT, as shown in Fig. 4.2-2. This allows the development of scenarios and control schemes up to heated flat top durations of 100’s of seconds to address integration and control issues relevant to DT plasmas with minimum neutron fluence consumption;
- The high available heating power in DT-1 allows the gradual build-up of T concentration for each current/ field step in DT, while maintaining a constant heating power in the plasma. This allows the gradual build-up of the alpha particle density as well as the step-by-step re-optimization of control schemes, disruption mitigation schemes, etc., with increasing alpha particle densities/fusion powers independently from other control/integration issues (e.g. divertor power load control, ELM control, etc.);
- The amount of injected T will increase gradually as the H-mode operational space current/field widens. This allows the development of operational strategies to minimize in-vessel T retention to be gradually developed together with H-mode development. It ensures that a sound in-vessel T minimization strategy has been developed before Q = 10 operation, in which the highest injected T amounts in DT-1 takes place.

a)

Step	I_p/B_t	q_{95}
1	7.5 MA/2.65 T	3
2	7.5 MA/3.4 T	4
3	7.5 MA/5.3 T	6
4	9.5 MA/3.4 T	3
5	9.5 MA/4.5 T	4
6	12.5 MA/4.5 T	3
7	12.5 MA/5.3 T	3.5
8	15 MA/5.3 T	3

b)

Step	I_p/B_t	q_{95}
1	7.5 MA/2.65 T	3
2	7.5 MA/3.4 T	4
3	7.5 MA/5.3 T	6
4	9.5 MA/3.4 T	3
5	9.5 MA/4.5 T	4
6	11 MA/5.3 T	4
7	12.5 MA/5.3 T	3.5

Table 4.2-1. a) Path to Q = 10 based on conventional H-mode plasmas in DT with q_{95} = 3-4. b) Path to Q = 10 based on enhanced confinement H-mode plasmas in DT with q_{95} = 3.5-4.

The DD and DT development path includes an exploration of high q_{95} (≥ 6) H-mode plasmas in DD and DT. These plasmas have been studied in DIII-D and EAST (e.g. [Garofalo 2017, Zhang 2021]) and have the potential for significantly increased H-mode confinement providing Q ≥ 5 operation at ~ 7.5 MA/5.3 T [Ding 2021], although this requires operation at plasma densities exceeding the Greenwald limit, which appears challenging. To investigate the potential for such an approach, a step is included in both paths to Q = 10. If experimental results in ITER confirm the potential for such a high q_{95} approach for high Q operation (typically, H_{98} ~ 2 at high $\langle n_e/n_{GW} \rangle$) the DT development path would be modified to a constant field path (5.3 T) in which I_p, $\langle n_e \rangle$ and the H&CD level and mix would be optimized to maximize Q starting at 7.5 MA.

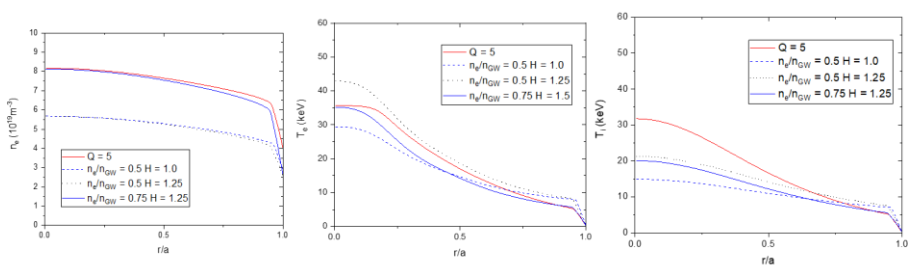

Scenario 12.5 MA/5.3 T	P_{tot} (MW)	$\langle n_e \rangle / n_{GW}$	P_{sep}/P_{LH}	β_N	β_p	W_{fast}/W_t	I_{CD}/I_p (%)	P_{sep} (MW)
Q = 5 H = 1.25	50	0.74	1.2	2.1	0.64	16	44	82
DD H = 1	93	0.5	1.4	1.4	0.44	12	44	76
DD H = 1.25	93	0.5	1.4	1.7	0.53	12	51	70
DD H = 1.25	93	0.75	1.1	1.8	0.6	6	40	72

Figure 4.2-2. Plasma density, electron temperature and ion temperature profiles for 12.5 MA/5.3 T DT long pulse plasma with Q = 5 and for similar plasmas in DD. The table shows overall characteristics of these plasmas in terms of auxiliary heating, plasma density normalized to the Greenwald density limit, power crossing the separatrix normalized to the H-mode threshold power, normalized and poloidal beta, normalized fast particle energy, current drive fraction and edge power flow.

For every DD step in the development path, specific experiments will be performed and control/mitigation schemes refined to:

a) provide high confinement/MHD stable plasmas by optimizing heating strategies, error field correction (using error field correction coils and ELM control coils for this purpose), NTM control, etc.;

b) characterize power fluxes for controlled-ELM H-mode plasmas with ELM control coils and achieve radiative divertor power dissipation and control of W sources in these conditions, while avoiding sizeable fast particle losses;

c) provide appropriate control of plasma density in the stationary H-mode phase as well as in the access to and exit from H-mode by optimization of gas and pellet fuelling;

d) ensure appropriate mitigation of disruptions, and;

e) explore different scenario options for access to /exit from H-mode in the current ramp-up and ramp-down including optimization of fuelling and heating waveforms to minimize excursions in plasma parameters (internal inductance, plasma energy, etc.), power fluxes to PFCs and corresponding W influxes into the confined plasma, etc.

For the DT steps, in addition, the experimental programme for H-mode plasmas will assess in detail, and for a range of heating powers/heating mixes and plasma densities, the impact of T concentration on:

a) the power required to access the H-mode;

b) edge and pedestal plasma characteristics and control of ELM power loads;

c) core plasma MHD stability including fast particle effects (NBI, ICH and alpha particles);

d) core plasma transport (including W), and;

e) He core plasma concentration and exhaust.

For each of the T concentrations, plasma densities and power levels, etc., explored, a fully integrated H-mode scenario will be developed. This will require the assessment and retuning of the previously developed control schemes to provide optimum T fuelling and DT mix control (e.g. by optimizing pellet size, velocity, etc.), the redevelopment of robust H-mode scenarios including access to/exit from H-mode phases, control of the divertor power fluxes and of W sources, ELM control by ELM control coils, NTM control, etc. Once alpha heating becomes a significant fraction of the power that is required to sustain the H-mode scenario, the additional heating will be reduced and burn control experiments will take place. Since plasma thermal energy and, especially, RE seed sources will increase significantly in these plasmas compared to DD, specific experiments will be carried out to optimize disruption mitigation with the DMS to ensure that the required degree of mitigation for thermal, electromagnetic and RE loads is achieved before expanding operations towards the next step.

A short description of the activities of the outline DT-1 plan and their logic is provided below.

4.2.1 FPO-1 campaign

The FPO-1 campaign is expected to have two parts one with hydrogen plasmas and one with deuterium plasmas.

- **Hydrogen FPO-1 campaign**

The main objective of the hydrogen campaign in FPO-1 is to re-start and re-commission the tokamak with all post-AFP components and systems installed. It is executed with hydrogen plasmas to minimize in-vessel activation in case human access to the vacuum vessel is required as a result of issues arising during commissioning with plasma. The target plasma scenarios for commissioning are L-modes with I_p = 7.5 - 15 MA. The foreseen experimental plan is similar to that of the L-mode programme in the PFPO-2 campaign of the 2016-IRP with one additional item for disruption mitigation risk retirement.

A specific experiment will be carried out towards the end of the hydrogen phase of the FPO-1 campaign to retire the risks associated to beta decay during disruption mitigation. These have not been addressed in AFP and can materialize during DT operation. If this is the case, significant damage to first wall panels may occur needing their replacement in an activated environment during DT. Modelling studies show that schemes that provide disruption mitigation with moderate RE production may fail to do so when T decay seeds are included, as shown in Fig. 4.2.1-1.

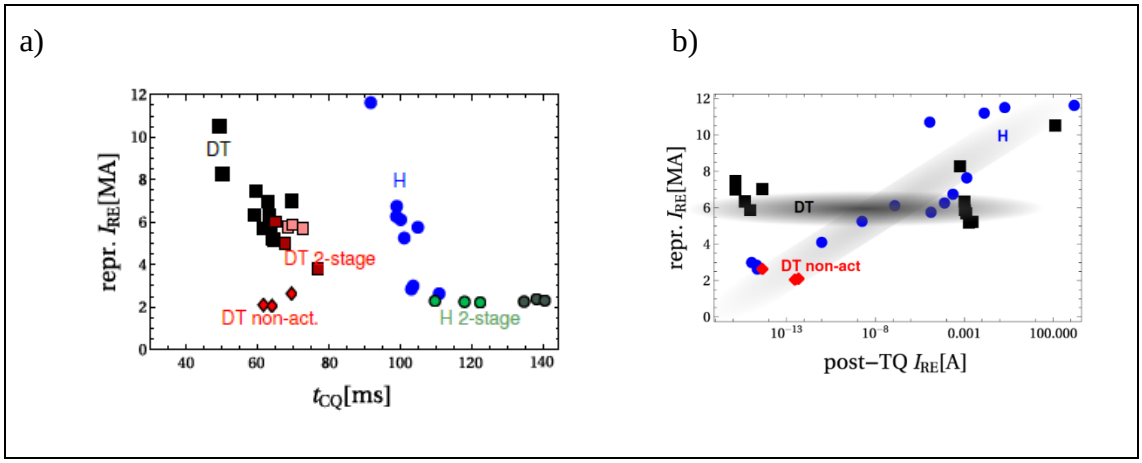

Figure 4.2.1-1. a) Resulting RE current following the application of DMS for disruption mitigation versus current quench time for L-mode H plasmas and DT H-mode plasmas with Q = 10 at 15 MA and single stage or double stage mitigation. For the DT plasmas a comparison is made in which the T beta-decay source of high energy electrons is removed (labelled DT non-act) to show the effect of these sources on the generated RE current. b) Resulting RE current versus post-TQ RE seed from the hot tail following disruption mitigation for the same discharges showing that the increased RE current for DT plasmas is associated with the beta-decay electron source from T [I. Pustzai 2023].

To retire this risk it is thus considered to perform a short campaign (~ 1 operational month) in hydrogen plasmas up to 15 MA/5.3T with increasing levels of T, starting from trace-T up to ~ 50 % T in which the disruption mitigation schemes developed for AFP are re-tuned to account for both hot electrons and beta decay electrons. If successful, it is expected that the risk

associated with beta decay electrons from T can be retired at this stage. It cannot be ruled out that in the execution of the disruption mitigation programme to retire the T beta decay risk, significant REs are produced causing significant damage to the water cooled first wall panels, even if their design is being improved to sustain as high as possible RE impacts. If this damage is considered excessive for the remaining DT-1 programme, the affected first wall panels will need to be removed after this phase of FPO-1. The advantage of the proposed approach with regards to leaving this risk for later DT operation is that this replacement will be done with low activation in-vessel since the proton-tritium reaction ($p+T \rightarrow n + He^3$) has an energy threshold above 1 MeV.

We note that in the hydrogen campaign in FPO-1 the NBI injectors will be commissioned with plasma injecting hydrogen neutrals, whose negative ion current density levels compared to those required in ITER has been demonstrated already in present facilities. It is proposed to maintain the NBI in this configuration for FPO-1. Depending on results obtained, this could be possibly extended to the end of the DT-1 campaigns as a risk mitigation for NBIs, if problems in deuterium beam development are encountered. The impact on fusion performance for Q = 10 plasmas of plasma heated by hydrogen compared to deuterium beams has been evaluated with fully integrated JINTRAC simulations. It has been found that this impact is very low, in the few percent range (loss of 10 MW fusion power because of the lack of fast-D+T reaction and an additional core dilution of few % hydrogen), as shown in Fig. 4.2.1-2. However, the use of hydrogen beams imposes restrictions to the use of NBI power due to shine-through losses at low currents and this, in turn, implies the need for higher RF heating in the earlier stages of the DD (and DT) H-mode development plan as shown in Fig. 4.2.1-3. The implications of the implementation of such risk mitigation measure need to be evaluated in detail before it can be decided to be implemented as reference operation for DT-1 or not.

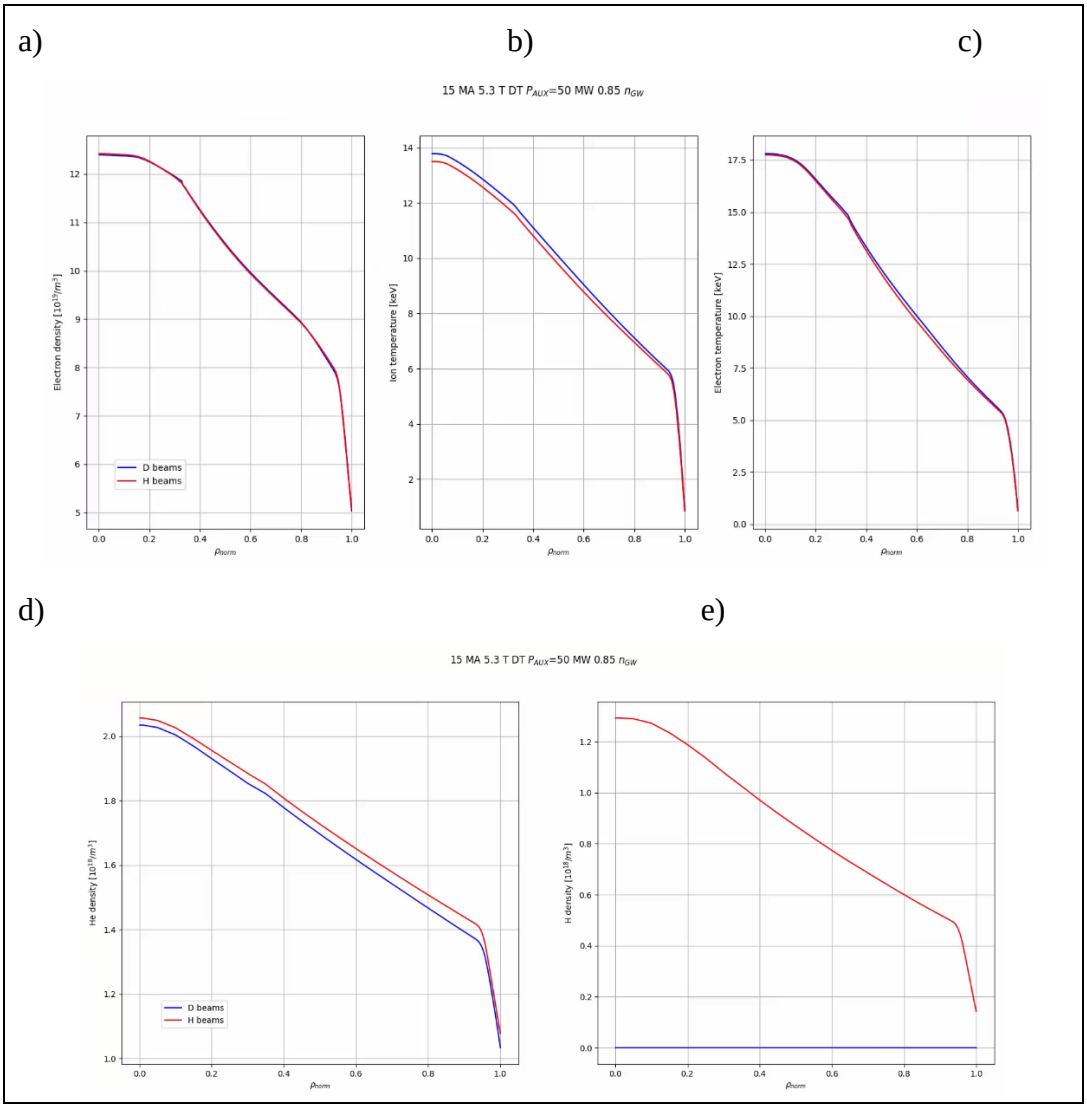

Figure 4.2.1-2. Plasma parameters for two Q = 10 discharges 15 MA/5.3T one heated by hydrogen (in red) and deuterium beams (in blue). a) Plasma density, b) Ion temperature, c) Electron temperature, d) Helium density and e) Hydrogen density.

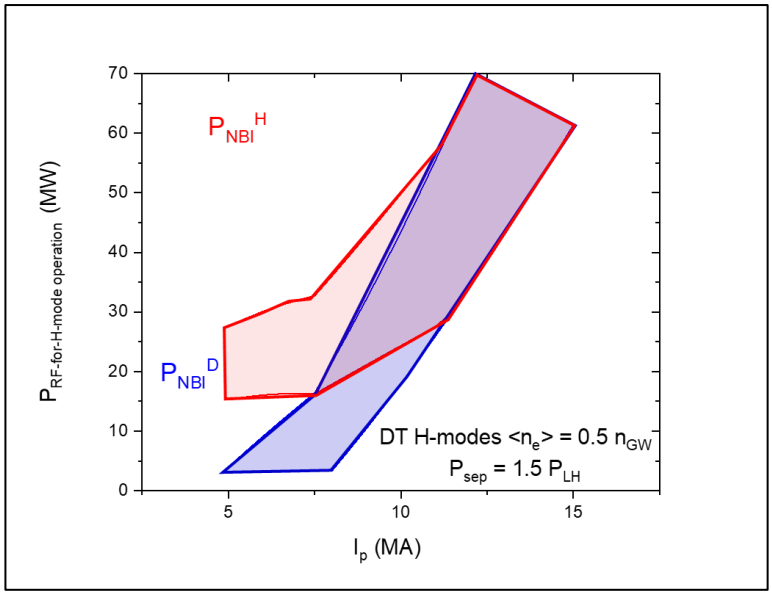

Figure 4.2.1-3. Required RF power for H-mode operation (assuming $0.25 < P_{rad}^{core}/P_{tot} < 0.5$) for DD H-modes at <ne> = 0.5 n_{GW} with hydrogen beams (NBI limited by shine-through) and deuterium beams.

- **Deuterium FPO-1 campaign**

The second part of the FPO-1 campaign aims at starting operation in DD plasmas and the expansion of the operational space up to 15 MA/5.3 T L-modes and up to 7.5 MA/2.65T H-modes with high heating power level for heated flat top durations of at least ~ 50 s and to investigate H-mode access in DD plasmas with B_t up to 5.3 T. The experimental activities and required time are similar to those foreseen in the FPO-1 campaign of the 2016-IRP. It includes a wall change over from H (+T) to D and scenario development, plasma control commissioning, etc., for which 45 days are allocated. The wall change-over experiment will provide first evidence of the efficiency of the operational strategies and schemes to remove in-vessel T from ITER.

In this campaign, and subsequently in FPO-2, DD H-mode plasmas comparable to those in AFP will be explored and this will allow the identification of effects from the TBMs and the NBMFRS (Neutral Beam Magnetic Field Reduction System) on H-mode plasmas and their mitigation by the re-tuning of error field correction and/or the use of the ELM control coils for this purpose.

4.2.2 FPO-2 – FPO-5 campaigns

The detailed plan to demonstrate the final DT-1 goal of Q = 10 for 300 – 500 s from FPO-2 onwards remains to be developed. This will follow the logic above by interleaving DD and DT scenarios and with specific experimental time allocation for tritium removal in the DT campaigns. This phase will also include specific time for demonstration of routine high Q operation that will also be used to address TBM-specific objectives of DT-1.

4.3 DT-2

The objective of DT-2 is to demonstrate routine operation in all ITER reference high Q scenarios addressing burning plasma physics, scenario integration issues and nuclear technology R&D, as defined in the Project Specifications and substantiated in the Project Requirements, up to the achievement of the Project Specification fluence goal.

The details of the research plan for this phase and the time required for its execution will strongly depend on the findings in DT-1 and need to be developed in detail. The main goals of DT-2 are:

- Development of the Q = 5 long pulse scenario and the demonstration of high Q/high duty operation with burn lengths 500 -1000s;
- Development of the Q = 5 steady-state scenario with 3000s burn;
- Exploration of Q > 10 scenarios and fusion reactor targeted studies.

The foreseen research plan for DT-2 is similar to that developed for the corresponding experiments in the 2016-IRP, since it is speculative to substantially modify it before high Q DT plasmas are obtained in ITER.

The final DT-2 campaigns could include experiments targeted to demonstrate Q > 10 plasmas, dedicated operation at high Q with a reduced set of sensors and actuators, assessments of the power exhaust solution based on high core radiative faction, as shown in Fig. 4.3-1, or specific experiments to demonstrate the pros and cons of different heating mixes with a view to high Q operation in DEMO. The available level of heating and variety of heating schemes in DT-2 should allow a conclusive result to be obtained. As an example, modelling of the optimization of access to Q = 10 in ITER with various heating mixes is shown in Fig. 4.3-2.

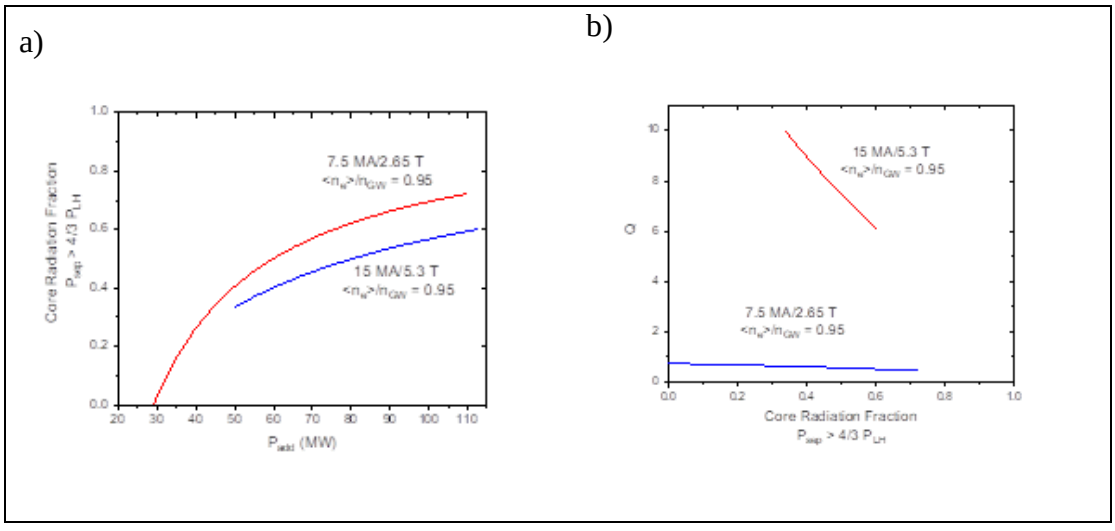

Figure 4.3-1. a) Level of core radiation fraction versus additional heating power, P_{add}, for $\langle n_e \rangle / n_{GW} = 0.95$ in DT plasmas with 15 MA/5.3 T and 7.5 MA/2.65 T (extrapolated from integrated plasma simulations for 50 MW additional heating and a simple 0-D model with $H_{98} = 1$ plus constant impurity and helium fractions independent of radiation fraction level). b) Fusion gain, Q, for the two cases as a function of the core radiation fraction.

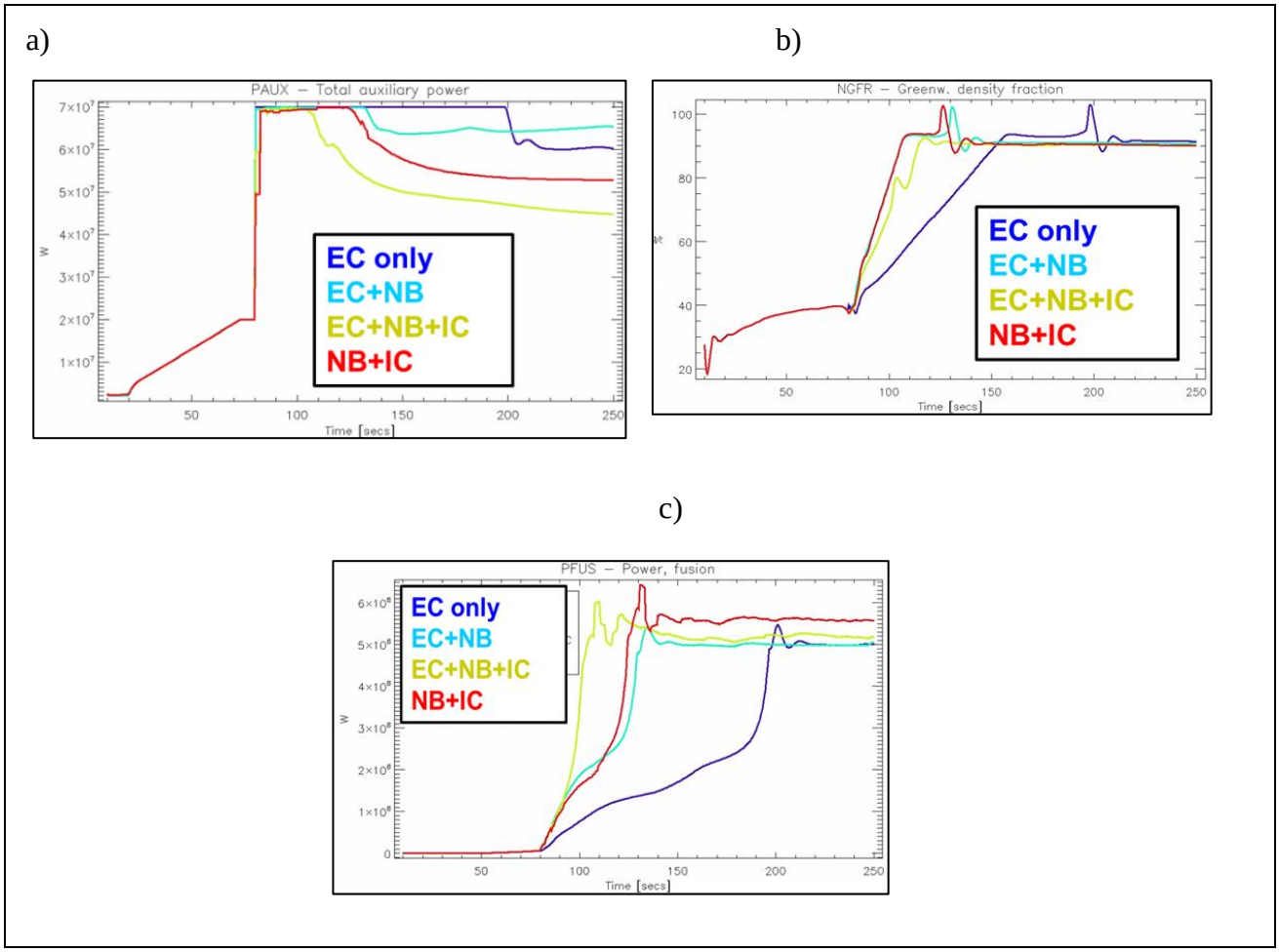

Figure 4.3-2. a) Additional heating power waveform to achieve Q = 10 in ITER 15 MA plasmas assuming the core radiated power level is 30% of the total heating power (alpha + additional heating). b) Density waveform including the fastest rise to stationary burning conditions with robust access to Q = 10. c) Resulting fusion power in these scenarios.

5. Summary and Conclusions

The present report describes the outline operational and research plan for the new ITER baseline with three main phases: AFP, DT-1 and DT-2. The experimental exploitation of ITER towards the achievement of the goals in these phases is described. This operational and research plan aims to be a realistic plan and this is taken into account in the proposed machine configuration, risk retirement strategy and time allocation to different activities. To firm up the foreseen activities and time allocations further analysis, in cooperation with the ITER Members' fusion communities, will be carried out. In addition, experimental and modelling support to resolve open issues already identified [e.g. 8YFSB3] is required to refine the details of these plans.

6. References

[Project Specification] Project Specification (PS) (2DY7NG)

[ITER INB Decree 2012] ITER INB Decree 2012

[Project Requirements] Project Requirements (PR) (27ZRW8)

[PFPO-1] ITER Research Plan (IRP) - Level 2 - Pre-Fusion Power Operation - 1 (24S8PK)

[PFPO-2] ITER Research Plan (IRP) - Level 2 - Pre-Fusion Power Operation - 2 (25STUD)

[Martín-Solís 2017] J.R. Martín-Solís et al 2017 Nucl. Fusion 57 066025

[Hoppe 2021] M. Hoppe, et al., Computer Physics Communications, 268 (2021) 108098

[Loarte 2021] A. Loarte et al 2021 Nucl. Fusion 61 076012

[Part I: Consequences of Changing First Wall Material in ITER] Part I of this technical report

[Matveev 2023] D. Matveev et al 2023 Nucl. Fusion 63 112014

[Garofalo 2017] A M Garofalo et al 2018 Plasma Phys. Control. Fusion 60 014043

[Zhang 2021] X X Zhang et al 2021 Plasma Phys. Control. Fusion 63 065013

[Ding 2021] S. Ding, et al. Proc. 28th IAEA Fusion Energy Conference, France 2021

[Pustzai 2023] I. Pustzai, 2023 EPS conference, Bordeaux, France. Paper I2-106

[8YFSB3] Open issues in the new ITER baseline with a W wall for Q = 10 operation that require experimental assessment (8YFSB3)

Disclaimer

The views and opinions expressed herein do not necessarily reflect those of the ITER Organization.

References

This ITER Technical Report may contain references to internal technical documents. These are accessible to ITER staff and External Collaborators included in the corresponding ITER Document Management (IDM) lists. If you are not included in these lists and need to access a specific technical document referenced in this report, please contact us at ITR.support@iter.org and your request will be considered, on a case by case basis, and in light of applicable ITER regulations.